ABSTRACT

Title of Thesis: ASSESSMENT OF PACKAGING MEDIA USED IN LONG-TERM STORAGE OF ELECTRONIC COMPONENTS

Suraj Ravimanalan,
Master of Science, 2021

Thesis Directed By: Dr. Diganta Das
Department of Mechanical Engineering

Companies that produce end-products with long-term sustainment requirements undertake long-term storage as one of the measures to overcome the problem of electronic component obsolescence. To protect the components from environmental degradation during storage, they are packed inside vacuum sealed moisture barrier bags along with desiccants and humidity indicator cards. The desiccants have a specific adsorption capacity at a particular temperature / relative humidity condition. They cannot absorb the moisture permeated through the moisture barrier bag beyond that capacity. The relative humidity inside the moisture barrier bag also changes during long-term storage. This thesis provides a methodology to estimate the time to reach the desiccant's adsorption capacity and to estimate the increase in relative humidity inside the moisture barrier bag. The methodology is based on the experimental results and the first principle physical equations used for moisture permeation and adsorption. Based on these estimations, companies can decide on replacement schedules for moisture barrier bags and desiccants, thus protecting the electronic components contained within moisture barrier bags from humidity-related reliability issues.

ASSESSMENT OF PACKAGING MEDIA USED FOR LONG-TERM STORAGE OF ELECTRONIC COMPONENTS

by

Suraj Ravimanalan

Thesis submitted to the Faculty of the Graduate School of the
University of Maryland, College Park, in partial fulfillment
of the requirements for the degree of
Master of Science
2021

Advisory Committee:
Dr. Diganta Das, Chair
Professor Peter Sandborn
Professor Patrick McCluskey
Dr. Michael Azarian
Dr. Robert Kinyanjui

Acknowledgements

I would first like to thank my thesis advisor Dr. Diganta Das of Mechanical Engineering Dept. at University of Maryland, College Park for his continued guidance, support and for all the opportunities I was given to conduct my research. I would also like to thank Prof. Michael Pecht and Dr. Michael Azarian of Center for Advanced Life Cycle Engineering, University of Maryland, College Park for their insightful comments and valuable feedback.

I would like to take this moment to thank Dr. Robert Kinyanjui of John Deere for sharing his expertise, and sincere and valuable guidance for this research.

Finally, I must express my very profound gratitude to my parents and to my friends for their wise counsel, unfailing support, and continuous encouragement throughout my years of study. This accomplishment would not have been possible without them.

Table of Contents

List of Tables

List of Figures

Chapter 1: Introduction

The electronics industry is continually evolving with innovations in component design and architecture. The component manufacturers concentrate on the products with the largest and fastest return on investments. This bottom-line pressure leads to frequent trimming of product portfolios. The introduction of newer electronic components into the market favors the consumer electronics industries that manufacture short-life electronic products such as smartphones. However, it acts as a problem of component obsolescence for the end-product manufacturers, primarily in the defense, aerospace, and automotive sectors. The lifecycle of the end-products manufactured by these sectors, such as weapon systems, ships, telecommunications infrastructure, farm machinery, and medical equipment, is longer than the lifecycle of the electronic components that go into them. Simultaneously, it is the electronic system that often defines functional complexity for the products in those sectors. For example, the communication and decision support electronic systems are critical to the farming equipment's performance, thereby influencing the farmer's farm output, plowing, and planting. The obsolescence of the components due to their discontinuation results in downtime when the farm machinery is serviced. This downtime can be very costly to the farmer/customer affecting their farm output.

To mitigate the component obsolescence, certain measures such as negotiating with the component manufacturer, redesigning the end-product and associated manufacturing processes, buying from aftermarket sources, and performing a lifetime-buy (LTB) or bridge-buy of near-obsolete or end-of-life component can be taken. In

most cases, lifetime-buy is the most commonly adopted measure by end-product manufacturers. This is because of the fact that undergoing redesign every time a product discontinuation notice is issued will be difficult for the end-product to get manufactured and serviced [1]. Lifetime-buy for an end-product manufacturer is defined as the process of buying sufficient quantity from the component manufacturers to meet the end-products' lifetime needs before the anticipated termination of component production [2].

While lifetime-buy helps to support uninterrupted manufacturing operations following component obsolescence, it requires careful planning and a well-thought-out storage management system so as to maintain these components in as-received condition until the support for the end-product's lifecycle is discontinued. For example, a company manufacturing the same model tractor for 10 years is expected by its customers to provide maintenance and repair support for more than 30 years. This requires the company to store the electronic components purchased as a part of lifetime-buy in the warehouse for an extended period of time. During this long-term-storage (LTS) of electronic components, various environmental factors such as temperature, humidity, oxygen, dust particles, and other contaminants can cause the components to degrade. For example, prolonged exposure of electronic components in a high-humid environment during storage causes the moisture to permeate through the electronic components' epoxy molding compound (EMC). If uncontrolled, such exposure reduces the interfacial adhesion strength between the EMC and die, causing delamination and induces vapor pressure during solder reflow resulting in popcorn cracking [3].

Electronic manufacturing companies rely on standards, manufacturer's handbooks, and literature that provide recommendations on storage conditions and suggestions on reliable practices to protect the components during long-term-storage from physical damage and degradation due to environmental factors. The most common practice suggested by these documents is to contain the components within carriers and pack them inside moisture barrier bags (MBBs) along with desiccant and humidity indicator card (HIC) during long-term storage. This is defined as long-term storage system in this thesis and is depicted in Figure 1. A long-term storage system consists of replaceable and non-replaceable elements. MBBs, carriers, HICs, and desiccants are labeled as replaceable elements as they can be replaced during the long-term storage until the electronic components are used for either manufacturing or repair processes after storage. The carriers such as tape and reel, tray and tubes protect the components from physical damage and electrostatic discharge damage to the components. Carriers are also used for manufacturing and assembly operations of components after storage. Tape and reel carriers are considered in this thesis. The desiccants are packed within the MBB to adsorb the moisture present within the MBB and adsorb the moisture that gets permeated through the MBB, and HICs indicate a fixed level of relative humidity (RH) inside the MBB. MBBs are vacuum sealed to protect the components from moisture-related degradation mechanisms and also protect the components from electrostatic discharge and electromagnetic interference. The detailed function of each of these replaceable elements of the long-term storage system is provided in Appendix A.

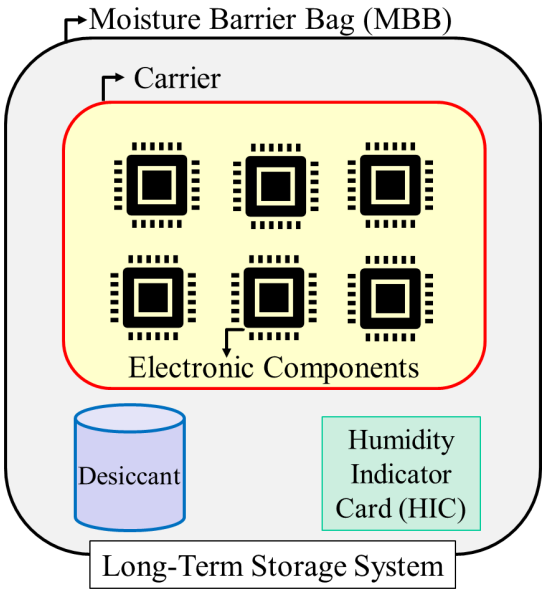

Figure 1 Long-term storage system and its elements

The long-term storage system is placed in a controlled storage environment. Usually, there are two environments – outside environment and inside environment. Outside environment is the temperature and relative humidity of air outside the MBB and Inside environment is the temperature and relative humidity of air inside the MBB. The long-term storage system environment considered in the thesis is shown in Figure 2. Outside the MBB, temperature and relative humidity is maintained at 17 °C – 25 °C and 30% RH – 60% RH respectively. The chemical environment outside the system is air. The environment inside the system is vacuum and dry initially. However, this environment can change depending on the properties of MBB, desiccant and carrier, which has been discussed in Chapter 3: Materials and its Properties.

Even though the electronic components and the carriers are packed within the MBB, the reliability of components can get compromised over time because the moisture from the outside environment permeates through the MBB and reaches the

inside where the permeated moisture gets adsorbed by the desiccant. The desiccant cannot adsorb the permeated moisture beyond its adsorption capacity, and as the desiccant is approaching to its adsorption capacity, relative humidity inside MBB increases over time, thus potentially affecting the reliability of stored components with respect to humidity related degradation mechanisms. Also, the surface resistivity property of the carriers and MBBs can degrade during long-term storage which could potentially affect the reliability of the stored components with respect to electrostatic discharge. As a result, the packaging media must be replaced in order to prevent the degradation of the components from affecting its manufacturability and reliability requirements.

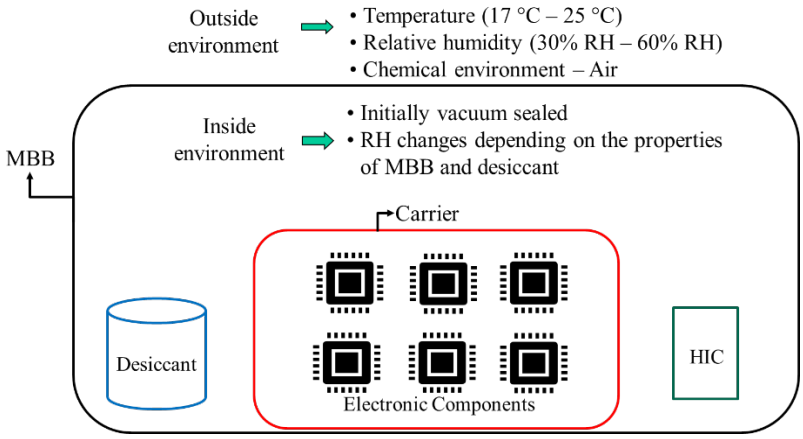

Figure 2 Long-term storage system environment

This thesis discusses the methodology to determine the estimates of RH increase inside MBB versus time based on which engineering decisions can be made to obtain the replacement schedules for the desiccants and MBBs. It also reports on the experiments conducted to determine of the criticality of the surface resistivity degradation mode of the carriers and MBBs.

Chapter 2: Review of Standards and Prior Work on Long-Term Storage

In this section, the literature review of the standards used for long-term storage of electronic components and a review on long-term storage study conducted by Texas Instruments is reported. Table 1 lists standards that are reviewed in this thesis. These standards provide the practices and recommendations for storing components for long-term.

Table 1 Long-Term Storage Standards for Electronic Components

Standard Name	Developed by	Coverage	Last Updated
JEDEC JEP 160 [4]	Joint Electron Device Engineering Council (JEDEC) Solid State Technology Association	Recommendations on best practices for packing and storing the solid-state electronics for long-term storage	Sep 2016
GEIA-STD-0003A [5]	SAE International	Recommendations on long-term storage environment control guidelines	Jan 2017
IEC 62435 (Series of 9 standards) [6]	International Electrotechnical Commission (IEC)	Recommendations on methods of long-term storage	Varies for each member of the series

JEDEC JEP 160 Standard

The Joint Electron Device Engineering Council (JEDEC) standard JEP 160 defines the long-term storage as uninterrupted storage where the conditions and requirements of JEDEC J-STD-033 do not otherwise apply. The long-term storage requirements and conditions stated in JEP 160 are applicable when stored for more than one year as opposed to J-STD-033, which provides the requirements for storage less than one year.

To prevent the electronic components from environmental damage and to maintain the reliability of the components during long-term storage, the JEP 160 standard recommends the following three methods – dry cabinet storage, vacuum MBB storage, and nitrogen flush or positive-pressure MBB storage. In dry cabinet storage, the components are recommended to be stored inside a cabinet that is humidity and oxygen controlled. In vacuum MBB storage, the components are recommended to be packed within a vacuum MBB that contains HIC and oxygen sensor. MBBs are recommended to be flushed with dry nitrogen before vacuuming in this method. In positive-pressure MBB storage, MBBs are initially vacuumed, followed by filling with dry nitrogen or dry air at a positive pressure compared to the outside environment, to create an inert atmosphere inside the MBB. However, in this method, the MBBs are susceptible to get punctured because of the positive pressure inflation of the bag. Irrespective of the above methods, this standard also recommends packing an MBB within another MBB, which is named as double containment, if required.

The standard also suggests performing certain verification tests on a regular schedule for both the packaging media and the components. Based on the results of the verification tests, the time to store further is recommended to be either increased or decreased. Verification tests for the packaging media include monitoring the HIC for any change in color, verifying the integrity of the MBB seal, and monitoring the oxygen sensor for any increase in the amount of oxygen inside the storage container or MBB. For the components, the verification tests are recommended to be performed by introducing “surrogate hardware” along with the other components. The surrogate hardware is expected to act as a representative sample for the stored electronic

components that is suggested to be evaluated for any signs of damage or deterioration by undergoing pass/fail tests in a periodic schedule. For example, the surrogate hardware can undergo cross-sectioning of the leads periodically to measure and compare the length of the grown intermetallic layer against the pass/fail criteria. Decisions involving choosing the environmental conditions for long-term storage are recommended to be evaluated by the users themselves based on the types of components and the packaging media used for storage.

Although this standard provides the methods of storing the electronic components for long-term, the standard did not report on how long one can use these packaging methods to store the components. While the standards provide recommendations for periodic evaluation of surrogate electronic components, it did provide any information on periodic evaluation of packaging media and also it did not report on how long one can use the packaging media before which they should be replaced during long-term storage.

GEIA-STD-0003A Standard

The standard GEIA-STD-0003A developed by SAE International recommends long-term storage practices for electronic devices by providing guidelines to packaging based on the required protection level. The standard defines the long-term storage as "any device storage for more than 12 months but typically allows for much longer (years)".

The standard recommends the storage environment to be maintained at a temperature of 17 °C – 25 °C and relative humidity of 7% - 25%. Similar to JEDEC JEP160, components are required to be stored within the sealed MBB that is either vacuumed or filled with dry nitrogen. In addition to packing those components inside either vacuum MBB or dry nitrogen MBB, it also recommends storing the sealed MBBs containing components inside the rigid containers that provides temperature-controlled protection, ionizing and non-ionizing radiation protection, extraneous chemical contamination protection, and mechanical protection (e.g., shock, vibration, movement). Based on the nature of the electronic components stored, protection levels are defined with the packaging requirement, as shown in Table 2. Along with all other aspects of how the protection should be provided, the standard covers the general aspects of the long-term storage control that starts right from the initial inspection to the removal or partial removal from storage.

Similar to JEDEC JEP 160, this standard also did not report on the time to store the components and their packaging media without affecting the manufacturability and reliability requirements of electronic components. Also, this standard explicitly mentions that the packing requirements provided in the standard help to mitigate only "some" of the degradation mechanisms while there are many known and unknown factors that cause other degradation mechanisms to the packaging media especially. However, identifying the critical degradation mechanisms for both the components and packaging media will be crucial in estimating the replacement schedules based on those critical degradation mechanisms.

Table 2 Packing requirement for the protection level mentioned in SAE GEIA-STD-0003A standard

Protection Level	**Are components highly valued and/or irreplaceable?**	**Are components sensitive to outgassing?**	**Are components moisture-sensitive?**	**Packaging requirement**
Level 1	No	No	No	Components placed in a sealed MBB along with desiccant. MBB is then placed in a protective container
Level 2	No	No	Yes	Components placed in a sealed MBB filled with dry N_2. MBB is then placed in a protective container
Level 3	No	Yes	Yes	Components placed in a sealed MBB filled with both dry N_2 and desiccant. MBB is then placed in a protective container
Level 4	Yes	---	---	Components placed in a sealed MBB filled with both dry N_2 and/or desiccant. MBB is then placed in a dry N_2 container that shall contain desiccant external to MBB.

IEC 62435 Standard

In this standard, long-term storage is defined as the planned storage of components to extend the life cycle for a duration with the intention of supporting future use. The standard recommends undergoing long-term storage at a temperature maintained between 5 °C and 40 °C and relative humidity maintained between 20% and 50%. This standard also provides recommendation on periodic evaluation of surrogate hardware for electronic components with specific validation requirements before and after long-term storage. However, no such recommendations were provided for packaging media.

The three long-term storage standards considered in this thesis do not provide any recommendations for estimating the replacement schedules for packaging media, degradation mechanisms of the packaging media, risks involved in re-packing of the components, and risks involved in cyclic storage practices. This thesis addresses the limitations of long-term storage standards by identifying the criticality of certain degradation mechanisms for packaging media and developing a methodology to estimate the replacement schedules of MBBs and desiccants based on its properties.

Long-Term Storage Study by Texas Instruments

Texas Instruments performed a study on packaging media along with the components to obtain its shelf life by storing them together at <40 °C and <90% RH for periods of time ranging from 2 to 17 years [7]. Along with the evaluation of long-term stored components, carriers such as tubes and tape and reel used as packaging media for those components were also evaluated for any degradation in static

dissipative properties during their long-term storage study. The cover tape of tape and reel carriers were evaluated for any degradation or change in the peel strength when they were stored for long-term. MBBs were evaluated for any moisture leak into the inside environment and any fading of marking and labels printed on MBBs.

From the results of the evaluations made on packaging media, it was concluded that the moisture diffusion through MBB limits the life of packaging media. A standard MBB can be used for 32 months and MBBs intended for long-term storage can be used for more than 5 years. Although their study reported on the operating life of MBB, it may vary for different properties of MBBs and the permeation property for standard MBB and long-term stored MBB was not reported. As a result, it is difficult to correlate the life of MBB with its properties based on their study. Also, their study did not report on how long one should use and replace the desiccant sealed inside MBB before reaching its adsorption capacity. This thesis provides a methodology to estimate the replacement schedules based on the properties of MBBs and desiccants before undergoing long-term storage.

Chapter 3: Materials and its Properties

Moisture barrier bags, desiccants, and tape and reel carriers are the packaging materials evaluated in this thesis. This section details the manufacturer information, construction, and important properties of those materials. Some of the important properties, which will be used for the evaluation of experimental results performed on them, are not provided by the manufacturers. Those properties are determined by either conducting experiments or using the available information provided by the manufacturer, which is also included in this section.

Moisture Barrier Bags

Moisture barrier bags (MBBs) are used for dry packing of electronic components. They act as a barrier for moisture permeation from the outside to the inside environment of the long-term storage system. They are also provided with antistatic and static dissipative coatings that shields the components from the electrostatic discharge (ESD), thus, protecting the components from moisture and ESD related degradation mechanisms.

Manufacturer Provided Information

Dri-Shield 3700 series MBBs manufactured by SCS are used in this thesis. The SCS manufacturer claims that their MBBs provide superior protection for ESD sensitive and moisture sensitive electronic components [8]. The SCS manufacturer provides 1 year of warranty from the date of purchase and also claims that the shelf life

of these bags is 5 years from the date of purchase when stored in a climate-controlled environment with ventilation [9]. Though the shelf life of the MBBs is not the same as that of the use-life, degradation mechanisms that occur during its shelf-life can be extended to its use-life. For example, manufacturers claim that the aluminum foil layer of the MBB could oxidize if exposed to environmental factors such as ultraviolet sunlight, moisture, or heat during storage [8]. While these environmental factors can cause oxidation of the aluminum foil layer during shelf life, they can also cause the same degradation mechanisms during their use-life as well.

Construction of MBB

Dri-Shield 3700 series MBB is made of layers of polymers and aluminum foil along with a static dissipative coating. Figure 3 shows the construction of this MBB as provided by the manufacturer. From the construction provided by the manufacturer, it can be figured out that the outer layer is made of static dissipative polyester, and the inner layer is made of static dissipative polyethylene. Also, an aluminum foil is laminated in between these two polymeric layers. This construction is usually named as a metalized film with aluminum foil acting as a barrier layer to moisture, and polymers are laminated to aluminum foil for better heat sealing and improved crease resistance of the aluminum foil [10]. The aluminum foil also acts as a Faraday cage to shield the electronic components sealed within it from any electromagnetic interference from the outside. The static dissipative coating offers protection to the components from electrostatic discharges because of its conductive native by carrying away the developed static charges from a localized spot and redistributing it along the surface.

Table 3 lists the properties of the MBB and its corresponding values as provided by the manufacturer along with the standard that is used to test that corresponding property [11]. Cross-section analysis, Fourier Transform Infra-Red (FTIR) spectroscopic analysis, Energy-Dispersive X-Ray Spectroscopic (EDS) analysis and surface resistivity analysis performed on the MBB is discussed in Appendix B.

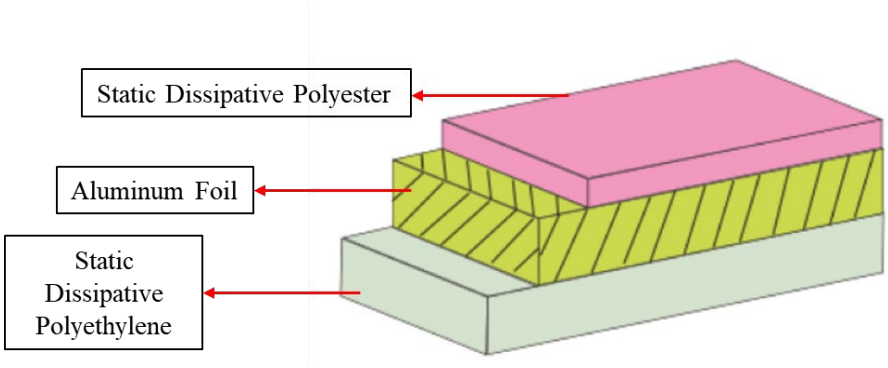

Figure 3 Construction of the SCS Dri-Shield 3700 series MBB as provided by the manufacturer

Table 3 Properties of the MBB as provided by the manufacturer [11]

Property	Value	Testing Standard
Thickness	106.7 ±10% µm	MIL-STD-3010 Method 1003
Moisture vapor transmission rate (MVTR)	≤ 4.7 mg/m^2/day (at 38 °C / 90% RH)	ASTM F1249 and MIL-STD-3010C (Method 3030)
Surface resistance (Both inner and outer layer)	1 x 10^4 to < 1 x 10^{11} Ohms	ANSI/ESD STM 11.11
Puncture resistance	111 N	MIL-STD 3010C Method 2065
Seal strength	66 N	ASTM D882
Tensile strength	68 MPa	ASTM D882

Moisture Permeation Property of MBB - Permeability

Moisture vapor transmission rate, abbreviated as MVTR, and permeability are the two properties associated with the moisture permeation mechanism of the MBB. MVTR is the time rate of water vapor flow normal to the surfaces, under steady-state conditions, per unit area [12]. The unit of MVTR is g/m^2/day, which represents the amount of the water vapor that permeates through the area of 1 m^2 in a day. The MVTR property of MBB varies with temperature, outside and inside relative humidity. The relationship between MVTR, temperature, and relative humidity is obtained by using the Fick's first law of diffusion [13]. The equation for Fick's first law is shown in equation ((1), where F represents the flux which is defined as the mass of water vapor permeated through unit cross-section area of the MBB per unit time. The flux term used in the Fick's law is commercially named as MVTR in the units of g/m^2/day. D is diffusion constant of the MBB in m^2/s. $\frac{\partial C}{\partial x}$ is concentration gradient, as shown in Figure 4, represents the difference between the concentration of water vapor at the inner surface of the MBB, C_{i1} $(\frac{g}{m^3})$, and the outer surface of the MBB, C_{o1} $(\frac{g}{m^3})$, divided by the thickness of the MBB, L (m). K in equation (2) represents the partition coefficient or equilibrium constant that establishes the equilibrium between the concentration of water vapor at the surface and the concentration of water vapor of the surrounding air to which the surface is exposed. K is defined as the ratio of concentration of water vapor at the inner surface of the MBB, C_{i1} $(\frac{g}{m^3})$, to the concentration of water vapor in the air inside the MBB, C_i $\left(\frac{g}{m^3}\right)$. Similarly, K can be defined for the outer surface of

the MBB. Substituting (2) in (1), and replacing flux, F as MVTR, permeability, P ($\frac{m^2}{s}$), , of MBB is obtained in the equation (3), which is defined as the product of diffusion constant of MBB and partition coefficient of MBB. Permeability can also be defined as the mass of water vapor permeated through unit cross sectional area of MBB per unit time per unit difference between the concentration of the water vapor in air between the inside and outside of MBB multiplied by the thickness of MBB. The equations (1) to (3)shows the difference in concentration of water vapor as the driving force for the moisture to permeate from the outside to the inside of MBB, which can also be replaced by relative humidity (RH) as MVTR is directly proportionally to ΔRH as it is proportional to ΔC as shown in equation (4). However, the units of permeability changes to $\frac{g\,.\,m}{m^2\,.\,day\,.\,\Delta RH}$ as the driving force changes from ΔC to ΔRH and equation (3) becomes equation (5), where RH_{out} represents the relative humidity outside the MBB and RH_{in} represents the relative humidity inside the MBB. Permeability depends on temperature as shown in the equation (6) [14] [15] [16], where a and b are coefficient of permeation constant ($\frac{g\,.\,m}{m^2\,.\,day\,.\,\Delta RH}$) and exponential factor (K) respectively. Substituting equation (6) in (5), we obtain the relationship between MVTR, temperature and relative humidity as shown in equation (7).

$$F = -D\frac{\partial C}{\partial x} = -D\frac{C_{i1} - C_{o1}}{L} \tag{1}$$

$$K = \frac{C_{i1}}{C_i} = \frac{C_{o1}}{C_o} \tag{2}$$

$$F = MVTR = -(D \times K)\frac{C_i - C_o}{L} = P \times \frac{C_o - C_i}{L} \tag{3}$$

$$MVTR\ \alpha\ \Delta C\ \alpha\ \Delta RH \tag{4}$$

$$MVTR = \frac{P}{L}(RH_{out} - RH_{in}) \tag{5}$$

$$P = a \times e^{-b/T} \tag{6}$$

$$MVTR = \frac{a \times e^{-b/T}}{L}(RH_{out} - RH_{in}) \tag{7}$$

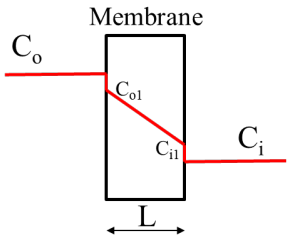

Figure 4 Concentration terms in the Fick's first law of diffusion equation

To obtain the permeability of MBB, the constants a and b in equation (7) need to be determined. If the MVTR values of the MBB at two temperature/RH conditions are known, then can be substituted in the equation (7) to obtain two equations and two unknowns which can be solved to obtain the values of constants - a and b. From the Table 3, it can be observed that the manufacturer of MBB provided the MVTR value at 38 °C / 90% RH as the outside condition and 38 °C / 0% RH as the inside condition. To obtain the values of MVTR at another condition, it is assumed that MVTR can be a linear function of difference in partial pressure of water vapor between the outside and inside of MBB, as shown in equation (8) [14] [4]. Here, p_{out} represents the partial pressure of water vapor in air outside the MBB and p_{in} represents the partial pressure of water vapor in air inside the MBB. If the inside condition is 0% RH, the partial pressure of water vapor in air inside the MBB is also zero. So, the MVTR is directly proportional to the partial pressure of water vapor in air outside the MBB. Substituting

the partial pressure inside the MBB to be zero, the MVTR values for the MBB are calculated for the two conditions - 60 °C / 85% RH and 40 °C / 93% RH at which the experiments are run for MBBs by linearly multiplying the outside partial pressure values of the corresponding condition. The calculated values of MVTR at different conditions are shown in Table 4.

$$MVTR\ \alpha\ (p_{out}\ -\ p_{in}) \tag{8}$$

Table 4 Calculated values of MVTR at different temperature / RH conditions

Outside temperature / RH condition	**Partial pressure of water vapor at the outside condition (atm), p_{out}**	**MVTR ($\frac{g}{m^2\ day}$)**
38 °C / 90% RH	0.0592	4.70E-3
40 °C / 93% RH	0.0678	5.38E-3
60 °C / 85% RH	0.1673	13.28E-3

The values of MVTR at 38 °C / 90% RH and 40 °C / 93% RH as outside temperature / RH conditions are substituted in the equation (7) to obtain two equations and two unknowns, which are solved to obtained the values of a and b that are reported in Table 5. The value of b is represented as $E_a/_R$, where E_a is activation energy in $\frac{J}{mol}$ and R is universal gas constant in $\frac{J}{mol\ K}$. Substituting the value of R, activation energy is found to be 41.41 $\frac{kJ}{mol}$ or 0.4 eV. The obtained activation energy is observed to lie within the ranges of moisture permeation mechanism. Also, the calculated constants a and b are substituted back in equation (7), to compare the MVTR values calculated from obtained a and b constants and the values from Table 4. The difference, as shown

in Table 6, is found to be 5×10^{-4}. Since these two MVTR values are comparable to two significant digits, the constant values a and b are validated and are substituted in the equation (6) at the required temperature to calculate the values of permeability at the corresponding temperature. Table 7 lists the calculated values of permeability property of MBB at 60 °C and 40 °C.

Table 5 Calculated values of constants – a and b in equation (6)

Parameters	Values
a ($\frac{g\,.\,m}{m^2\,.\,day\,.\,\Delta RH}$)	5.39
b (K); b = $E_a/_R$	4980.85

Table 6 Comparison of MVTR values calculated based on linear assumption and calculated by substituting the obtained the constants - a and b in equation (7)

	MVTR Value
Value calculated based on linear assumption as shown in Table 4	13.28E-3
Value calculated by substituting the obtained constants a and b in equation ((7)	12.78E-3
Difference	5E-4

Table 7 Calculated permeability values at temperatures - 60 °C and 40 °C

Temperature	Permeability, P ($\frac{g\,.\,m}{m^2\,.\,day\,.\,\Delta RH}$)
60 °C	17.21E-7
40 °C	6.62E-7

Electrostatic Discharge (ESD) Protection Property – Surface Resistivity

Properties such as surface resistivity and electro-static discharge shielding are used as a measure to indicate the MBB's protection from ESD damages to components

stored within them. Static dissipative materials are evenly dispersed or coated on the surface of the polymeric layers of MBB to improve the conductivity. As a result, the static charges that could get developed on the surface are carried away from a localized spot and are dissipated, thus protecting the components from any ESD damage. The conductivity of the polymeric layers is represented in terms of surface resistivity. The surface resistivity of the MBB is reported to be between 10^5 and 10^{12} ohms/sq by the manufacturer, which lies in the static dissipative region, according to ANSI/ESD S541 [17]. Any change in the surface resistivity from the static dissipative region to the insulative region ($\geq 10^{12}$ Ohms/Sq) can increase the risk of component damage due to ESD.

Carriers

Carriers are packaging media that are used to protect the components from physical damage and electrostatic discharge damage during transportation and storage. In addition to the function of protecting the components from physical and environmental damage, they are used as an aid in the manufacturing or assembly processes after storage. For example, carriers containing the integrated circuits such as microprocessors are fed along the rails of the pick and place machines that automatically pick those microprocessors from the carriers and place them in a specific orientation at a specific location on the circuit board for reflow soldering.

Tape and reel carriers are considered in this thesis. Tape and reel carriers are usually of two types and consist of three sub-elements – carrier tape, cover tape and reel as shown in Figure 5. In this thesis, experiments were conducted on embossed pocket type

tape and reel with a focus on carrier tape and cover tape sub-elements. Tray carriers are molded in rectangular shapes that nest the electronic components within a matrix of pockets that are uniformly spaced, as shown in Figure 6. Information related to tray carriers is provided in Appendix A.

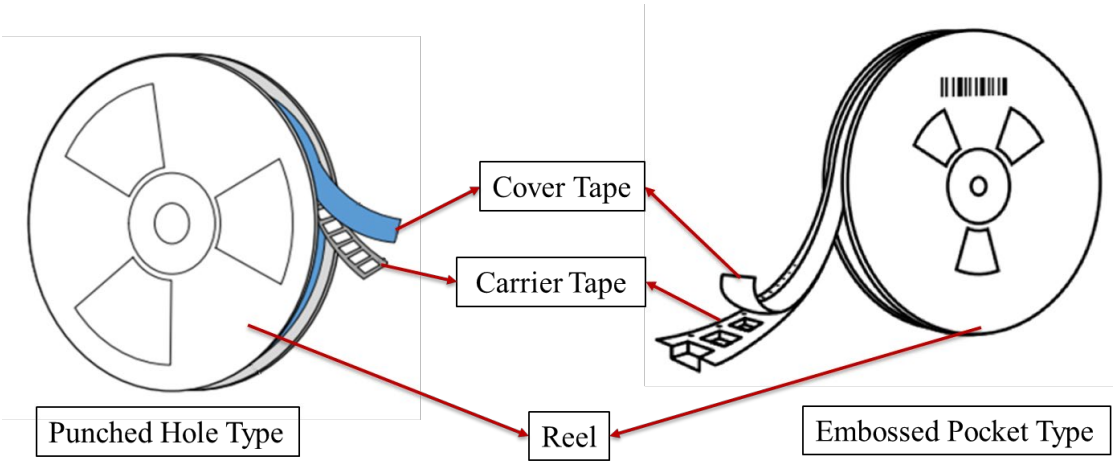

Figure 5 Two types of tape and reel along with its sub-elements

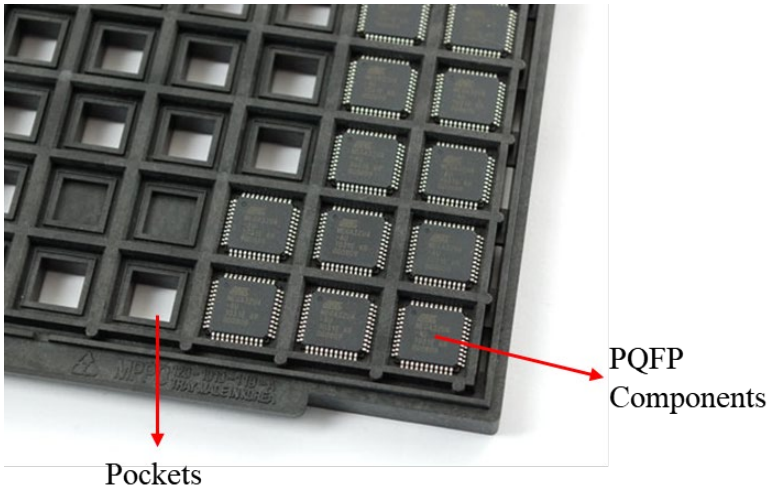

Figure 6 Tray carriers with pockets and loaded with Plastic Quad Flat Packages (PQFP) components

Manufacturer Provided Information

Table 8 lists three carriers used in this thesis along with their manufacturer name, series, and shelf-life information provided by the manufacturer. The carrier tapes are addressed based on the manufacturer part number of the component contained within it throughout this thesis.

Table 8 Manufacturer information of the tape and reel carriers used in this thesis

Manufacturer part number of the component contained within the carrier	**Carrier tape manufacturer and series**	**Cover tape manufacturer and series**	**Shelf-life information provided by the manufacturer**	
			Carrier Tape	**Cover Tape**
ST10F276	Advantek PS+C Trilaminate	Advantek HUE	5 years from the date of manufacture when stored at 21 ºC ± 17 °C [18]	24 months from the date of manufacture when stored at 5 °C – 35 °C and 15% RH – 85%R H [19]
XC2288H	Advantek PS+C Trilaminate	Advantek HUB	5 years from the date of manufacture when stored at 21 °C ± 17 °C [18]	24 months from the date of manufacture when stored at 20 °C – 30 °C and 30% RH – 80% RH [20]
C167CR	Cpak-PS-BC1051L	Unknown	5 years from the date of manufacture when stored at ≤ 45 °C [21]	Unknown

Material Composition Information

The material composition information of the Advantek PS+C and Cpak-PS-BC1051L carrier tapes as provided by the manufacturer is shown in Table 9 and Table 10, respectively. The material composition information for the cover tapes is not available from the manufacturer.

Table 9 Material composition information of Advantek PS+C carrier tape [22]

Chemical Name	Ingredients (CAS#)	% (Weight)
Acrylonitrile-butadiene-styrene (ABS)	9003-56-9	<65
Polystyrene (PS)	9003-53-6	<20
Carbon Black	1333-86-4	<10
Additives (trade secret)		<5

Table 10 Material composition information of Cpak-PS-BC1051L carrier tape [23]

Chemical Name	Ingredients (CAS#)	% (Weight)
Styrene copolymer	9003-53-6	90 - 95
Carbon Black	1333-86-4	5 - 10

Electrostatic Discharge Protection Property of Carriers – Surface Resistivity

Carrier's protection to the components from ESD damage is defined in terms of surface resistivity property. For the "carrier tape" of the tape and reel carriers used in this thesis, carbon black is dispersed in the polymeric matrix of the carrier tape. Carbon

black, being conductive in nature, increases the conductivity of the polymeric matrix. As a result, the static charges that could get developed on the surface are carried away from a localized spot and are dissipated.

For the cover tape of the tape and reel carriers used in this thesis, both the top and bottom layer of the cover tape is reported to be coated with an antistatic layer by the manufacturer. This layer prevents the development of any static charges protecting the components from ESD damage while peeling the cover tape from the carrier tape. However, the surface resistivity of carrier tape of the tape and reel carrier is considered to be critical compared to the cover tape as the components are in direct contact with the carrier tape. Should any electrostatic discharge occur, carrier tapes should be able to dissipate the charges to protect the components, which are in direct contact with it, from any damage. The surface resistivity values of both the carrier tapes and cover tapes used in this thesis, as provided by the manufacturer, are reported in Table 11. According to the manufacturer, the surface resistivity values were obtained by following the standard ASTM D 257.

Table 11 Surface resistivity values of the carrier tapes and cover tapes of the tape and reel carrier used in this thesis

Manufacturer part number of the component contained within the carrier	**Carrier tape manufacturer and series**	**Cover tape manufacturer and series**	**Surface Resistivity (Ohms/Sq)**	
			Carrier Tape	**Cover Tape**
ST10F276	Advantek PS+C Trilaminate	Advantek HUE	$\geq 10^5$ to $<10^{12}$ [18] [21]	$\geq 10^5$ to $<10^{10}$
XC2288H	Advantek PS+C Trilaminate	Advantek HUB		$\geq 10^5$ to $<10^{12}$
C167CR	Cpak-PS-BC1051L	Unknown		Unknown

Mechanical Properties of the carriers

This section provides the mechanical properties reported by the manufacturer for the tape and carrier used in this thesis. The mechanical properties that are included here are the tensile strength of the carrier and cover tape and peel strength of the cover tape of tape and reel carriers used in this thesis.

Tensile Strength

Along with the ESD protection to the components, carriers provide protection to any physical damage to the components that could occur during physical handling and transportation of the components. They are also used as an aid to the manufacturing/assembly process of the stored components after their long-term storage. The carriers get loaded onto the guided rails of the pick and place machines, where they get pulled by sprocket wheels that get engaged with the sprocket holes

provided on the edges of the carrier tapes of tape and reel carrier. Tensile strength is an important property for this specific operation of carrier tape of tape and reel carrier after storage. Any change to the strength can cause cracks in between the sprocket holes of the carrier tape, making misalignment or disengagement with the sprocket wheels, causing feeding error and trampoline (jumping off of the components from the carrier tape) of the components. This affects the manufacturability of the components after long-term storage.

While the carrier tapes are getting pulled by the sprocket wheels, the cover tapes are peeled back from the carrier tape by pulling it in the opposite direction to the moving direction of the carrier tape. Any change in the tensile strength can cause the tearing of the cover tape. As a result, the cover tape does not get peeled from the carrier tape and is still adhered to the carrier tape. When this reaches the pick and place spot, it can result in manufacturability issues. The tensile strength of both the carrier tapes and the cover tapes used in this thesis, as reported by the manufacturer, is shown in Table 12. According to the manufacturer, the tensile strength values were obtained by following the standard ASTM D882.

Table 12 Tensile strength values of the carrier tape and cover tape of the tape and reel carriers used in this thesis

Manufacturer part number of the component contained within the carrier	Carrier tape manufacturer and series	Cover tape manufacturer and series	Tensile Strength (MPa)	
			Carrier Tape	Cover Tape
ST10F276	Advantek PS+C Trilaminate	Advantek HUE	45.5 [18]	69 [19]
XC2288H	Advantek PS+C Trilaminate	Advantek HUB		≥ 48 [20]
C167CR	Cpak-PS-BC1051L	Unknown	26 - 49 [21]	Unknown

Peel Strength of Cover Tapes of Tape and Reel carrier

Peel strength represents the ability of the cover tape to get peeled from the initially adhered carrier tape for further manufacturing operations. Peel strength is defined as the average load per unit width of bond line required to separate progressively one member from the other over the adhered surfaces [24]. Any change in the peel strength cause inconsistent peeling resulting in the trampoline of the components. Table 13 lists the peel strength of the cover tapes used in this thesis, as reported by the manufacturer. The values were obtained by following the standard EIA 481.

Table 13 Peel strength of the cover tapes used in this thesis

Manufacturer part number of the component contained within the carrier	Cover tape manufacturer and series	Peel strength of the cover tape (grams)
ST10F276	Advantek HUE	50 ± 25 [19]
XC2288H	Advantek HUB	50 ± 20 [20]
C167CR	Unknown	Unknown

Desiccants

Desiccant is an adsorbent material that adsorbs water vapor onto its surface from the environment to which the desiccant is expose. Typically, desiccant packets are packed inside the sealed MBBs to adsorb any moisture inside the bag, thus protecting the components from humidity related degradation mechanisms. The different types of materials used as desiccants are silica gel, clay, zeolite, activated alumina, molecular sieve, calcium oxide, anhydrous calcium chloride, and calcium sulfate. Based on the materials, desiccants adsorb water under different distinctive adsorption isotherms that are classified from type-I to type-VI, according to the International Union of Pure and Applied Chemistry (IUPAC) [25]. Using these adsorption isotherms, desiccant adsorption capacity is calculated based on the units of desiccant. According to MIL-D-3464E, a unit of desiccant is defined as that quantity of desiccant, as received, which will adsorb 3g and 6g of water vapor at 25 °C, 20% RH and 25 °C, 40% RH respectively [26]. The adsorption capacity of the desiccant is a function of temperature and relative humidity, which differs for different materials. For example, at room temperature of about 25 °C and relative humidity less than 35%, silica gel and clay desiccant have the similar moisture adsorption capacity whereas, at the same room temperature and relative humidity greater than 35%, silica gel has relatively higher moisture adsorption capacity than clay desiccant [27]. Therefore, the selection of desiccant material and adsorption capacity is based on the storage environmental conditions and adsorption isotherm of that material at those storage conditions.

Manufacturer Provided Information

S-5165 Tyvek bag desiccants distributed by Uline is used in this thesis. The material of the desiccant is bentonite clay. 33g of this desiccant is equal to 33 grams of clay. The shelf life of the desiccant is 1.5 to 2 years if the pail is opened and 5 years for an unopened pail. The condition at which the desiccant is recommended to be stored is <30 °C and <80% RH [28].

Adsorption Capacity Property

Adsorption capacity is defined as the mass of water vapor adsorbed by unit gram of desiccant in equilibrium with air at that temperature / RH condition [26]. Manufacturer of this desiccant reported that the desiccant adsorbs 20% of its weight when exposed to 25 °C / 70% RH. This indicates that the desiccant's adsorption capacity at 25 °C / 70% RH is 0.2 g/g. Experiments were run on desiccants to determine its adsorption capacity at 60 °C / 60% RH and 40 °C / 60% RH. Three desiccants were taken at each test conditions and their mass were weighed before placing them at the conditions. The increase in mass of the desiccant was recorded at certain time intervals till it reached its saturation. The observed increase in mass of desiccant divided by the initial mass of desiccant is plotted against time as shown in the Figure 7. Adsorption capacity, in this graph, represents the stabilized values of the curves. Table 14 lists the adsorption capacity values of the desiccant at the run conditions which are calculated by taking average of the stabilized values of the three desiccants at each condition. It can be interpreted that the difference between the adsorption capacity of the desiccant at 60 °C and 40 °C is comparable to one significant digit. Also, the rate of adsorption

at 60 °C is higher than at 40 °C which can be interpreted that increasing the temperature can make the desiccant to reach its saturation faster.

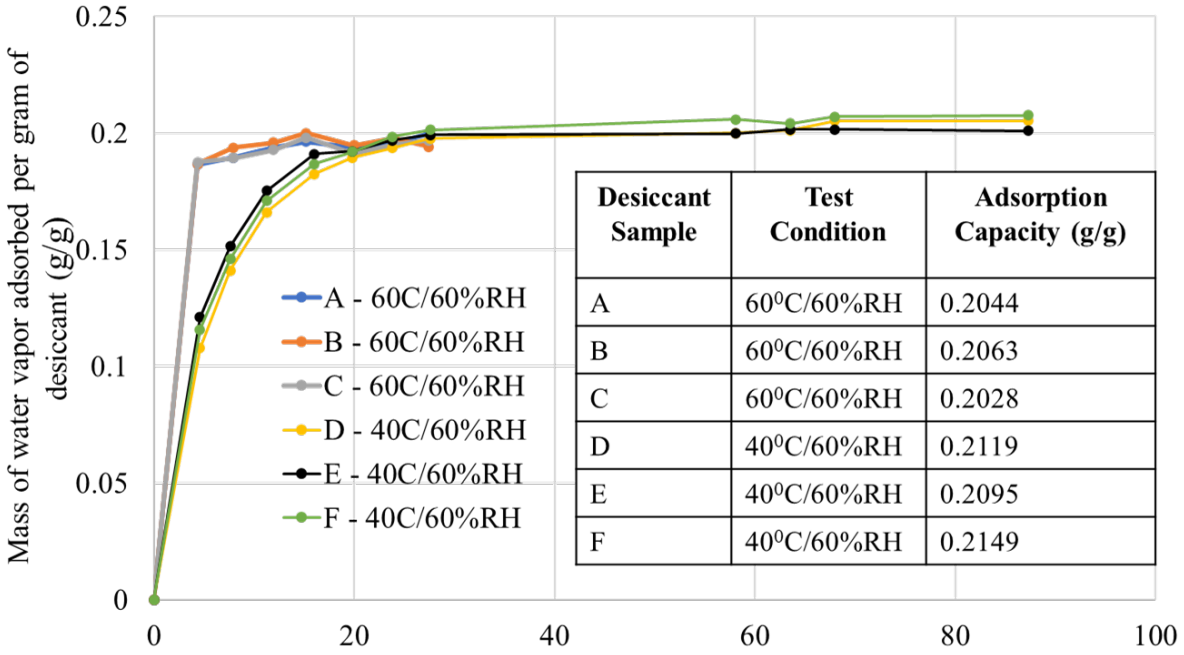

Desiccant Sample	Test Condition	Adsorption Capacity (g/g)
A	60^{0}C/60%RH	0.2044
B	60^{0}C/60%RH	0.2063
C	60^{0}C/60%RH	0.2028
D	40^{0}C/60%RH	0.2119
E	40^{0}C/60%RH	0.2095
F	40^{0}C/60%RH	0.2149

Figure 7 Graph showing the mass of water vapor adsorbed by desiccant vs. time at 60 °C / 60% RH and 40 °C / 60% RH

Table 14 Adsorption capacity values of the desiccant at 60 °C / 60% RH and 40 °C / 60% RH

Test Condition	Adsorption Capacity ($\frac{g}{g}$)
60 ^{0}C / 60% RH (Average of A, B, and C Samples)	0.2045
40 ^{0}C / 60% RH (Average of D, E, and F Samples)	0.2121

Adsorption Isotherm

Adsorption isotherm establishes the relationship between the adsorption capacity of the desiccant (g_{H_2O} / g_{clay}) and relative humidity (RH) to which the desiccant is exposed at a constant temperature. From the literature [29], it is found that Freundlich

adsorption isotherm can be used for clay desiccant. The formula for the isotherm is shown in equation (9). g_{H_2O} represents mass of water vapor adsorbed by desiccant in grams. $g_{desiccant}$ represents the mass of clay desiccant in grams. $\frac{g_{H_2O}}{g_{desiccant}}$ is the adsorption capacity of the desiccant in g/g. RH is the relative humidity to which the desiccant is exposed. k represents the Freundlich constant representing adsorption capacity. n represents Freundlich constant representing adsorption strength. The constants, k and n, of this equation should be determined for obtaining the adsorption isotherm equation of the clay desiccant.

$$\frac{g_{H_2O}}{g_{desiccant}} = k \times (RH)^{1/n} \tag{9}$$

The literature [27] reported the adsorption isotherm graph for the clay desiccant at 25 °C and 40 °C which has been reproduced in Figure 8. The values obtained from this graph are compared against the known values to decide if the graph represents the clay desiccant or not. The manufacturer reported that the bentonite clay desiccant adsorbs 20% of its weight at 25 °C / 70% RH, which means the adsorption capacity is 0.2 g/g at 25 °C / 70% RH, whereas the Figure 8 shows 0.26 g/g. Similarly, comparing the desiccant's adsorption capacity at 40 °C / 60% RH, which is shown in Table 14, the Figure 8 shows that the desiccant adsorbs 0.25 g/g at 40 °C / 60% RH. Although there are some variations, compared to other graphs obtained from the literature, the Figure 8 showed comparable results with type of desiccant used in the thesis. Equations (10) and (11) represent the Freundlich adsorption isotherm equations with the numerical values substituted for constants which are obtained by curve fitting the values obtained

from this Figure 8 at 25 °C and 40 °C from 0% RH to 20% RH. The R^2 values obtained for the fit equation at 25 °C and 40 °C are 0.985 and 0.982 respectively.

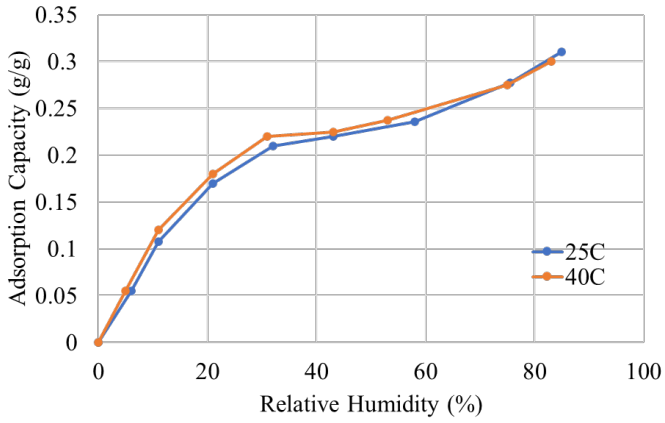

Figure 8 Reproduced adsorption isotherm graph of bentonite clay at 25 °C and 40 °C from literature [27]

$$For\ 25\ °C, \quad \frac{g_{H_2O}}{g_{desiccant}} = 0.7193 \times (RH)^{1/1.113} \tag{10}$$

$$For\ 40\ °C, \quad \frac{g_{H_2O}}{g_{desiccant}} = 0.6913 \times (RH)^{1/1.201} \tag{11}$$

Chapter 4: Degradation Mechanisms of Replaceable Elements

This section describes the degradation mechanisms that can be critical for the replaceable elements of the long-term storage system. Degradation mechanisms of tape and reel carriers and moisture barrier bags, along with the failure mode and effects, are discussed and tabulated in this section. Degradation mechanisms of tray carriers and desiccants are not discussed in this thesis and will be investigated as a part of future study.

Moisture Barrier Bags

This section describes the degradation mechanisms of the moisture barrier bags that can occur during long-term storage along with the failure modes and effects that are observed after storage. The degradation mechanisms such as degradation of the adhered layer of the seal and degradation of the static dissipative layer are considered to be critical for MBBs based on the effects that are induced after long-term storage.

Degradation of Adhered Layer of Heat Seal

To protect the components from moisture-related degradation mechanisms, the MBBs are vacuum-sealed. The heat seal is formed as a result of fusion of the inner polyethylene layer at a specific temperature, pressure, and time. These thermally bonded seals were found to permit the transfer of water vapor through the polymeric packages, and it has been found that seals contribute to 24% of the total water vapor permeance through the polymeric packages. This is possible due to the permeation of

water vapor through micro holes, weakened material, or some type of defect present in the seal that is defined by the seal strength [30]. Thus, seal strength is often defined as a measure of the total integrity of the package [31].

The internal bonds of the adhered layer degrade over time, and as a result, the thermophysical properties of the seal change that results in change of seal strength [32]. This decrease in seal strength can cause the moisture vapor transmission rate (MVTR) to increase unexpectedly that, if unnoticed, may result in humidity-related degradation to the components and packaging media sealed within it. The failure modes and effects for the degradation of the adhered seal are tabulated in the first row of Table 15. The experimental analysis for this particular failure mechanism is not performed by measuring the seal strength of MBB at specific intervals after accelerated aging. On the other hand, the use-life of MBB is measured indirectly by performing aging tests under accelerated test conditions.

Degradation of Static Dissipative Layer

MBBs used in this thesis are coated with a static dissipative layer on the inner and outer layers to provide protection to the components from the electrostatic discharge damage. The static dissipative property of the polymeric carrier tape is obtained by adding organic additives, which decreases the surface resistivity from insulative region ($>10^{12}$ Ohms/Sq) to static dissipative region ($>10^{5}$ to $<=10^{12}$ Ohms/Sq). These additives are organic compounds that degrade over time, increasing the surface resistivity of the polymeric layers of MBBs [17] [33]. As a result, the MBBs may lose their protection to contained components from electro-static discharge damages. Also, in some cases,

the products that are outgassed as a result of degradation of the antistatic layer can become a source of contamination on the contained electronic components during long-term storage. For example, an antistatic polyethylene bag contained n-octanoic acid that got vaporized and deposited on the leads of the components to form lead di (n-octanoate) [34]. The failure modes and effects for the degradation of the static dissipative layer of MBB are tabulated in Table 15. The experimental analysis for the degradation of the static dissipative layer is provided in Chapter 5: Experiments and Results.

Table 15 Long-term storage degradation mechanisms for moisture barrier bags

Degradation mode	**Degradation mechanism**	**Effects**
Change in the seal strength of the MBB	Degradation of the adhered layer of the heat seal	Unexpected increase in the moisture vapor transmission rate (MVTR) of the MBB
Change in the surface resistivity of the MBB	Vaporization of the static dissipative layer on the inner and the outer polymeric layers of the MBB	Risk of electronic components getting damaged by ESD The components may get contaminated with the outgassed elements

Carrier Tape of Tape and Reel

The tape and reel carrier consist of elements such as carrier tape and cover tape. This section describes the degradation mechanisms of the carrier tape of tape and reel that can occur during long-term storage, along with the failure modes and effects that are observed after storage. For carrier tape of tape and reel, degradation mechanisms

such as polymeric shrinkage and degradation of the static dissipative layer are considered critical based on the effects that are induced after long-term storage.

Polymeric Shrinkage

Polymers can continue to shrink after processing, causing a slow contraction of their polymeric chains. As a result, the chains get closer decreasing the free volume within them, resulting in continued shrinkage over time [35]. When the carrier tapes made of polymers are stored for long-term, they can also undergo continued shrinkage causing a change in the dimensions. Also, shrinkage of polymers causes the polymeric chains to come closer, making the polymer stiffer and stronger. As a result, they become brittle and lose their ductile nature.

Some manufacturers of carrier tapes have investigated the nature of this problem that can occur during long-term storage. 3M, a company that manufactures carrier tapes, has released a qualification report on dimensional changes associated with the polymeric shrinkage [36]. As a part of qualification testing, their polycarbonate carrier tapes were aged at 52 °C and 85 °C for 24 hours to determine the extent of dimensional change of their carrier tapes. According to EIA 481-E, the dimensions of the ten-pitch distance of the sprocket holes of the carrier tapes should be 40 ± 0.2 mm (Tolerance is $\pm$ 0.5%) [37]. The results of their aging tests showed that the dimensions of the carrier tapes showed a change in tolerance of less than 0.1% at both 52^0C and 85^0C, which were still within the range set by EIA 481-E. However, the carrier tapes used in this thesis are made of different material composition other than polycarbonate materials.

So, accelerated aging experiments are decided to be performed to determine if there is any noticeable change in the dimensions for the carrier tape that is used in this thesis.

Change in dimensions, especially the diameter and pitch of the sprocket holes of the carrier tape, can cause misalignment or disengagement of the carrier tape with the sprocket holes. This can lead to rough feeding, mis-picks by the pick and place machine, trampoline of the components, and physical damage to the leads of the components, affecting the manufacturability of the components after long-term storage.

Change in the ductility due to the continued shrinkage of polymers over time can cause the impact strength to decrease with the increase in the strength showing a ductile to brittle transition. As a result, the components contained within the carrier tapes may be subjected to impact damage after long-term storage when the carrier tapes are dropped accidentally while handling. Also, the ductile to brittle transition may cause cracks at the stress concentration sites of the sprocket holes while the carrier tapes are getting pulled, leading to feeding errors. The failure modes and effects for the polymeric shrinkage degradation mechanism of the carrier tape are tabulated in Table 12.

Degradation of Static Dissipative Layer

The static dissipative property of the polymeric carrier tape is obtained by adding additives, which decreases the surface resistivity from the insulative region ($>10^{12}$ Ohms/Sq) to the static dissipative region ($>10^{5}$ to $<=10^{12}$ Ohms/Sq). These additives are organic compounds that degrade over time, increasing the surface resistivity of the

polymer [17] [33]. As a result, the carrier tapes may lose their protection to contained components from electro-static discharge damages. Also, in some cases, the products that are outgassed as a result of degradation of the antistatic layer can become a source of contamination on the contained electronic components during long-term storage. The failure modes and effects for the degradation of the static dissipative layer are tabulated in Table 12. The experimental analysis for degradation of the static dissipative layer of MBB is provided in Chapter 4: Degradation Mechanisms of Replaceable Elements.

Cover Tape of Tape and Reel – Degradation of Adhesive Layer

The cover tape is adhered to the top of the carrier tape to make the components contained within the pockets of the carrier tape. The cover tapes used in this thesis contain a heat-activated adhesive layer that helps in adhering to the carrier tape upon applying heat and pressure. The adhesive layer can degrade overtime during the long-term storage causing a change in the peel strength. The factors that can cause a change in the peel strength over time are rearrangement of molecules due to the relaxation of residual stress, migration of chemical species between the polymer and the adhesive layer over time, and bulk movement of the polymeric chains in and around the bonded interface over time [24].

3M has performed qualification tests on observing the change in the peel strength of their heat-activated cover tapes. They aged their cover tapes at room temperature, 40 °C, and 60 °C for 60 days to determine the extent of change in the peel strength. The results that were published in their qualification reports are shown in Figure 9 [38]. It

is observed from the graphs that the peel strength of the cover tape increased initially and then stabilized at the end of 60 days for all three temperatures. Although the results did not show a significant change in the peel strength, this qualification report was specifically performed for their cover tapes. So accelerated aging experiments are decided to be performed for the cover tapes that are used in this thesis to determine the criticality of this degradation mechanism. The details of the experiment are provided in the section.

When the cover tape is peeled from the carrier tape for the components to get picked up by the pick and place machines, the consistent peel strength is required. EIA 481-E standard defines the peel strength of the cover tape to be between 10.2g and 132.56g for 44mm width of carrier tape [37]. Any change in the peel strength beyond the limits specified by the standard affects the manufacturability of the components after long-term storage. The components pop out from the pockets of the carrier tape when there is a change in the peel strength and may result in components not getting picked up by the pick and place machines leading to feeding error. The failure modes and effects for the degradation of the adhesive layer are tabulated in Table 12.

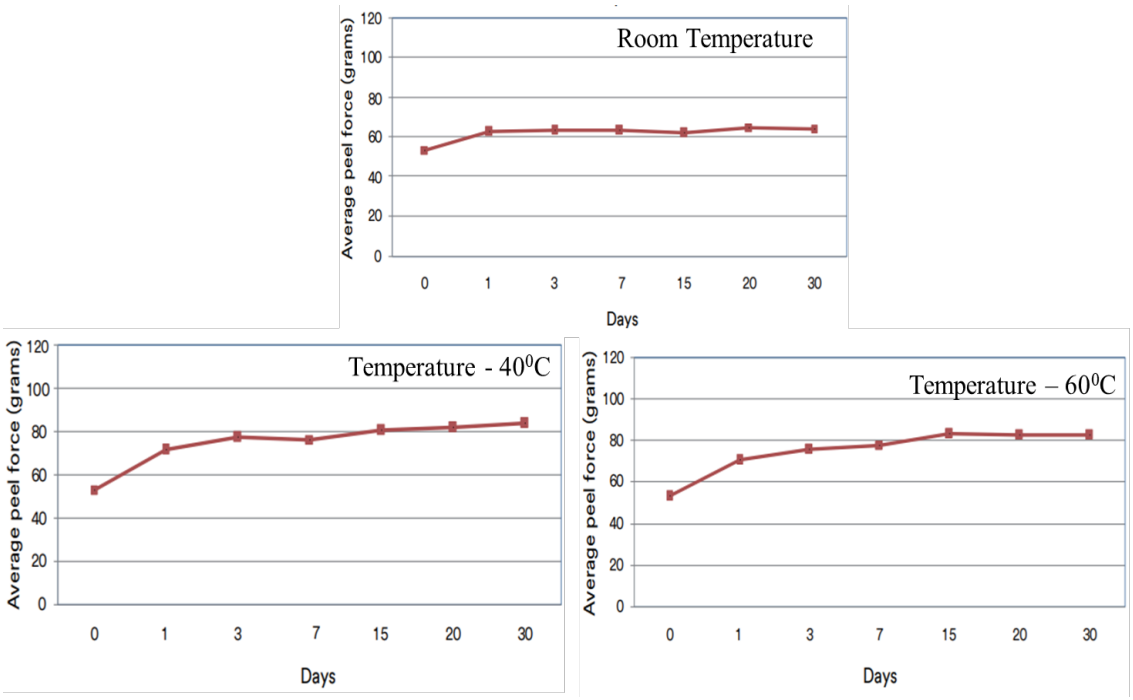

Figure 9 Change in average peel strength of 3M heat-activated cover tapes at room temperature, 40^0C and 60^0C for 60 days

Table 16 Long-term storage degradation mechanisms for tape and reel carrier

Elements of tape and reel carrier	Degradation mode	Degradation mechanism	Effects
Carrier tape	Change in dimensions of the carrier tape	Continued dimensional shrinkage of the polymers	Rough feeding, Mis-picks by the pick and place machine, trampoline of components, Physical damage to the leads of the contained components
	Change in the tensile strength and impact strength of the carrier tape	Polymeric shrinkage causing continued transformation from the ductile to brittle nature of the polymers	Protection of components from impact damages may be compromised during handling after storage Decrease in the ductility can cause cracks in the gaps between the sprocket holes leading to feeding error
	Change in the surface resistivity of the carrier tape	Degradation of the static dissipative layer of the carrier tapes	Risk of electronic components getting damaged by ESD The components may get contaminated with the outgassed elements
Cover tape	Change in the peel strength of the cover tape	Degradation of the adhesive layer of the cover tape	Uneven peeling resulting in the trampoline of components

Chapter 5: Experiments and Results

This section describes the details of the experiments that were conducted on MBBs, desiccants and carriers. It includes the testing conditions, run time, number of samples, and measurements that were recorded for each of the conducted experiments. The results obtained from these experiments are also discussed in this section.

Experiments for Determining RH Inside MBB vs. Time

According to JEDEC J-STD-033D, when the relative humidity inside the MBB containing MSL 2A-5A electronic parts reaches 10% RH, the components should be baked [39]. However, the RH inside MBB sealed with desiccant increases from 0% RH to 10% RH as the desiccant is reached its adsorption capacity. As a result, it is critical to investigate how the RH inside MBB changes over time in order to make informed decisions about replacing MBBs and desiccants during long-term storage. In this experiment, MBBs are vacuum-sealed with wireless temperature/relative humidity sensor to monitor the change in RH inside MBB when placed at conditions – 60 °C / 85% RH and 40 °C / 93% RH. This section details the equipment used in this experiment, design of experiments and preliminary testing performed to determine the accelerated test conditions, experiment procedure, and the obtained results.

Equipment Used in the Experiment - Vacuum Sealing Machine

In this experiment, MBBs are vacuum sealed, necessitating the use of a vacuum sealing machine prior to performing experiments. The manufacturer's conditions for

sealing the MBB, as mentioned in [11], that includes sealing at a temperature of 204 °C, a sealing pressure of 206 - 482 kPa, and a sealing time of 0.6 - 4.5 seconds. For economic reasons, a vacuum sealing machine that only controls the sealing time parameter is used to vacuum seal the MBB. The seal strength of the MBB sealed by this vacuum sealing machine is compared to the seal strength of the MBB sealed by the manufacturer.

ASTM F88 standard is used for measuring the seal strength of the MBB samples [31]. As per the standard, the sealed MBB samples were cut into rectangular strips, as shown in Figure 10. The rectangular strip contains the seal portion and the portion for clamping the strip onto the tensile testing machine's grips. The seal lies in the middle of the two strips that are sealed together. The rectangular strip is then clamped onto the tensile testing machine's grips so that the distance between the grips is maintained between 10 and 25 mm, which is represented in Figure 11. The grips are pulled apart at a displacement ramp rate of 200 -300 mm/min. The result is recorded as a load vs. displacement graph from which the seal strength is measured.

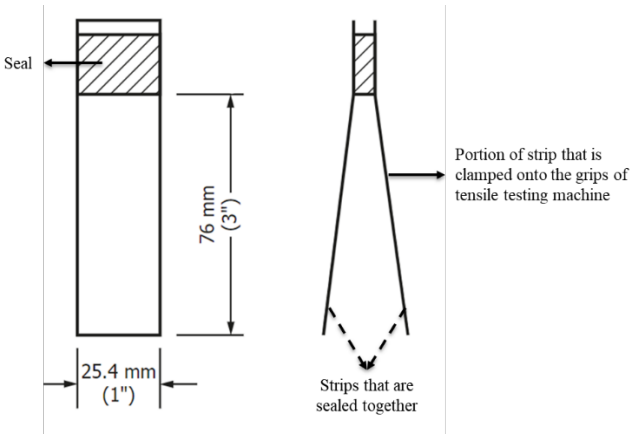

Figure 10 Recommended dimensions by ASTM F88 standard for the samples to measure the seal strength [31]

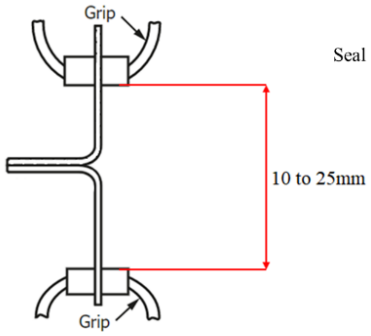

Figure 11 Representation of the sealed cut strip that is clamped onto the grips of the tensile testing machine [31]

Two samples – sample I and sample II were prepared according to the dimensions recommended by the ASTM F88 standard, which is shown in Figure 12. The samples were sealed using the vacuum sealing machine, and the sealing time was 8 seconds. Sample II was made by cutting the MBB with the seal portion that was sealed by the manufacturer. The seal marked in Figure 13 indicates the portion that was sealed by the MBB manufacturer. The tensile testing machine used in this experiment and its calibration details is reported in Table 17. The experiment was performed on November

9, 2020, and the testing conditions were reported to be 19.1 °C / 20.3% RH. Figure 14 shows the picture of the MBB samples clamped onto the grips of the tensile testing machine. The output for sample I and II is recorded and compared in the form of load vs. displacement graph, which is shown in Figure 15. The displacement in the x-axis of this graph represents the distance moved by the grips as they were pulled apart at a displacement ramp rate of 300 mm/min. The load in the y-axis of this graph represents the force resisted by the seal of the samples as they were pulled apart. The maximum seal strength was observed to be 158 N (35.52 lbs) for sample I and 183 N (41.14 lbs) for sample II. From the results, it can be observed that the difference between the maximum seal strength values of the manufacturer sealed MBB samples and the samples that were sealed using the vacuum sealing machine is 25 N (5.62 lbs). This difference is negligible when compared to magnitude of the absolute values of seal strength. The results of this comparison experiment justified the decision to seal the MBBs using this vacuum sealing machine before performing the accelerated experiments.

Figure 12 Sample I and sample II prepared for measuring the seal strength using the tensile testing machine

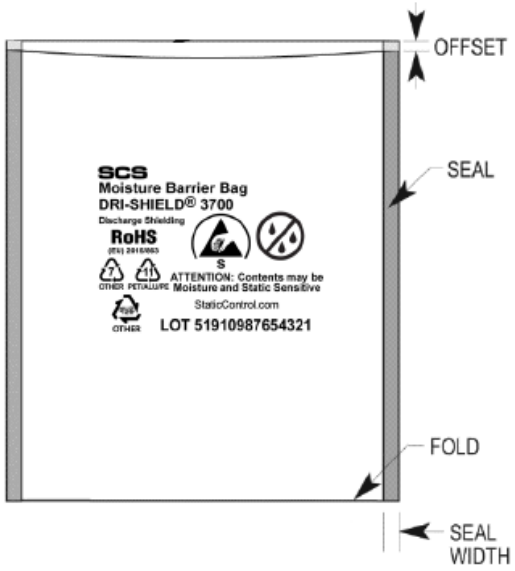

Figure 13 Picture showing the MBB with the seal made by its manufacturer

Table 17 Details of tensile testing machine used for measuring the seal strength of MBB samples

Asset Number	Manufacturer	Description	M/N	S/N	Last Calibration	Calibration Due
WC051746	Instron	Tensile Tester	5982	B10355	09/16/2020	09/17/2021
WC051748	Instron	Tensile Tester Load Cell 100kN	2580-301	300229	09/16/2020	09/17/2021

Figure 14 Picture showing the MBB samples that are being clamped onto the grips of the tensile testing machine

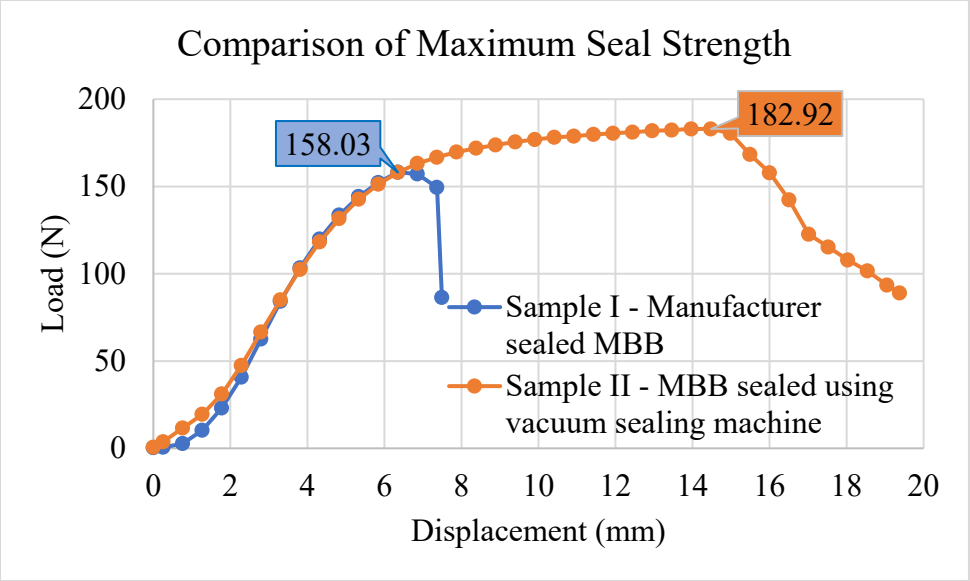

Figure 15 Graph showing the load vs. displacement results obtained for sample I and sample II

Equipment Used in the Experiment - Wireless Temperature/RH Sensor

To make an observation of the change in relative humidity inside the MBB after sealing, wireless temperature/relative humidity sensors and data loggers are used. This sensor is sealed inside the MBB and transmits the data wirelessly over WiFi. The data gets stored in the cloud and can be monitored. Table 18 lists the details of the wireless TH sensor used in this experiment.

Table 18 Technical specifications of the wireless TH sensor used in this experiment

Manufacturer	Elitech
Model number	RCW – 360
Temperature measurement range	-20 °C to 70 °C
Temperature accuracy	±0.5 °C
Humidity measurement range	0% to 99% RH
Humidity accuracy	±5% RH
Humidity resolution	1% RH
Battery	Rechargeable lithium battery
Battery life before recharging	Approximately 3 months at 1-hour recording interval

Determination of Accelerated Test Conditions

This section details the steps involved in choosing the test conditions for performing the accelerated experiments on MBBs. The test conditions are chosen based on the long-term storage system elements such as MBBs and desiccants and equipment such as wireless TH sensors used in this experiment. The chosen test conditions are then used as input for the design of experiment matrix to choose the combinations of appropriate test conditions for performing the experiments.

In this accelerated experiment, desiccants are vacuum sealed inside the MBB and are put together inside the temperature/RH chamber. The accelerated test conditions should be chosen so that the desiccant's functionality is not compromised. Literature shows that the clay desiccant loses its moisture adsorbing effectiveness above 50 °C [27]. The manufacturer of the desiccant used in this experiment has also reported that its desiccant works best at temperatures below 48.9 °C [40]. However, choosing all the accelerated test conditions below 50 °C may not accelerate the moisture permeation mechanism into MBBs, making it more time-consuming to yield any conclusive

results. Therefore, desiccants were tested for their moisture adsorbing capability above 50 °C, and the following paragraphs discuss the details of the experiment performed on desiccants.

Experiments on Desiccants to Determine the Accelerated Test Condition Above 50 °C

This section describes the details of the experiment performed on desiccants to select accelerated test conditions above 50 °C. Figure 16 shows the test plan that was followed to determine the moisture adsorbing performance of the desiccants above 50 °C.

In this experiment for desiccants, two temperatures were chosen. One of them was chosen to be above 50 °C, and the other one was chosen to be below 50 °C. The relative humidity was kept constant for both temperatures. The chosen test conditions were 40 °C / 60% RH and 60 °C / 60% RH. For each test condition, three desiccant samples were chosen to observe the variability in the measurements. Each desiccant sample is weighed using a weighing scale before placing them inside the temperature/relative humidity (TH) chamber at the chosen test conditions. Figure 17 shows the representation of how the desiccant samples are placed inside the TH chamber. The calibration of the weighing scale used for measuring the weight of the desiccant along with calibration of TH chamber used for this experiment is included in Appendix C – Calibration Information of the Equipment. After placing three desiccants inside the TH chamber at each test condition, the desiccants were weighed at regular time intervals to record the increase in weight of the desiccant. This weight gain is caused by the

desiccant's adsorption of water vapor at the maintained relative humidity inside the chamber. This calculated gain in weight is divided by the weight of the desiccant measured before placing them inside the chamber to obtain the amount of water vapor adsorbed per gram of desiccant at each time interval. This process is repeated until the increase in weight of the desiccant values has stabilized.

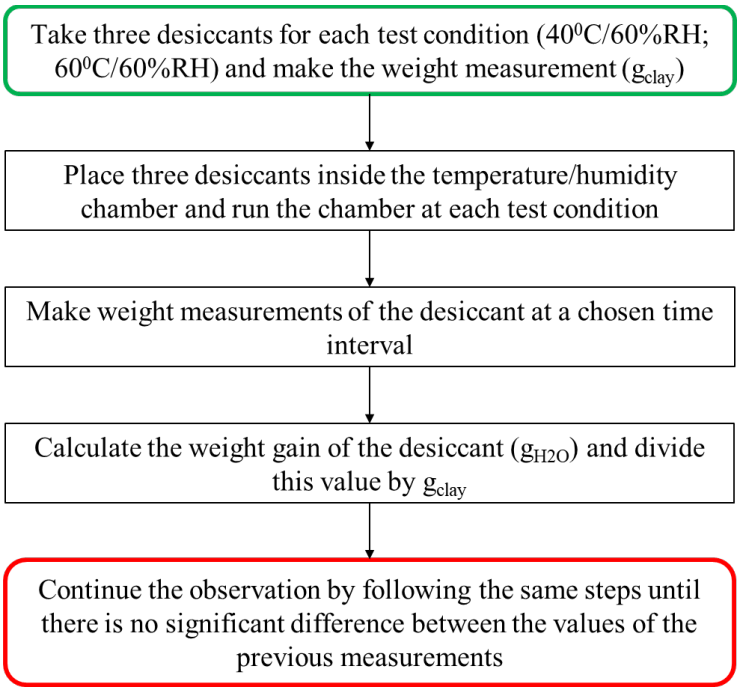

Figure 16 Flowchart describing the test procedure to determine the moisture adsorbing effectiveness of the desiccants above 50 °C

Figure 17 Representation of desiccants placed inside the temperature/relative humidity chamber

The graphs shown in Figure 18 depict the results of the experiment conducted for desiccants. On the y-axis of the graph, the amount of water vapor adsorbed by the desiccant per gram of desiccant is shown. The x-axis on the graph represents the number of hours the desiccants were inside the TH chamber. Desiccant samples A, B, and C were placed inside the chamber at 60 °C / 60% RH, and the samples D, E, and F were placed at 40 °C / 60% RH. The graph shows that the amount of water vapor adsorbed by the desiccant initially increased and then stabilized. This stabilized number is referred to as the desiccant's adsorption capacity, which represents the maximum quantity of water vapor that the desiccant can absorb at that temperature and relative humidity. Averaging the last three stabilized y-values of the same desiccant at both test conditions yields the adsorption capacity of each desiccant. Table 19 lists the adsorption capacity of each desiccant sample at the corresponding temperature and

relative humidity conditions. The adsorption capacities of the desiccant samples A, B, and C is observed to be comparable to those of the desiccant samples D, E, and F. This infers that the desiccant's water adsorbing capability at 60 °C (above 50 °C) is same as that at 40 °C (below 50 °C). From this experiment, it is possible to conclude that 60 °C can be used as one of the accelerated temperature conditions for accelerated experiments on MBBs.

The adsorption rate of the desiccant at a specific temperature and relative humidity is defined as the time it takes to reach the adsorption capacity at the same temperature and relative humidity condition. From Figure 18, it can also be observed that the adsorption rate of the desiccant samples A, B, and C that were tested at 60 °C / 60% RH is faster than the desiccant samples D, E, and F that were tested at 40 °C / 60% RH. This suggests that temperature can act as an accelerator, shortening the time required to reach the adsorption capacity of the desiccant sealed inside the MBB. As a result, running the accelerated aging experiments of MBBs at 60 °C is expected to shorten the total experiment time.

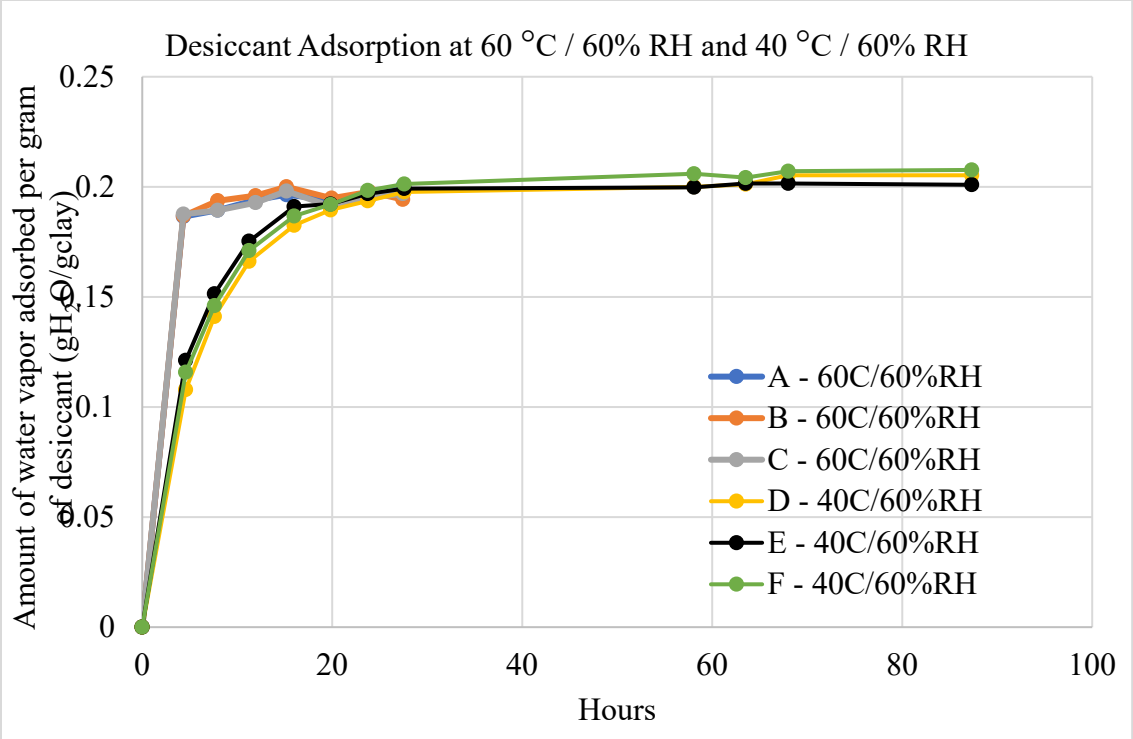

Figure 18 Graph showing the amount of water adsorbed per unit gram of desiccant vs the number of hours the desiccants were placed inside the TH chamber

Table 19 Adsorption capacity of the desiccants at different temperature/RH conditions

Desiccant Sample	**Test Condition**	**Adsorption Capacity ($g_{H_2O}/g_{desiccant}$)**
A	60^0C/60%RH	0.1966
B	60^0C/60%RH	0.1956
C	60^0C/60%RH	0.1943
D	40^0C/60%RH	0.2039
E	40^0C/60%RH	0.2013
F	40^0C/60%RH	0.2063

Test Conditions

Since accelerating the temperature accelerates the desiccant's adsorption rate, one can infer that temperature can be one of the testing conditions for performing the accelerated experiments on MBBs sealed with desiccant. MVTR is a linear function of relative humidity between the outside and inside of the MBB. As the relative humidity outside the MBB increases, so does the MVTR, shortening the time it takes to reach the adsorption capacity of the desiccant, and thus 10 percent RH inside the MBB. As a result, the two testing conditions that can be employed to accelerate the moisture permeation mechanism of MBBs are temperature and relative humidity.

The test conditions, temperature and relative humidity, are chosen based on the conclusions of the experiments conducted for desiccants, the maximum operating temperature of wireless TH sensor, the glass transition temperature of MBB, and the actual storage environment. The experiments conducted for desiccants revealed that the desiccant could perform its water adsorbing function at 60 °C. From Table 18, it can be observed that the maximum temperature that the Elitech wireless TH sensor can measure is 70 °C. The glass transition temperature of the MBBs used in this thesis was found to be 105 °C. The actual storage environment is 17 °C – 25 °C / 30% RH – 60% RH outside the MBB. Considering all of the aforementioned factors, 60 °C is the maximum possible temperature that can be used, as temperatures above 60 °C may affect the wireless TH sensor's measuring capability, resulting in inconclusive results. Therefore, three levels of temperature – 40 °C, 50 °C, and 60 °C and two levels of relative humidity – 50% RH and 85% RH are chosen as the two conditions for this experiment.

Design of Experiments

The chosen test conditions are utilized as input parameters in the design of experiments to establish the combinations of test conditions that can be employed for accelerated tests on MBBs. Using JMP Pro software, the maximum number of potential combinations for the three levels of temperature and two levels of relative humidity was determined to be 6 as shown in Table 20. As data on how long it takes to get to 10% RH inside the considered MBB is not available, it is unknown whether performing experiments for all six combinations of test conditions will be time-consuming or not. Thus, it has been decided to start with two different test combinations initially as shown in Table 21 and observe the experiment duration based on which the decision to perform accelerated experiments on the remaining four combinations of test conditions will be made.

It can be observed from Table 21 that 60 °C / 85% RH is chosen as one of the test conditions which represents high/high pattern for both temperature and relative humidity. The other test condition was initially chosen to be 40 °C / 85% RH that represents low/high pattern for temperature/relative humidity. However, due to reasons associated with availability of chamber, test condition 40 °C / 93% RH was used with the assumption that the moisture permeation rate did not differ significantly between 85% RH and 93% RH.

Table 20 Combinations of temperature/relative humidity obtained from design of experiments software - JMP Pro

Temperature	Relative Humidity	Pattern (Temperature / Relative Humidity)
40	85	Low / High
50	50	Medium / Low
60	50	High / Low
40	50	Low / Low
60	85	High / High
50	85	Medium / High

Table 21 Combinations of test conditions that were chosen to run on MBBs and desiccants

Temperature	Relative Humidity
60	85
40	93

Experiment Procedure for Accelerated Aging of MBBs

Figure 19 shows the procedure following for accelerated experiments on MBBs. The MBBs are vacuum sealed using the vacuum sealing machine with the desiccants and wireless TH sensor placed inside it. The sealed MBBs are placed inside the chamber at the test conditions as specified in Table 21. The chamber is run at the selected conditions with the RH inside the MBB is continuously monitored by the wireless RH sensor that was vacuum sealed inside the MBB. The time taken to reach the adsorption capacity of the desiccant sealed inside MBB is calculated based on the results obtained from these experiments.

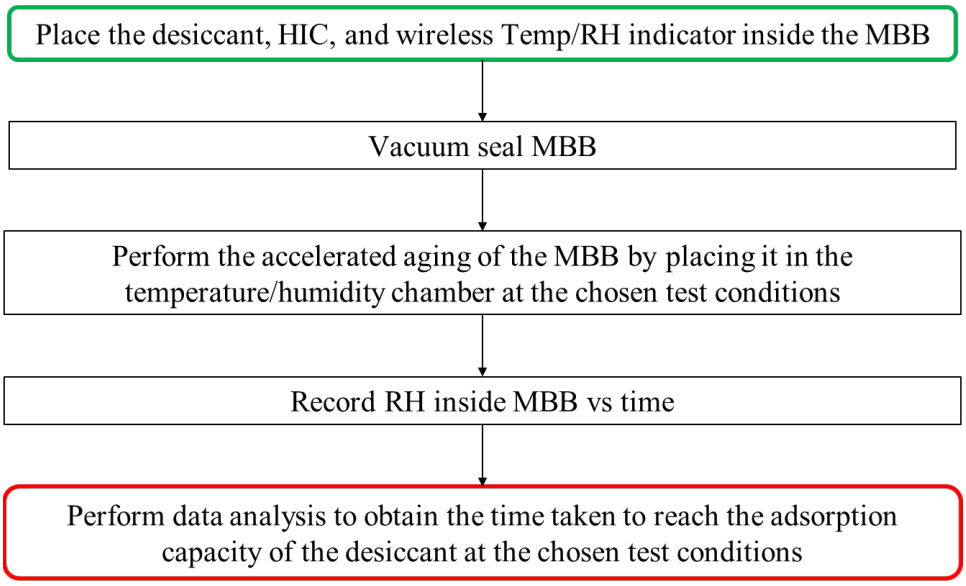

Figure 19 Flowchart showing the test procedure for accelerated experiments on MBBs

Sample Preparation

MBBs are cut into rectangular shape with a sealed area of 7.25 × 8 in^2. Elitech wireless temperature/relative humidity sensors are placed inside the cut MBB before vacuum sealing. Three samples were prepared out of which one was sealed without desiccant, one was sealed with 16.5g of desiccant and the last one was sealed with 33g of desiccant. Figure 20 shows an image of MBB of area 7.25 × 8 in^2 sealed with 33g of desiccant. Figure 21 shows an image of vacuum sealed MBB. The vacuum sealed MBBs were punched with holes through which stainless steel hooks are inserted and hung onto the trays that were fit in the temperature/relative humidity chamber, as shown in Figure 22.

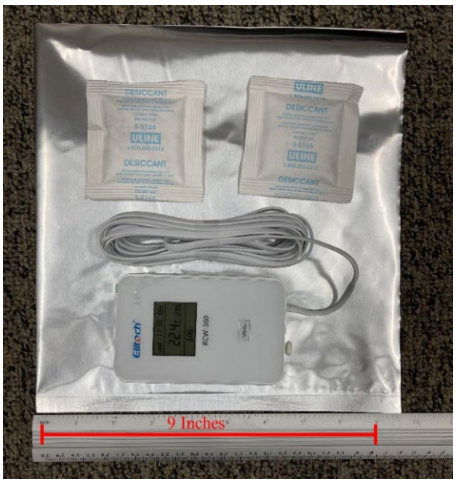

Figure 20 Image of MBB cut into a sealed area of 7.25 × 8 in^2, a wireless temperature/relative humidity sensor and 33g of desiccant before vacuum sealing

Front side

Back side

Figure 21 Image of vacuum sealed MBBs containing wireless temperature/relative humidity sensor and 33g of desiccant inside it

Figure 22 Image showing the vacuum sealed MBBs hanging inside the temperature/relative humidity chamber

Results

MBB samples were placed inside the chamber at two different conditions – 60 °C / 85%RH and 40 °C /9 3%RH. Figure 23, Figure 24 and Figure 25 shows the temperature and relative humidity recorded by the wireless sensor sealed inside MBB versus time for MBBs sealed without desiccant, with 16.5gof desiccant and with 33g of desiccant, respectively when placed inside TH chamber at 60 °C / 85%RH. Similarly, Figure 27, Figure 30 and Figure 31 represents the temperature and relative humidity recorded by the wireless sensor sealed inside MBB versus time for MBBs sealed without desiccant, with 16.5gof desiccant and with 33g of desiccant, respectively when placed inside TH chamber at 40 °C / 93%RH.

It can be observed from Figure 23 that relative humidity increased from 16% RH to 37% RH at the end of 50 days of placing the vacuum sealed MBB inside TH chamber at 60 °C / 85% RH. It is interpreted that sudden initial increase in inside RH from 16%

RH to 30% RH is due to the release of adsorbed water molecules from TH sensor as it is heated from laboratory atmospheric temperature (25°C) to TH chamber temperature (60°C) when placed inside TH chamber. Taking this into consideration, an increase of 7% RH is observed inside the vacuum sealed MBB at the end of 50 days when placed at 60 °C / 85% RH. Figure 23 can also be observed with abrupt increase and decrease in inside RH and temperature at around 2 days which is attributed to opening and closing of chamber at that time. When the chamber is opened, the temperature dropped from 60 °C to 51 °C that increased the RH inside MBB for the same moisture content contained within the MBB. When the chamber is closed, the temperature returns to 60°C, and the RH inside MBB returns to the level it was before the chamber was opened. It should be noted that the resolution of the wireless sensor is 1% RH, which has been stated in Table 18. As a result, any line connecting the absolute values of RH within MBB is not parallel to the x-axis. For example, the line connecting 34% RH and 35% RH is not parallel to the x-axis. It should be interpolated linearly to connect the two values that result in a line not parallel to the x-axis.

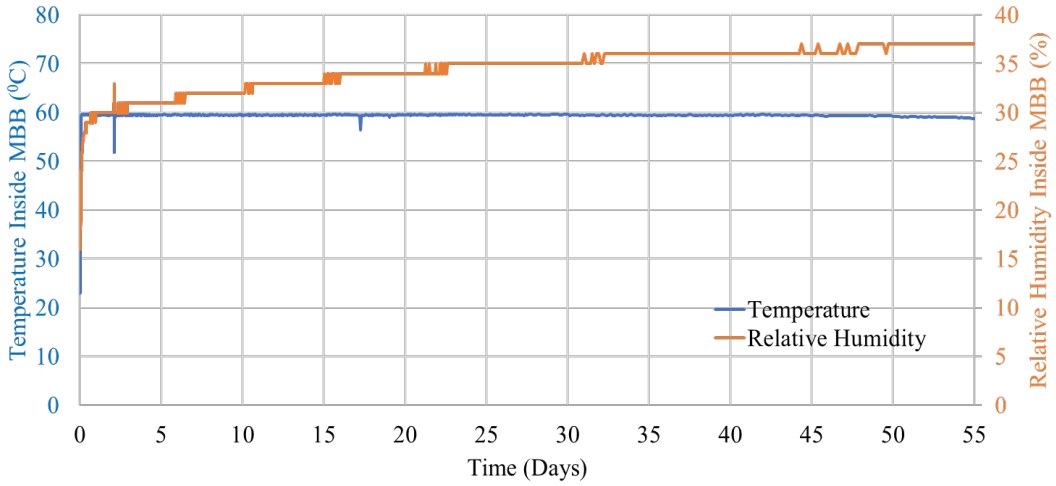

Figure 23 Graph showing the temperature and relative humidity inside MBB measured by wireless sensor vs time for MBB sealed without desiccant at 60°C/85%RH as external condition

From Figure 24 and Figure 25, it can be observed that the relative humidity inside MBB is reduced to 2% RH at the end of 35 days and 55 days for MBBs sealed with 16.5g and 33g of desiccant, respectively. The accuracy of the wireless TH sensor is ±5% RH as stated in Table 18. This indicates that the RH inside MBB containing desiccant can be anywhere in between 0% RH and 5% RH. It can be observed from the graph that it took 7 days for the RH inside MBB to reach 2% RH for 16.5g of desiccant. On the other hand, for the MBB having a same sealing area, it took 2.5 days for the RH inside MBB to reach 1% RH for 33g of desiccant. This means that by sealing a 7.25 x 8 in^2 MBB with 33g of desiccant, the RH inside the MBB can be decreased to 1% RH in a shorter amount of time. Figure 26 shows comparison of relative humidity inside MBB vs time for MBBs sealed without desiccant and with 16.5gand 33g of desiccant.

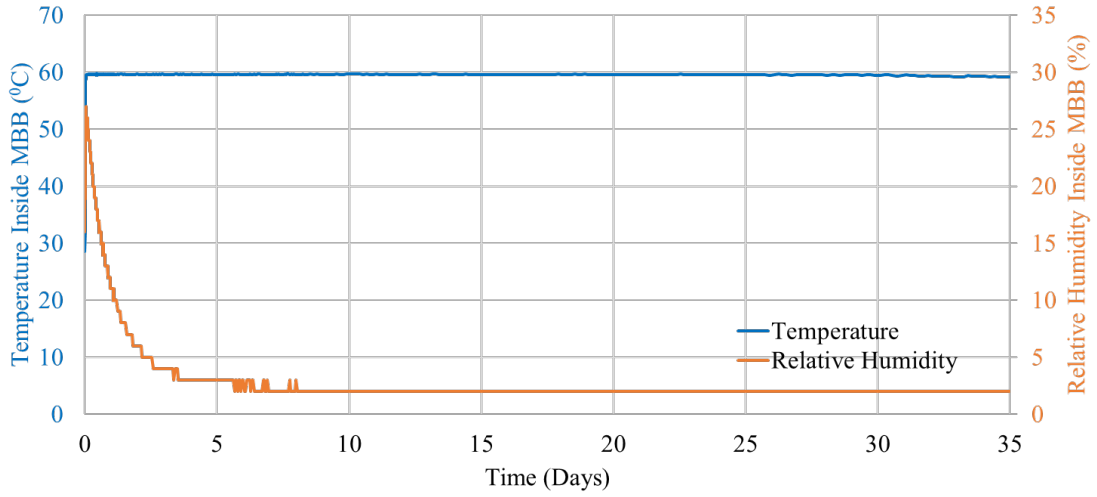

Figure 24 Graph showing the temperature and relative humidity inside MBB measured by wireless sensor vs time for MBB sealed with 1/2 unit of desiccant at 60°C/85%RH as external condition

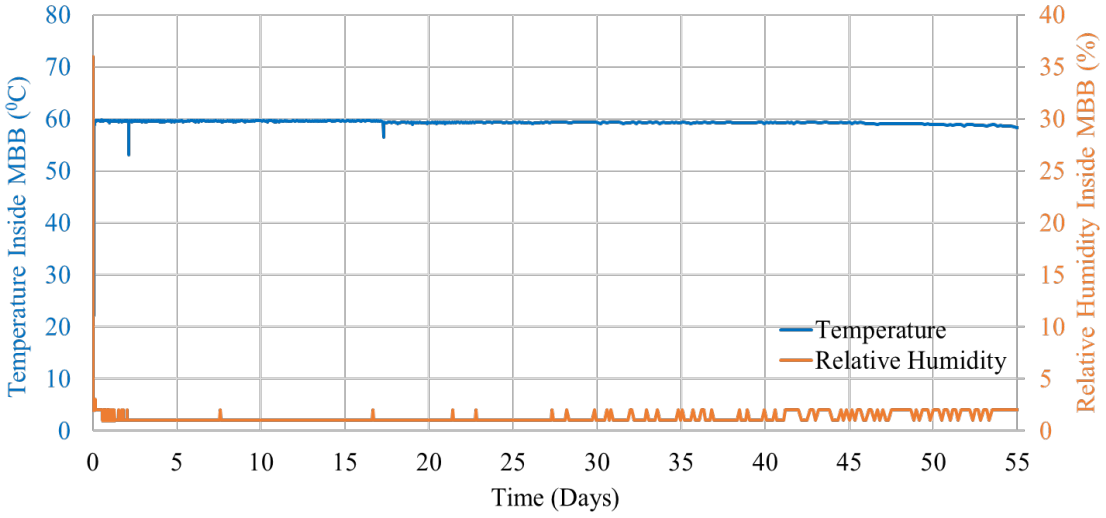

Figure 25 Graph showing the temperature and relative humidity inside MBB measured by wireless sensor vs time for MBB sealed with 33g of desiccant at 60 °C / 85% RH as external condition

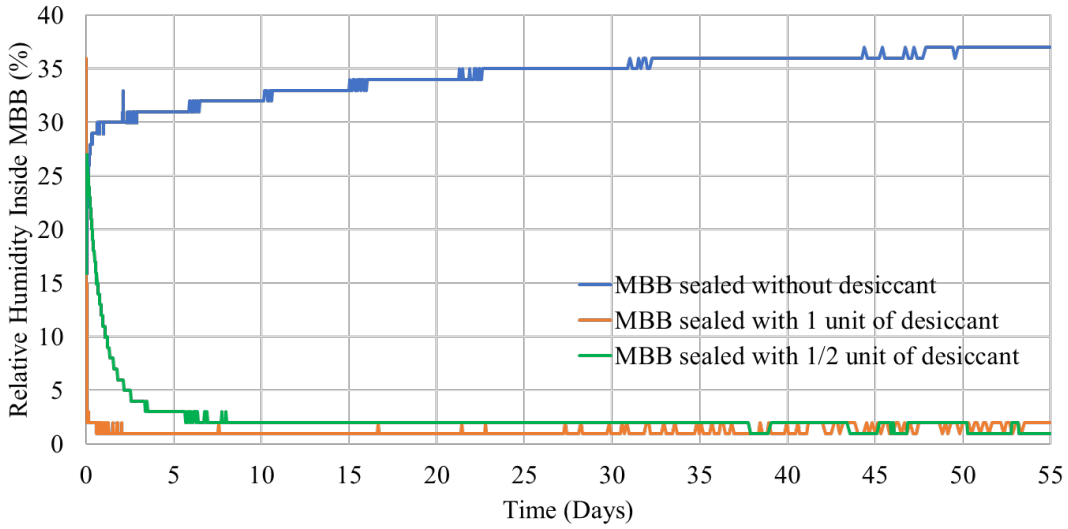

Figure 26 Graph showing the comparison of relative humidity inside MBB between MBBs sealed without desiccant, with 16.5gof desiccant and 33g of desiccant at 60 °C / 85% RH as external condition

The MBB vacuum sealed with wireless TH sensors was placed inside the TH chamber at 40 °C / 93% RH after 12 hours of performing vacuum sealing operation. This can be clearly observed from the temperature plot of Figure 27 that shows an increase in temperature from 25 °C to 40 °C at end of 0.5 days. At the time of placing the MBB inside the chamber, RH inside the chamber was 30% RH. It can be noticed that RH inside MBB increased from 30% RH to 38% RH at the end of 44 days when placed inside the TH chamber at 40 °C / 93%RH. The explanation provided for the release of adsorbed water molecules from the wireless TH sensor when placed inside chamber at 60 °C / 85%RH can be extended to 40 °C / 93%RH condition for explaining a sudden increase in inside RH from 26% to 35%. So, the actual increase in inside RH is from 35% RH to 38% RH at the end of 44 days of placing the MBB sealed without desiccant at 40 °C / 93%RH.

Figure 28 shows the comparison of inside RH vs time for MBBs sealed without desiccant between external conditions – 60 °C / 85%RH and 40 °C / 93%RH. It might seem from Figure 28 that MBB placed at 40 °C / 93%RH condition reached higher inside RH compared to MBB placed at 60 °C / 85%RH at the end of 40 days. However, the RH inside MBB at the time of placing it inside chamber at 40 °C / 93%RH is 26% RH, higher than the RH inside MBB at the time of placing at 60 °C / 85%RH, which is 16% RH. Therefore, to compare the increase in inside RH between the MBB samples placed at these two conditions, the y-axis (RH) and x-axis (time) is shifted to zero as shown in Figure 29. It can be inferred from Figure 29 that RH inside MBB placed at 60 °C / 85% RH increased by 20% RH whereas at 40 °C / 93% RH it is increased only by 12% RH. This shows that temperature plays a role in increasing the permeation rate of water vapor from outside to inside of the MBB.

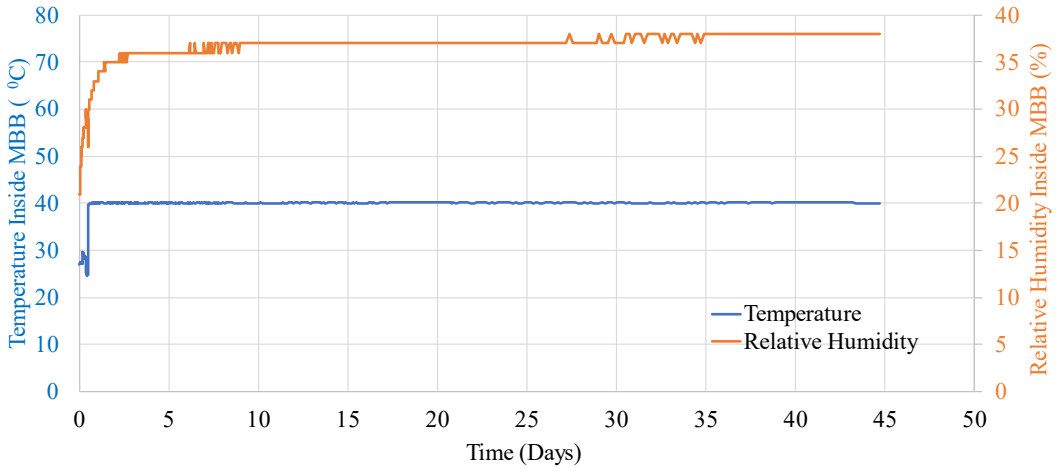

Figure 27 Graph showing the temperature and relative humidity inside MBB measured by wireless sensor vs time for MBB sealed without desiccant at 40 °C / 93% RH as external condition

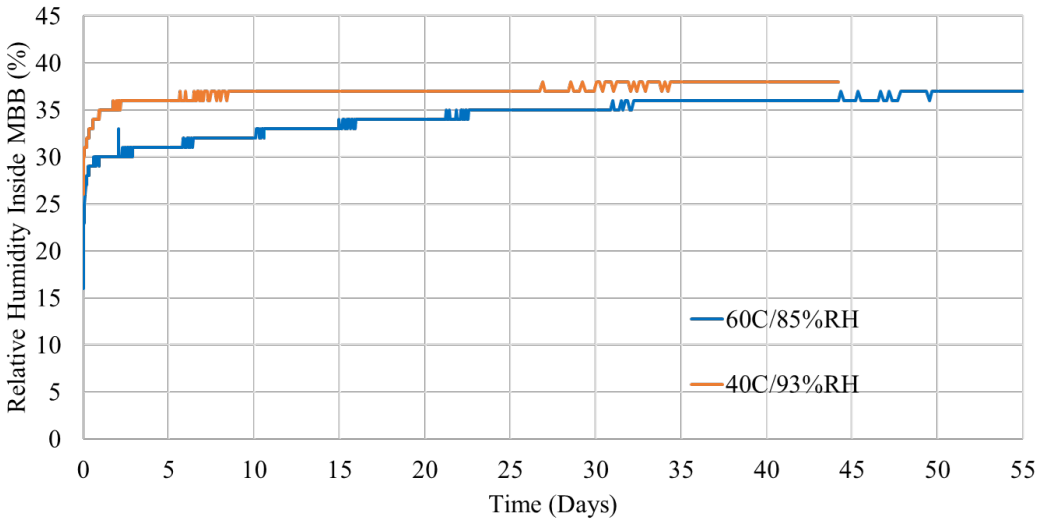

Figure 28 Graph showing the relative humidity inside MBB vs time as comparison between MBBs sealed without desiccant when placed at 60 °C / 85% RH and 40 °C / 93% RH

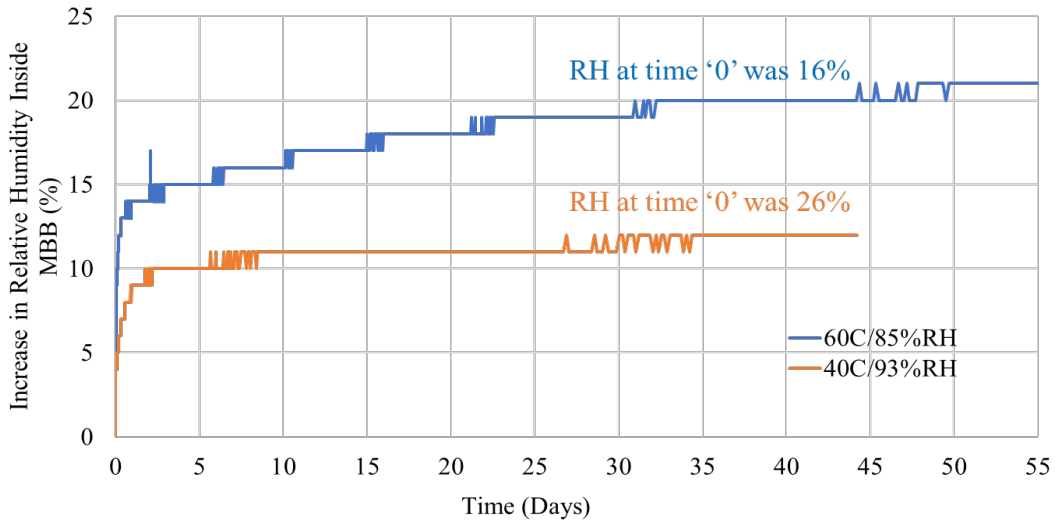

Figure 29 Graph showing the increase in relative humidity inside MBB when placed at 60 °C / 85% RH and 40 °C / 93% RH after shifting and RH and time scale of Figure 28 to zero

From Figure 30 and Figure 31, it can be observed that the RH inside MBB is reduced to 4% and 1% at the end of 45 days for MBBs sealed with 16.5g and 33g of desiccant, respectively. Figure 32 shows the comparison of relative humidity inside

MBB vs time for MBBs sealed without desiccant and with 16.5g and 33g of desiccant at 40°C/93%RH.

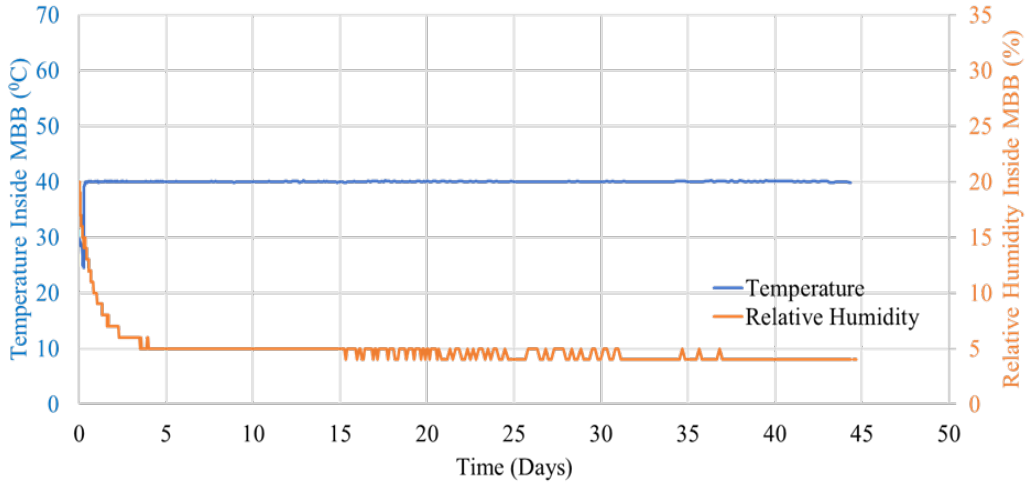

Figure 30 Graph showing the temperature and relative humidity inside MBB measured by wireless sensor vs time for MBB sealed with 16.5g of desiccant at 40 °C / 93%RH as external condition

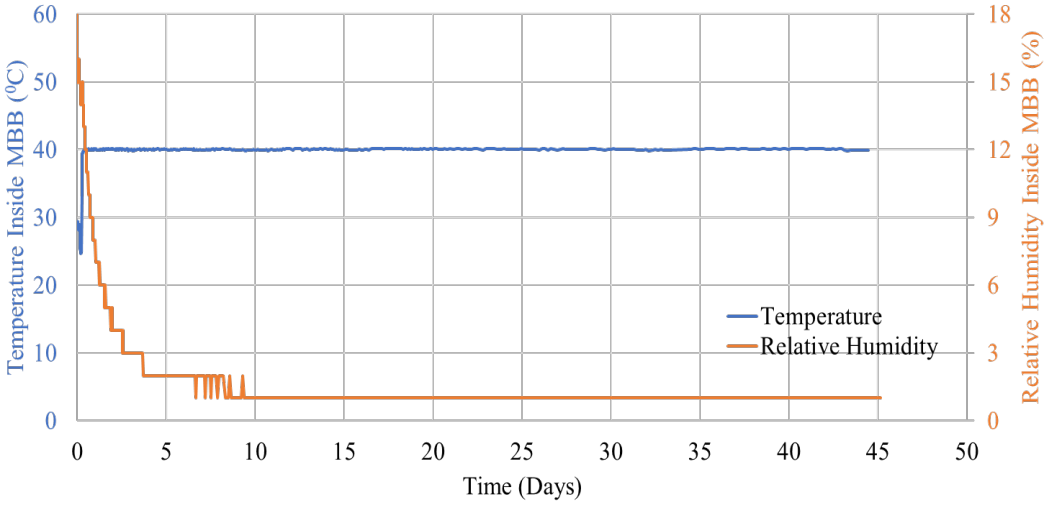

Figure 31 Graph showing the temperature and relative humidity inside MBB measured by wireless sensor vs time for MBB sealed with 33g of desiccant at 40 °C / 93% RH as external condition

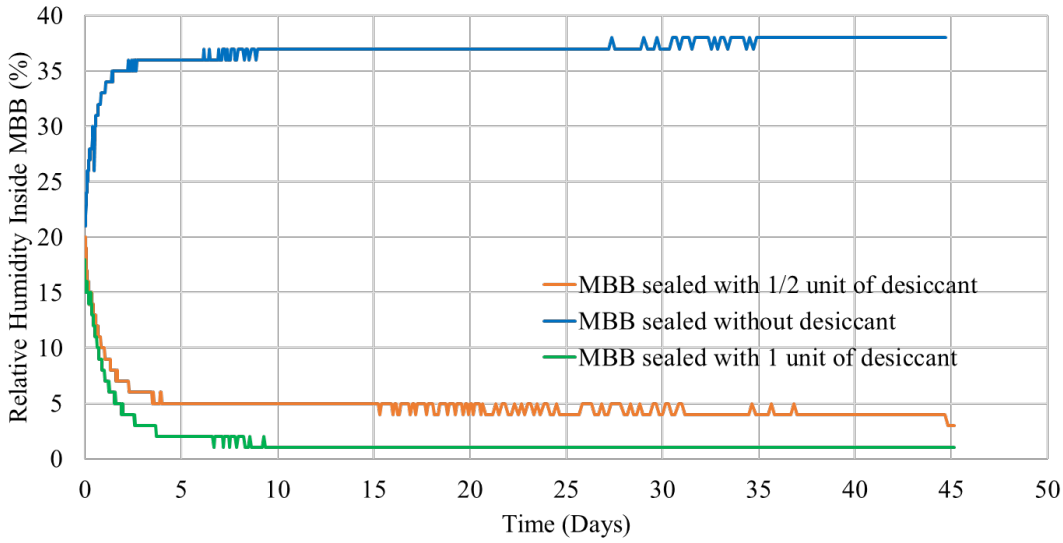

Figure 32 Graph showing the comparison of relative humidity inside MBB between MBBs sealed without desiccant, with 16.5g of desiccant and 33g of desiccant at 40 °C / 93% RH as external condition

Accelerated Aging Experiment for Change in Surface Resistivity

The failure mode of change in surface resistivity due to the degradation of organic compounds, which are added as additives to the polymeric layers, for improving the surface resistivity property is analyzed for its criticality in the following section.

For measuring the surface resistivity of the MBB samples before and after aging, the samples were cut into rectangular shapes of dimension 8*4 cm^2. Similarly, the three carrier tapes were cut into samples, as shown in Figure 33. These samples were then placed under the four-point probe of the Pro-4 system, which is shown in Figure 34. The four-point probe of the Signatone Pro-4 surface resistivity system was pressed against the surface of the samples to record the surface resistivity. The input parameter that is required for obtaining the surface resistivity from the Pro-4 system is the

thickness of the sample being measured. After having entered the thickness from Table 29 (appendix), the lever of the Pro-4 system was pushed against the surface of the sample. The system auto-selects the current range and displays the resistivity for the selected current passed through the surface of the sample. 5 measurements of the surface resistivity were obtained by placing the four-point probe at 5 different locations on the surface for the same sample. The values were then averaged. The surface resistivity values of both the MBBs and carrier tapes samples were measured before and after accelerated aging, which is discussed in the below sections.

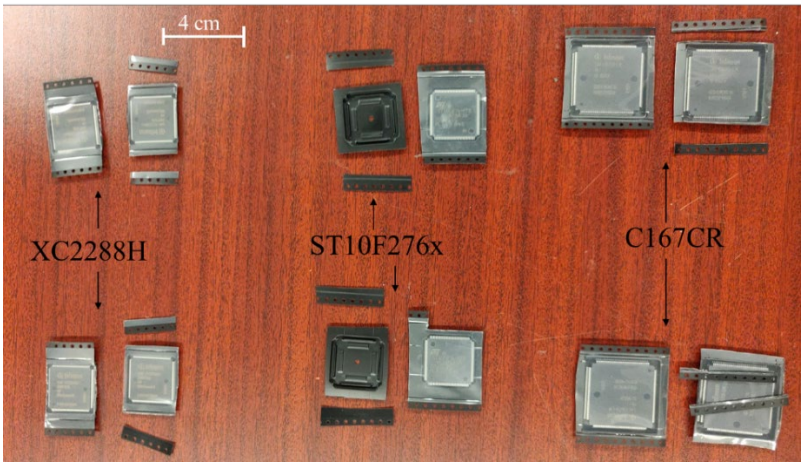

Figure 33 Picture showing the different set of carrier tape samples used for accelerated aging experiments

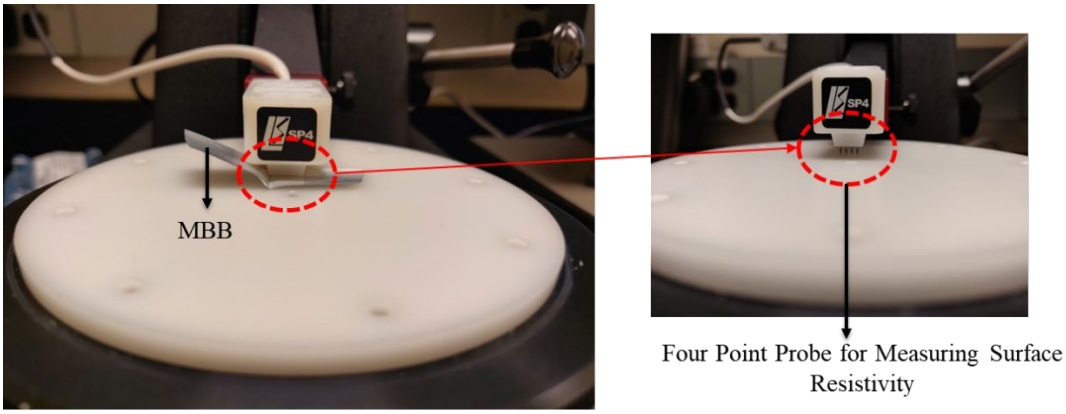

Figure 34 Image showing the Signatone Pro-4 Four-Point Resistivity System

To observe the change in surface resistivity in both MBB and carrier tape samples after aging, the samples were placed in a Temperature/Relative Humidity chamber at two different conditions — 85^0C/5%RH and 60^0C/25%RH. The aging conditions and the run time has been tabulated in Table 22. The surface resistivity values were measured at 5 different locations for each sample at each time interval for each run. The average of those 5 measurements was calculated and reported in the graph along with the maximum and minimum values. It is hypothesized that upon aging at higher temperatures, the organic compound additives degrade, resulting in an increase in surface resistivity. When the surface resistivity of the MBB and the carrier tape reaches the insulative region (> 10^{12} Ohms/Square), it is considered to be a failure criterion, at which point the aging experiments for measuring surface resistivity will be stopped.

Table 22 Aging conditions and aging time for measuring the change in surface resistivity

	Run 1	Run 2
Temperature/Relative Humidity Condition	85^0C/5%RH	60^0C/25%RH
Run Time (Aging Period)	28 days	28 days
Number of measurements at each time interval	5	5

Moisture Barrier Bags

Surface resistivity values of the MBBs were measured before aging by following the procedure are tabulated in Table 23. The surface resistivity values for both the inner and the outer layers of the MBB were found to be at 10^7 Ohms/square (Ω /sq), which matches with the specification provided by the manufacturer and lies within the static dissipative region.

Table 23 Surface resistivity values obtained for the inner and outer layer of the MBB from Pro-4 four-point resistivity system before aging

Surface Resistivity Measurement (Ω /sq)	**1st Measurement**	**2nd Measurement**	**3rd Measurement**	**4th Measurement**	**5th Measurement**	**Average**
MBB outer layer	1.62 x 10^7	4.31 x 10^7	3.72 x 10^7	4.7 x 10^7	5.41 x 10^7	3.95 x 10^7
MBB inner layer	8.72 x 10^7	4.39 x 10^7	4.18 x 10^7	2.87 x 10^7	3.73 x 10^7	4.78 x 10^7

Figure 35 and Figure 36 show the graph of the change in surface resistivity observed for the outer and inner layer of the MBB after aging. The solid black lines at 10^5 and 10^{12} Ohms/Sq in the graph show the lower and the upper limit for the static dissipative region. The blue and red line representing the run 1 and 2 respectively

passes through the mean of the 5 measurements that were taken at each time interval. The maximum and minimum values among the 5 measurements at each time interval is indicated as caps above and below the mean for both the runs. The whole range of surface resistivity values, including the maximum and minimum values, should be taken into account for any interpretation of the results.

For run 1, the surface resistivity of the outer layer of the MBB stayed within the 10^7 - 10^8 Ohms/Sq for the aging period of 28 days. The experiments for run 1 were stopped at the end of 28 days as the surface resistivity is observed to have reached a stable value and did not show any significant increase or decrease beyond 10^8 Ohms/Sq. For run 2, the surface resistivity of the outer layer of the MBB showed a varying - increasing and decreasing trend and the maximum increase was observed to be 10^9 Ohms/Sq at the end of 4 and 28 days. Since the trend did not show any consistent increase or decrease in the surface resistivity values when aged for 28 days at run 2 conditions, the experiments were stopped for run 2. Similarly, for both runs 1 and 2, the surface resistivity of the inner layers of the MBB showed an increase from 10^7 to 10^8 Ohms/Sq initially, but then the value got stabilized by the end of 28 days.

Although changes were observed in the mean values of surface resistivity for both the inner and outer layers of the MBBs, they were found to have the same range of values up to 28 days of aging. Also, the failure criteria of $>10^{12}$ Ohms/Sq was never reached at the end of 28 days of aging. Therefore, the accelerated aging experiment for measuring the change in surface resistivity of the MBBs was stopped from running at the conditions set for runs 1 and 2.

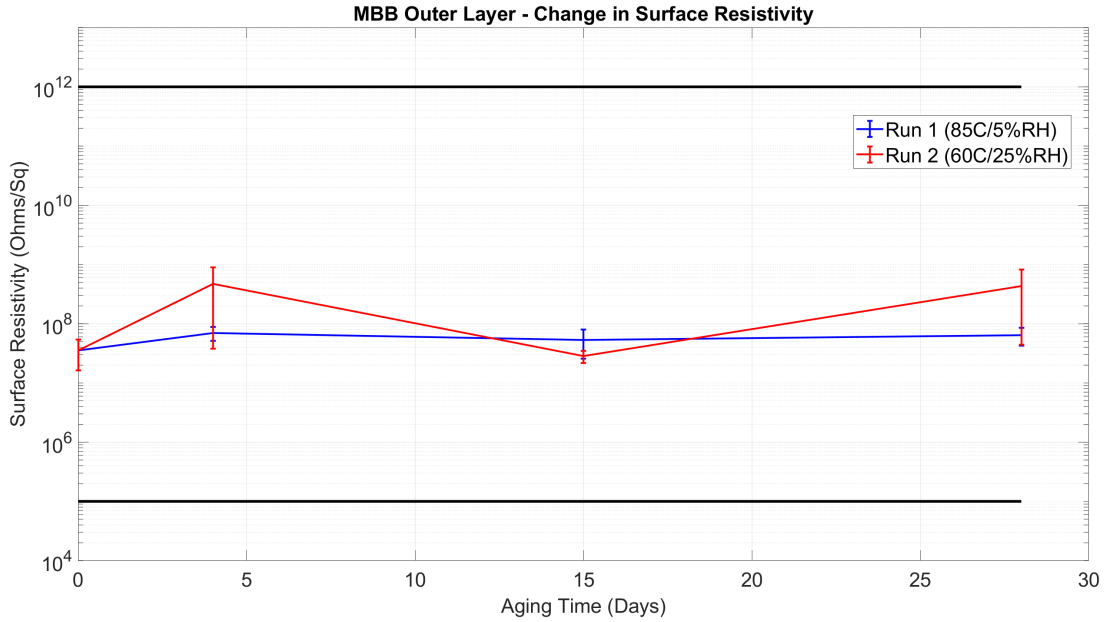

Figure 35 Graph showing the change in surface resistivity of the outer layer of the MBB vs. aging time for different runs

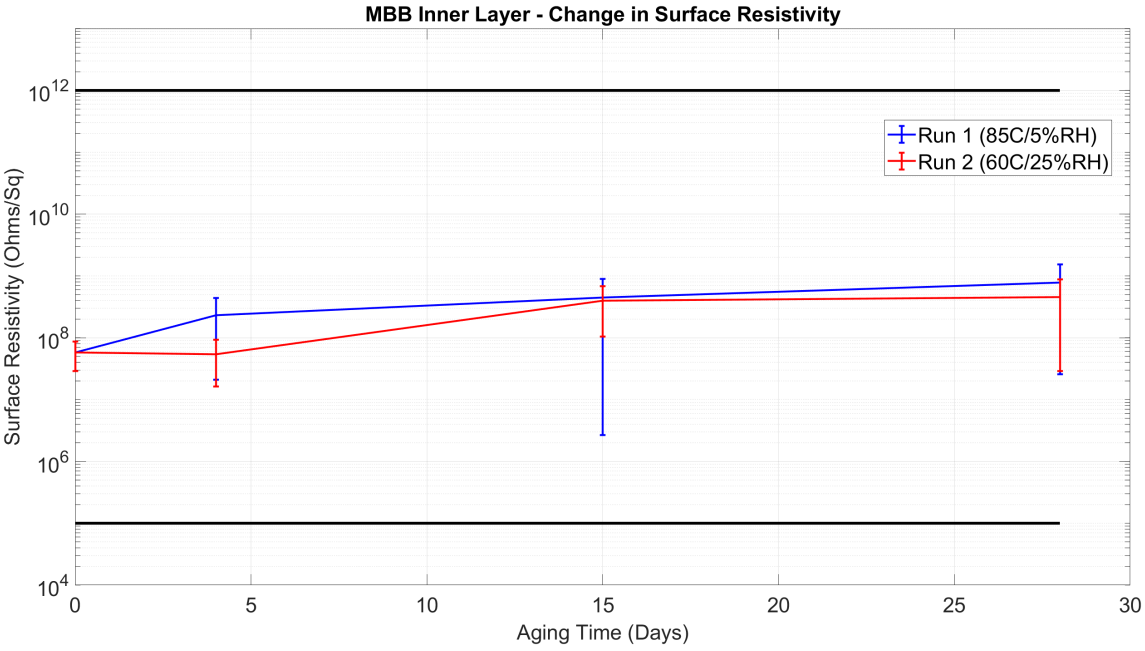

Figure 36 Graph showing the change in surface resistivity of the inner layer of the MBB vs. aging time for different runs

Carrier Tapes of Tape and Reel Carriers

Carrier tapes are addressed by the manufacturer part numbers of the components contained within them. The surface resistivity values provided by the manufacturer are discussed in Table 11.The surface resistivity values of the carrier tapes - C167CR, ST10F276, and XC288H carrier tapes that were measured before aging is shown in Table 24. C167CR and XC2288H carrier tapes show an average of 10^8 and 10^5 (Ω /sq) respectively before aging, which is within the specification limits provided by its manufacturer. However, the surface resistivity value of ST10F276 carrier tape before aging was observed to be $10^{4,}$ which is below the lower limit specification provided by its manufacturer.

Table 24 Surface resistivity values obtained for the carrier tapes used in this thesis from the Pro-4 four-point resistivity system before aging

Surface Resistivity Measurement (Ω /sq)	1st Measurement	2nd Measurement	3rd Measurement	4th Measurement	5th Measurement	Average
C167CR carrier tape	1.68×10^5	1.6×10^8	1.51×10^8	1.52×10^8	1.77×10^8	1.62×10^8
ST10F276 carrier tape	8.07×10^4	5.62×10^4	6.77×10^4	8.72×10^4	6.45×10^4	7.13×10^4
XC2288H carrier tape	3.01×10^5	2.84×10^5	2.36×10^5	3.65×10^5	2.96×10^5	2.96×10^5

Figure 37 shows the graph of change in surface resistivity values for C167CR carrier tape after accelerating to aging conditions specified for run 1 and run 2. For both runs, C167CR carrier tape showed an increase of the mean value of surface resistivity

from 10^5 Ohms/Sq to 10^9 Ohms/Sq at the end of 28 days. This increase was significant compared to other carrier tapes and MBBs used in this thesis, and so they were continued to age beyond 28 days to observe if it reaches the failure criteria of $>10^{12}$ Ohms/Sq. However, the range of the surface resistivity values was observed to be stabilized after 28 days. The maximum values of surface resistivity did not increase beyond 10^{10} Ohms/Sq all through the 45 days of aging at conditions specified for both runs 1 and 2. The reason for the increase in surface resistivity value for C167CR carrier tape, unlike other carrier tapes, can be attributed to the different manufacturer of this carrier tape compared to the manufacturer of the ST10F276 and XC2288H carrier tapes.

Figure 38 shows the graph of change in surface resistivity vs. aging time for ST10F276 carrier tape. For run 1, the range of values of surface resistivity did not increase beyond 10^5 Ohms/Sq at the end of 28 days, and so the experiments were suspended for ST10F276 carrier tape at run 1 conditions. For run 2, the mean value showed an increase from 10^5 to 10^6 Ohms/Sq at the end of 28 days. This increase was considered to be significantly less compared to the change in surface resistivity observed for C167CR carrier tape, and so the experiments were suspended for ST10F276 at run 2 conditions as well.

The change in surface resistivity values for XC2288H carrier tape is shown in Figure 39. Both run 1 and run 2 showed a similar trend of varying - increasing and decreasing mean values of surface resistivity. However, the range of the values for the aging period of 28 days was found to be consistent, and so the accelerated aging

experiments were stopped from measuring the surface resistivity values for XC2288H carrier tape at the end of 28 days.

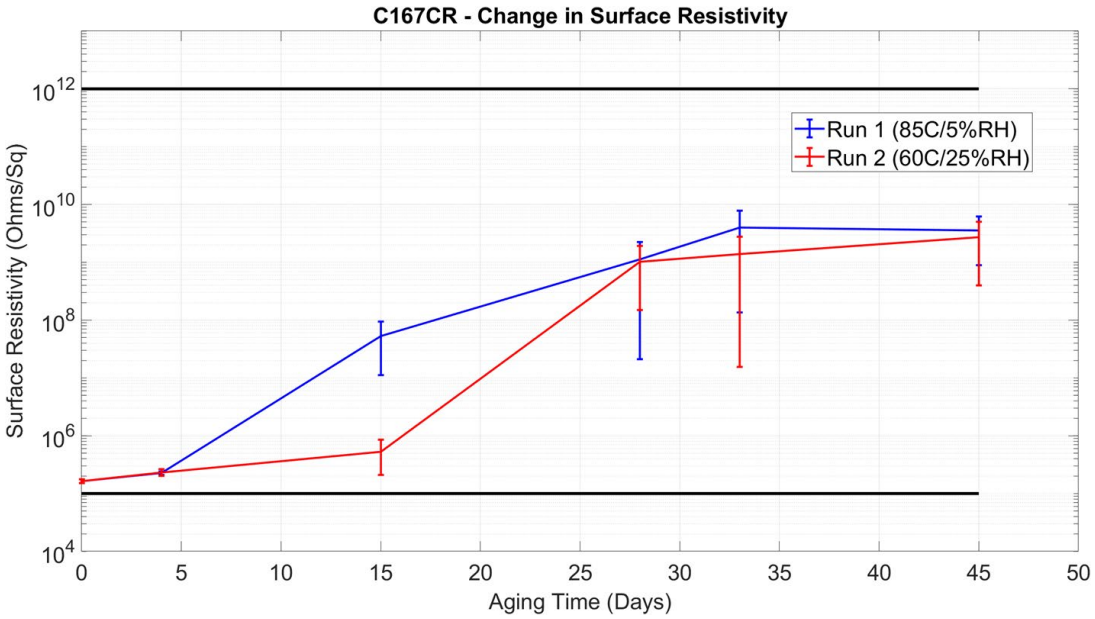

Figure 37 Graph showing the change in surface resistivity of the C167CR carrier tape vs. aging time for different runs

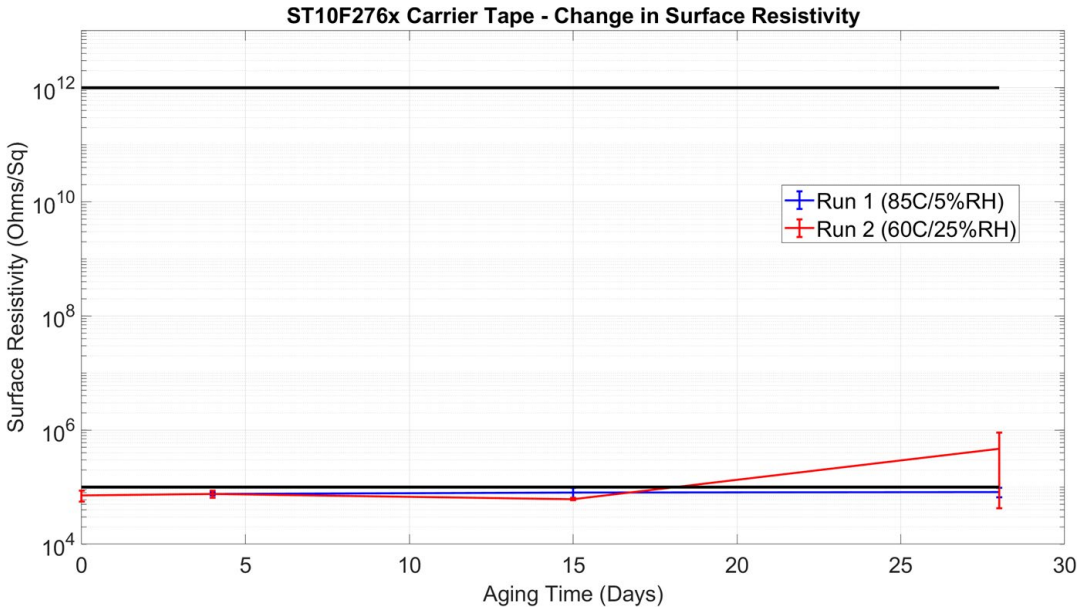

Figure 38 Graph showing the change in surface resistivity of ST10F276x carrier tape vs. aging time for different runs

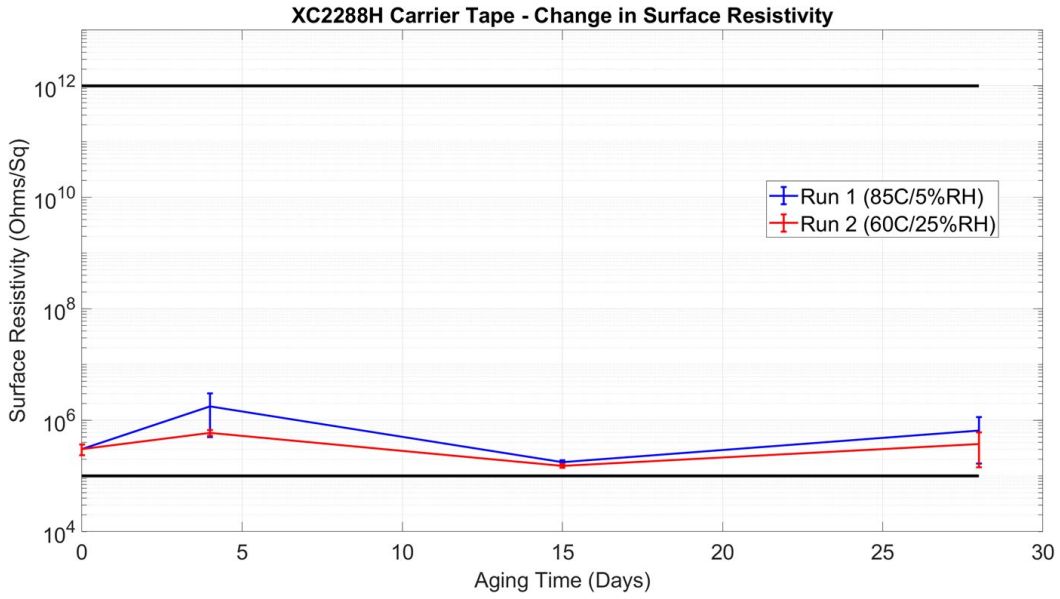

Figure 39 Graph showing the change in surface resistivity of XC2288H carrier tape vs. aging time for different runs

Accelerated Aging Experiment for Change in Dimensions of Carrier Tape

Polymeric shrinkage mechanism that could cause the dimensions of the carriers to change over time. This section details the accelerated aging experiments that were run to determine the criticality of the degradation mechanism by observing the change in dimensions of the carrier tape after aging.

In this thesis, the diameter and pitch of the sprocket holes of the carrier tapes are the two dimensions that are evaluated to observe for any change after aging. The diameter and pitch are represented as D_0 and P_0, as shown in Figure 40. EIA 481-E has set the dimensional requirements for the diameter and pitch of the sprocket holes of the carrier tape that is shown in Table 25. To analyze the criticality of the polymeric shrinkage mechanism that causes the change in dimensions during the long-term storage, the carrier tapes were aged in a temperature/relative humidity chamber at two conditions – 85^0C/5%RH and 60^0C/25%RH. The aging conditions and the run time have been tabulated in Table 26. A different set of carrier samples were used for each run, as shown in Figure 33. The dimensions – diameter and pitch of sprocket holes of the carrier tapes were measured using the Zeiss Axiovert optical microscope. Figure 41 shows an optical microscopic image representing an example of a measurement of the diameter and pitch of the sprocket holes of a carrier tape. 4 different diameters of the sprocket holes were measured for each sample and for each time interval of each run, and the average was calculated. 2 different measurements of pitch between any two of the 4 different sprocket holes were measured for each sample and for each time interval of each run, and the average was calculated. The dimensions were measured

for every carrier tape before and after aging, and the percentage change in dimensions was calculated. It is hypothesized that upon aging at higher temperatures, the diameter increases, and pitch decreases due to the polymeric shrinkage.

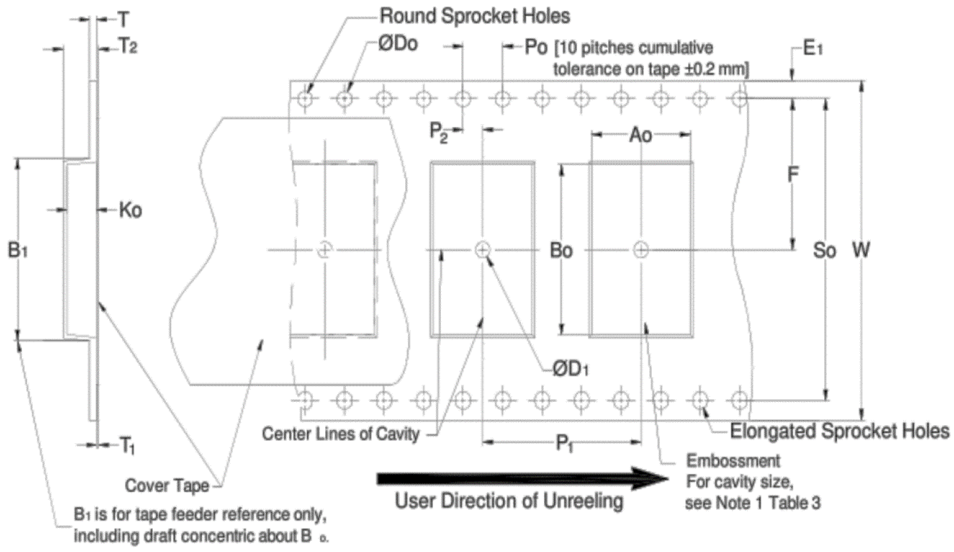

Figure 40 Picture showing the dimensions (D_0 and P_0) of the carrier tape as provided by EIA 481-E [37]

Table 25 Dimensional requirements for carrier tape set by EIA standard 481-E

Width (W)	44 mm
Diameter of the Sprocket Holes (D_0)	1.5 + 0.1 mm
Pitch of the Sprocket Holes (P_0)	4 $\pm$ 0.1 mm

Table 26 Aging conditions and aging time for the experiments conducted for polymeric shrinkage mechanism

	Run 1	**Run 2**
Temperature/Relative Humidity Condition	85^0C/5%RH	60^0C/25%RH
Run Time (Aging Period)	19 days	19 days
Number of Samples	2 Pockets containing components from each carrier tape (Totally 6 pockets)	

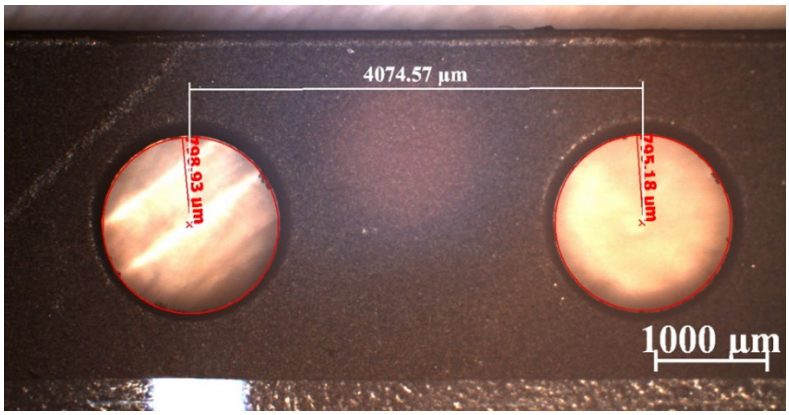

Figure 41 Optical microscopic image showing the measurement of pitch and diameter of sprocket holes

Figure 42, Figure 43, Figure 44, and Figure 45 show the percentage change in dimensions – diameter and pitch of the sprocket holes of different carrier tape samples used in this thesis for the conditions specified at run 1 and run 2. For the change in diameter graphs - Figure 42 and Figure 44, the solid line is drawn through the mean value of 4 different diameter measurements that were measured at each time interval for each carrier tape sample. For the change in pitch graphs - Figure 43 and Figure 45, the solid line is drawn through the mean value of the 2 different pitch measurements that were measured at each time interval for each carrier tape sample.

When the carrier tape samples were aged at 85^0C/5%RH - run 1, the change in percentage of the diameter of the sprocket holes of the carrier tapes did not show a monotonous trend. It can be observed from Figure 42 that for run 1 at the end of 19 days, the diameter of the sprocket holes of C167CR carrier tape increased from 1.598 mm to 1.612 mm, ST10F276 increased from 1.56 mm to 1.585 mm, and XC2288H carrier tape increased from 1.533 mm and 1. 581 mm. Comparing with dimensional

requirements set by EIA 481-E standard for the diameter of the sprocket holes (1.4 mm – 1.6 mm) as shown in Table 25, the increase in diameter was observed to be within the upper limit specification except for ST10F276 carrier tape (1.612mm), which is a little above 1.6mm. However, this little increase in the diameter of the sprocket holes does not cause any feeding errors or mis-picks during the pick and place operation after long-term storage.

Figure 43 shows the change in the pitch of the sprocket holes of the different carrier tapes for the run 1 condition for an aging period of 19 days. While it is hypothesized that the pitch of the sprocket holes is decreased upon aging, ST10F276 showed an increase in pitch from 4.045 mm to 4.053 mm. However, this increase is still within the upper limit (4.1 mm) of the pitch of the sprocket hole specification provided by EIA 481-E. On the other hand, C167CR and XC2288H showed a decrease in the pitch from 4.075 mm to 4.056 mm and from 4.069 mm to 4.058 mm, respectively. This decrease was also found to be within the lower limit specification (3.9 mm) for the pitch by the EIA 481-E standard. It can also be observed that similar to Figure 42, the graph of Figure 43 did not show any monotonous trend.

For run 2 conditions, as shown in Figure 44, the change in diameter of the sprocket holes was found to show an increase in diameter of the sprocket holes above the upper limit specification provided by EIA 481-E. However, as already discussed, this little above 1.6 mm increase does not cause any feeding errors or mis-picks. Figure 45 shows the change in percentage values obtained for change in the pitch of the sprocket holes for different carrier tapes for run 2 conditions. None of the values at the end of 19 days

were observed to be outside the limits of the specifications provided by the standard. As the graphs did not show a monotonous trend, and the change were observed to be less critical for dimensions, the experiments were stopped from running at the end of 19 days.

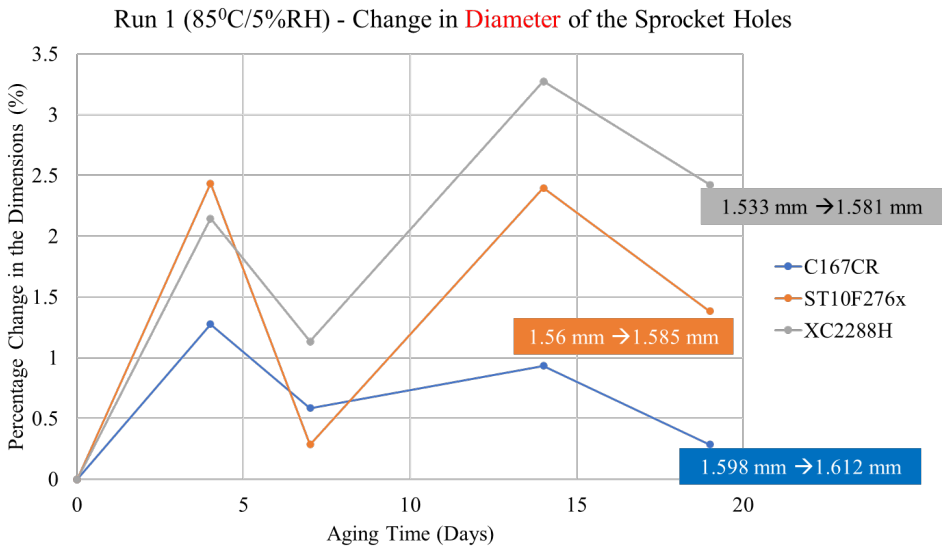

Figure 42 Graph showing the change in percentage of the diameter of the sprocket holes vs. aging time for different carrier tape samples at running 1 condition

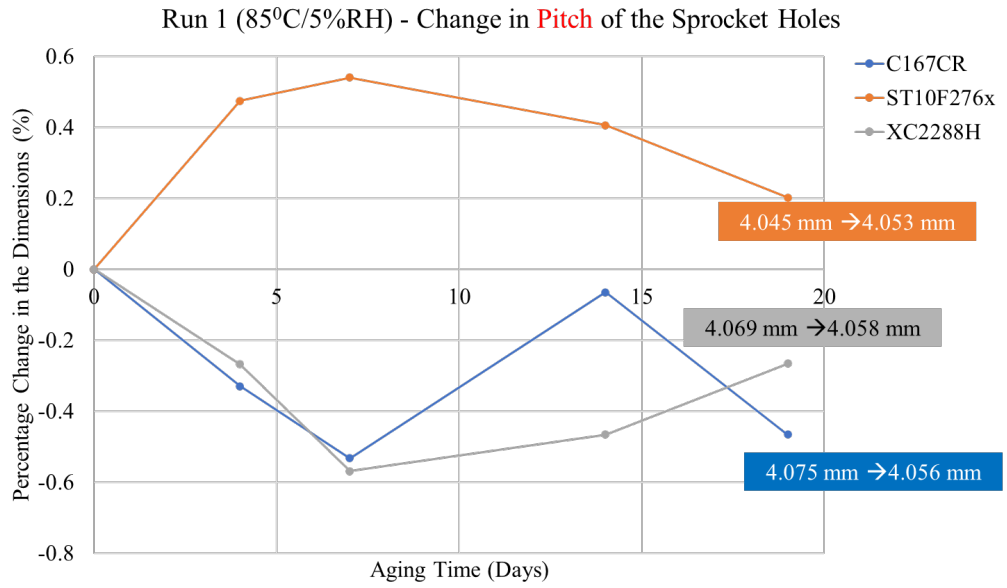

Figure 43 Graph showing the change in percentage of the pitch of the sprocket holes vs. aging time for different carrier tape samples at run 1 condition

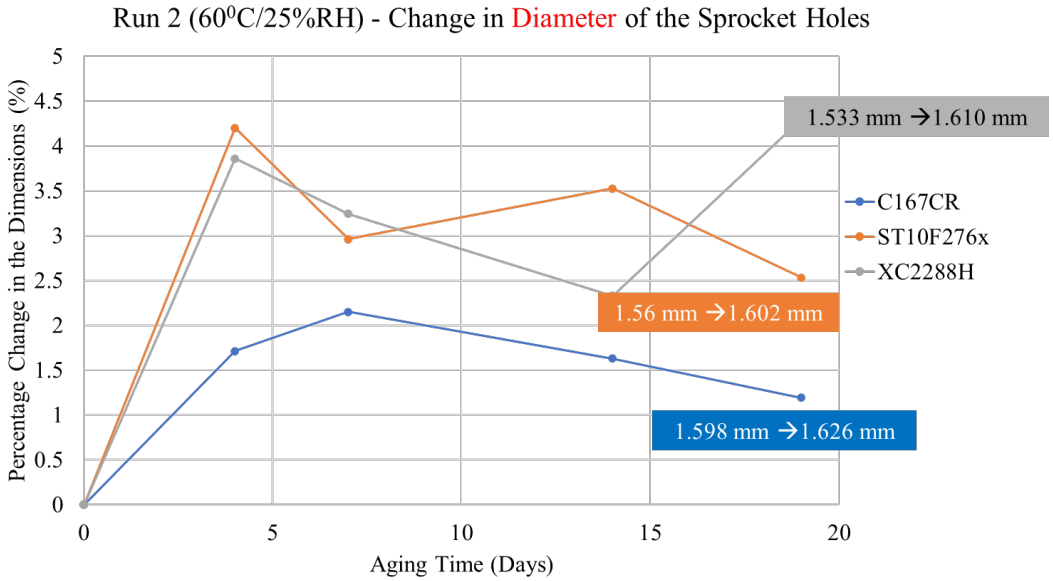

Figure 44 Graph showing the change in percentage of the diameter of the sprocket holes vs. aging time for different carrier tape samples at run 2 condition

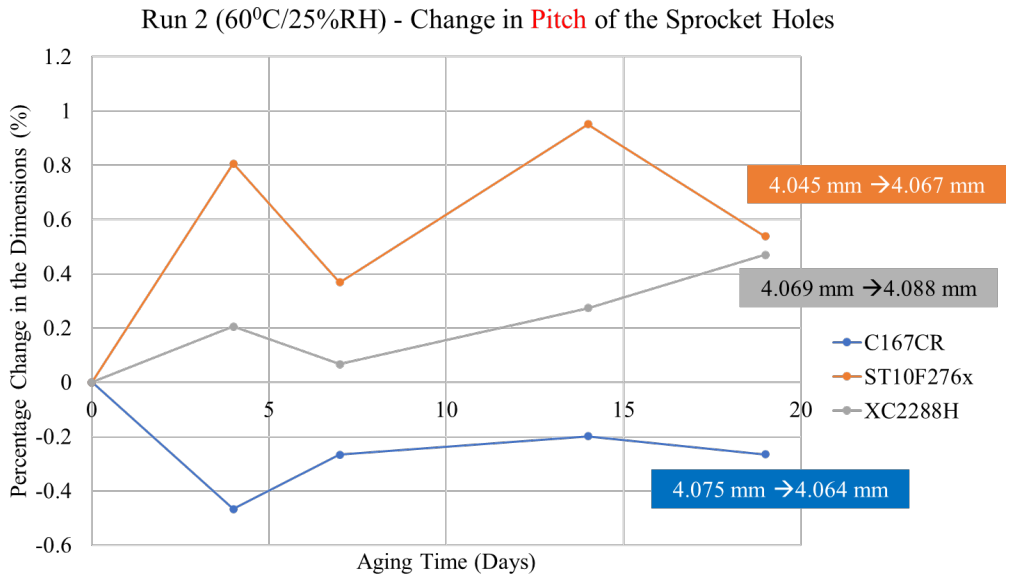

Figure 45 Graph showing the change in percentage of the pitch of the sprocket holes vs. aging time for different carrier tape samples at run 2 conditions

Chapter 6: Discussion

This section provides the discussion of the results obtained from the experiments conducted on MBBs, desiccants and carriers, that were provided in Chapter 5: Experiments and Results. The discussions include the method for obtaining the estimate of mass of water vapor adsorbed by desiccant sealed inside MBB vs. time and the estimate of RH inside MBB vs. time from the obtained experimental results.

Method for Obtaining the Mass of Water Vapor Adsorbed by Desiccant vs. Time

This section discusses the method for estimating the time to reach a certain percentage of adsorption capacity of desiccant when sealed inside MBB at a certain outside temperature / RH condition. This estimate is obtained by determining the relationship between the mass of water vapor adsorbed by desiccant and time. The method is explained for an example of MBB sealed with 16.5g of clay desiccant placed in an outside condition of 40 °C / 93% RH.

Equation (12) represents that MVTR equation, whose definition of terms and derivation are discussed in detail in moisture permeation property section. Here, Q represents the mass of water vapor permeated through MBB in grams, A represents the area of the MBB through which the moisture permeates in m^2, and t represents the time in days. The value of permeability, P, at 40 °C from Table 7 is 6.62E-7. Relative humidity outside the MBB, RH_{out}, is 0.93. Relative humidity inside the MBB, RH_{in}, is obtained from Figure 30 whose data was recorded from the wireless sensor placed inside MBB along with 16.5g of desiccant at 40 °C / 93% RH as outside condition.

However, in this example, it is assumed that there is no water vapor present initially. As a result, Figure 30 is modified by removing the decrease in RH data from 0 to 4.5 days that represents the adsorption of initial mass of water vapor present inside the MBB after sealing to obtain Figure 46. Area, A, and thickness, L, of the MBB are 0.07 m^2 and 0.11 × 10^{-3} m respectively. Substituting $P, L, A, RH_{out}, RH_{in}$ in equation (13) provides a linear relationship between the mass of water vapor permeated through MBB and time. Assuming that the moisture permeated through MBB is adsorbed by the desiccant, Q in the equation (13) can be replaced by g_{H_2O} representing the mass of water vapor adsorbed by desiccant. Also, assuming that the properties of MBB and desiccant may not degrade for the period of long-term storage, the linear relationship between the mass of water vapor adsorbed by desiccant and time when 16.5g of desiccant is inside sealed MBB at 40 °C / 93% RH as outside condition is shown in equation (14). This linear relationship may hold true only till the desiccant inside sealed MBB reaches 80% of the desiccant's adsorption capacity because the rate of adsorption gets slower and slower as the desiccant reaches its adsorption capacity, and it is not good to assume that it will still be linear after 80%. Using this equation, the time taken to reach 80% of the adsorption capacity of the desiccant at 40 °C / 60% RH as inside condition, as determined from Table 14, is estimated to be approximately 18 years. Similarly, this method can be used for estimating the time taken by desiccant to reach the required percentage of adsorption capacity at a required outside temperature / RH condition.

$$MVTR = \frac{Q}{A \times t} = \frac{P}{L}(RH_{out} - RH_{in}) \quad (12)$$

$$Q = \frac{P}{L}(RH_{out} - RH_{in}) \times A \times t \quad (13)$$

$$g_{H_2O} = 4.1 \times 10^{-3} \times t \quad (14)$$

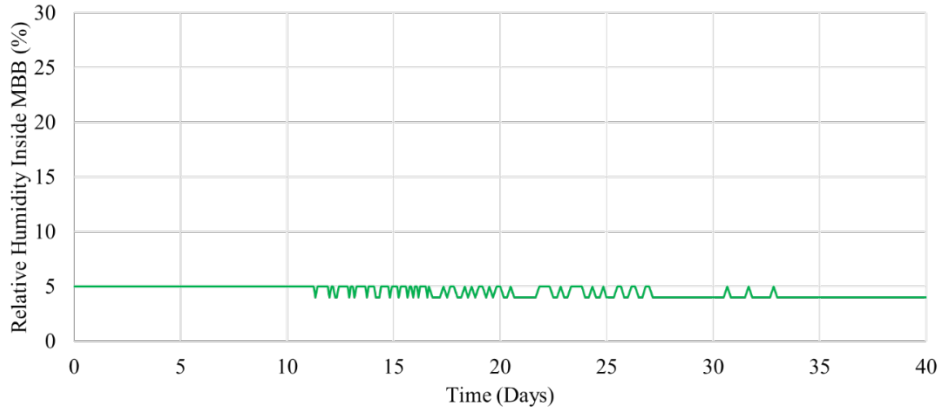

Figure 46 Graph showing the relative humidity inside MBB vs. Time recorded by wireless sensor inside MBB sealed with 16.5g of desiccant at 40 °C / 93% RH (Modified version of Figure 43)

Method for Estimating the RH Inside MBB vs. Time

In this section, the method for obtaining the relationship between RH increase inside MBB and time when desiccant is inside sealed MBB based on equation obtained in Section: Method for Obtaining the Mass of Water Vapor Adsorbed by Desiccant vs. Time is discussed. The outcome of this method is to estimate the time taken to reach a certain level of RH inside MBB based on which engineering and managerial decisions for replacing the MBB and desiccants can be made. The method is shown for an example of MBB sealed with 16.5g of desiccant inside it with outside temperature / RH condition to be 40 °C / 93% RH. The results estimated based on equation (14) is compared to validate against the theoretical results obtained from first principle moisture permeation and moisture adsorption equation.

Equation (14) provides the relationship between the mass of water vapor adsorbed by desiccant and time at 40 °C / 93% RH as the outside condition. Equation (11) from adsorption isotherm section provides the adsorption isotherm equation for the desiccant at 40 °C. Under equilibrium, the mass of water vapor, g_{H_2O}, in equations (14) and (11) are equated to obtain equation (15) that provides the relationship between RH inside MBB and time in days. The equation (15) is obtained based on the assumption that the RH inside the MBB initially (time of sealing) is zero.

$$RH = 4.59 \times 10^{-6} \times t^{1.2} \tag{15}$$

The graph based on equation (15) is shown in Figure 47. The top subplot of the graph shows the relative humidity inside MBB vs. time and bottom subplot of the graph shows the mass of water vapor adsorbed by the desiccant vs. time correspondingly. The linear assumption for the mass of water vapor adsorbed by desiccant and time was made valid till the desiccant reaches 80% of its adsorption capacity at 40 °C / 60% RH inside the MBB. The estimate of time taken to reach 80% of its adsorption capacity is approximately 18 years and the corresponding increase in RH inside MBB is around 17.5% RH.

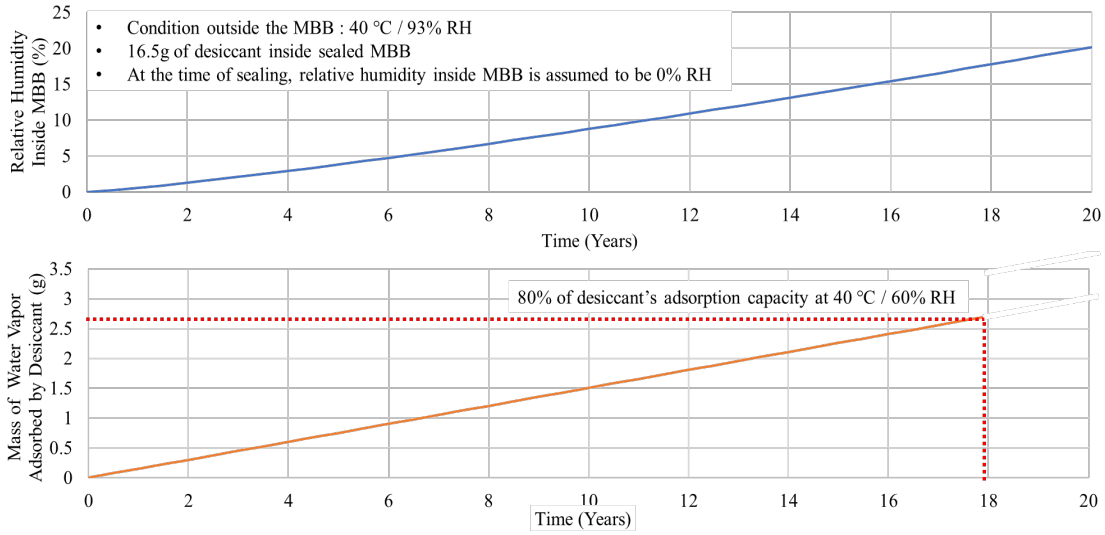

Figure 47 Graph showing two subplots - Top subplot shows the relative humidity inside MBB vs. time and the bottom subplot shows the corresponding mass of water vapor adsorbed by desiccant vs. time

Taking 10% RH as the limit based on IPC/JEDEC J-STD-033 standard, from Figure 48, the estimate of time taken to reach 10% RH inside the MBB is approximately 11 years and the desiccant would have adsorbed approximately 47% of its adsorption capacity at 40 °C / 60% RH. The humidity indicator card also indicates 5% RH level, and this 5% RH can also be taken as warning limit for the companies to taken engineering decisions and judgements for replacing the desiccants before it reaches 10% RH inside MBB. The estimate for 5% RH is approximately 6 years and the desiccant would have adsorbed 26% of its adsorption capacity at 40 °C / 60% RH. These estimates are obtained based on the equation (11) which was obtained from experiments.

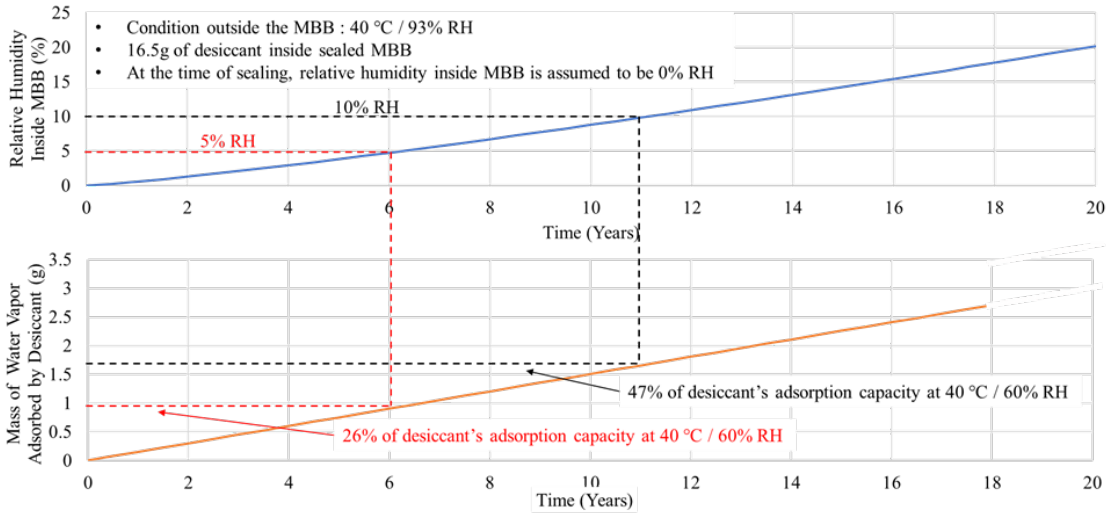

Figure 48 Graph showing two subplots with estimates of time to reach 5% RH and 10% RH inside MBB, and corresponding mass of water vapor adsorb by the desiccant

The estimated results obtained from the experiments conducted on MBBs and desiccants is compared against the theoretical results that can be obtained from equations for moisture permeation for MBB and moisture adsorption for desiccant. The first principle moisture permeation equation is obtained from equation (12). The moisture adsorption equation is obtained from equation (11). According to the conservation of mass, mass of water vapor permeated through MBB in equation (12), Q, is equal to the mass of water vapor adsorbed by the desiccant in equation(11), g_{H_2O}, plus the initial mass of water vapor in air inside the MBB, $g_{initial}$ to obtain equation (16). Assuming that mass of water vapor initially inside the sealed MBB is zero, the equation (17) is obtained from which the theoretical increase in RH inside MBB can be obtained.

$$Q + g_{initial} = g_{H_2O} \tag{16}$$

$$\frac{P(T) \times A}{L} \times (RH_{out} - RH_{in}) \times t = 0.69 \times (RH_{in})^{0.83} \times g_{clay} \quad (17)$$

Figure 49 shows the theoretical results obtained from the equation and results obtained based on experiments conducted on MBBs and desiccants at 40 °C / 93% RH. It can be observed from the graph that the theoretical results and the results based on experimental analysis diverge and the difference increases as the time increases. It can be inferred from this observation that the results based on experimental results can be considered as a conservative estimate compared to theoretical results because of linear assumption in experimental analysis. The theoretical results show that as the desiccant is approaching towards its adsorption capacity, the rate of adsorption becomes slower and slower and therefore a corresponding slower increase in RH. For reaching 5% RH, theoretical results show that it takes approximately 7 years, whereas results based on experimental analysis provide a conservative estimate of 6 years and correspondingly the desiccant adsorbs 26% of its adsorption capacity when it reaches 5% RH inside MBB. So this graph shows that both the theoretical and experimental methods can be used for obtaining estimates of time to reach 5% RH inside as the results are comparable for the lower levels of RH.

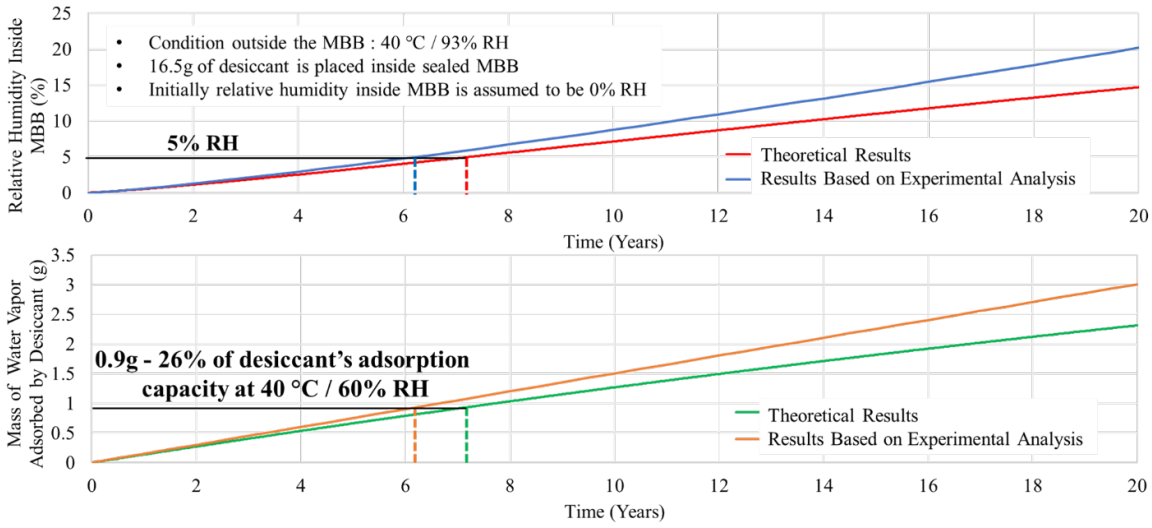

Figure 49 Graph showing the comparison of theoretical results and results based on experimental analysis for

The theoretical results were obtained for 25 °C / 60% RH as outside condition. From the graph, it can be observed, it takes 22 years to reach the 5% RH inside MBB at 25 °C / 60% RH condition and correspondingly the desiccant adsorbs 20% of its capacity at 25 °C / 60% RH. The reason for this longer time to reach 5% RH at 25 °C / 60% RH compared to 40 °C / 93% RH results is because the permeation rate decreases with the decrease in temperature which reduces the amount of water vapor permeated through MBB from the outside to the inside environment. This results in slower adsorption rate by the desiccant and thus, slower increase in RH inside MBB. When the RH inside MBB reaches 5%, the desiccant is estimated to adsorb 20% of its adsorption capacity at 25 °C / 60% RH.

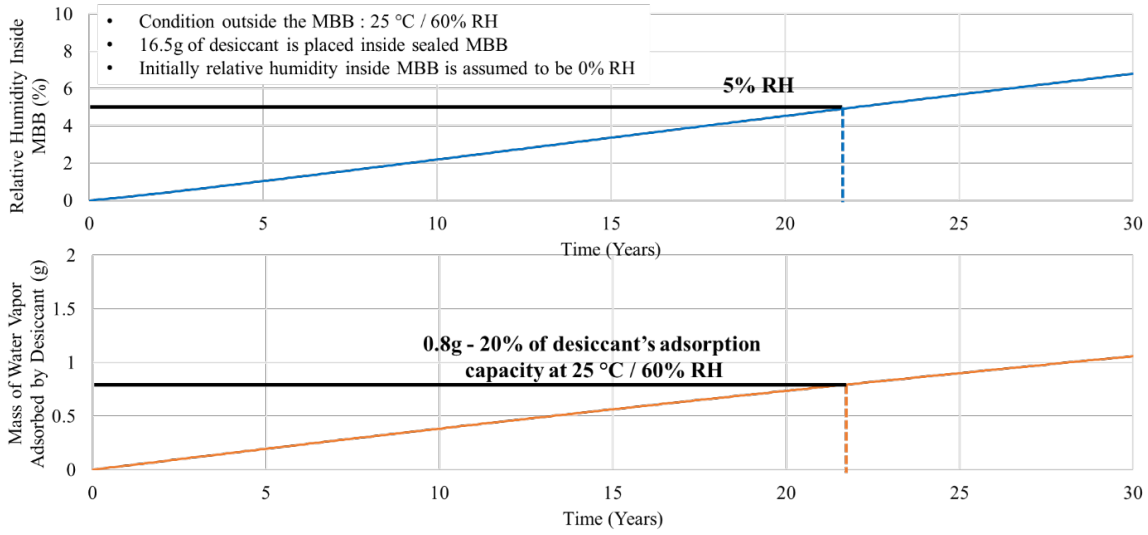

Figure 50 Graph showing theoretical results for relative humidity inside MBB vs. time and mass of water vapor adsorbed by desiccant vs. time at 25 °C / 60% RH as outside condition

Table 27 Summary of results

Condition (Temperature/ Relative Humidity)	**Estimate of time to reach 5% RH inside MBB when 16.5g of desiccant is inside the sealed MBB**		**Estimate of mass of water vapor adsorbed by 16.5g of desiccant at 5% RH inside MBB**
	Theoretical Results	**Results Based on Experimental Analysis**	
40 °C / 93% RH	6 years	7 years	0.9g (26% of desiccant's adsorption capacity at 40 °C / 60% RH)
25 °C / 60% RH	22 years	-	0.8g (20% of desiccant's adsorption capacity at 25 °C / 60% RH)

Table 27 shows the summary of the results obtained in the thesis. For 40 °C / 93% RH, the estimate of time to reach 5% RH inside MBB when 16.5g of desiccant is sealed inside MBB is 6 years, which is based on results obtained from experimental analysis, and 7 years from theoretical results. And the desiccant is estimated to adsorb 26% of

desiccant's adsorption capacity when RH reaches 5% RH. For 25 °C / 60% RH, theoretical results show an estimate of 22 years to reach 5% RH inside MBB and 20% of the desiccant adsorption capacity is estimated to be utilized when the RH reaches 5% RH inside MBB. These results assume that MBB or desiccant may not undergo degradation till the time that has been reported here.

Chapter 7: Conclusions

Companies undergo long-term storage to avoid the problem of component obsolescence. Long-term storage can be represented as a system containing replacements elements (packaging media) and non-replaceable elements (electronic components). The failure of long-term storage system is defined as when the electronic component's (non-replaceable elements) manufacturability and reliability requirements are not met. Defining the system and its lifecycle environment allows for the identification of the long-term storage system's various elements' degradation modes, mechanisms, and effects associated with it.

Degradation modes such as change in surface resistivity and change in dimensions can be observed on carrier tapes of tape and reel during long-term storage of electronic components. However, experimental results showed no increase or decrease in surface resistivity or dimensions of the sprocket holes and pitch of the carrier tape beyond the maximum or minimum limits specified by the standards when aged at accelerated conditions (85 °C / 5% RH and 60 °C / 25% RH). At the warehouse, the carrier tapes are packed inside MBB that is maintained at a maximum temperature of 25°C. Also, the recommendation for maximum relative humidity inside MBB is 10% RH before the desiccants and MBBs shall be replaced. Since only minimal changes were observed at accelerated conditions, the degradation modes – change in surface resistivity and dimension for the carrier tapes packed within MBB that is stored at <25°C / <10%RH inside MBB is concluded to be less critical to occur and affect the manufacturability or reliability of the electronic components. This conclusion holds good when the MBBs

and desiccants are replaced before the RH inside MBB reaches 10% RH. Change in surface resistivity degradation mode can also be observed on MBBs. Similar to the experiments conducted on carrier tapes to find criticality of this degradation mode, MBBs were also aged at accelerated conditions (85 °C / 5% RH and 60 °C / 25% RH) for observing its change in surface resistivity over time. The results of this experiment also led to the conclusion that the degradation mode of change in surface resistivity on MBBs when stored at <25°C / <10%RH inside MBB is found to be less critical to occur.

Desiccants used for long-term storage of electronic components has got adsorption capacity beyond which the permeated moisture will not get adsorbed and as the desiccant is adsorbing the permeated moisture, the RH inside the MBB increases. It is critical to estimate the trend of RH increase inside MBB vs. time based on the permeation characteristics of MBB and adsorption characteristics of the desiccant that is inside sealed MBB. Methods developed in this thesis estimated that it takes 22 years to reach 5% RH inside MBB when 16.5g of desiccant is inside sealed MBB at 25 °C / 60% RH as outside condition. Similarly estimates for time to reach 5%RH inside MBB and the corresponding increase in mass of any desiccant can be obtained from the methods developed in the thesis – which are based on experimental results and based on theoretical equations. These estimates can be used for determining replacement schedule for desiccants during long-term storage. However, these estimates were made on some assumptions. Therefore, it is recommended to introduce and distribute control samples for packaging media and inculcate periodic verification of those control samples as one of the management practices for long-term storage. Based on the

estimates obtained for time to reach 5% RH inside MBB, engineering and managerial decisions can be made to determine time interval for periodic evaluation of control samples. Also, if there any changes associated with mass measurement of desiccant at each time interval with the estimated trend developed by using the method proposed in the thesis, appropriate decisions and actions need to be taken.

As a part of risk management practices for long-term storage, storage conditions such as temperature and relative humidity for high-risk elements - components or the packaging media should be determined, based on which the changes should be made accordingly for the next level of assemblies, such as circuit cards and modules. The storage policies followed by the component manufacturers and distributors need to be obtained for determining the pre-storage stress factors. It is important to know how long the components and packaging media have been stored in the component and packaging media manufacturer's and distributor's warehouses so that the time to replace estimate can be adjusted accordingly. Any qualification reports, product change notifications (PCNs), and product discontinuation notifications (PDNs) available for the packaging media should also be obtained. Care should also be taken in not selecting any substandard or non-conforming MBBs, carriers, desiccants, and humidity indicator cards for long-term storage of electronic components.

Chapter 8: Appendices

Appendix A – Elements of Long-Term Storage System

Carriers

Carriers are packaging media that are used to protect the components from physical damage and electrostatic discharge damage during transportation and storage. Electronic components such as, but not limited to, transistors, capacitors, resistors, diodes, and integrated circuits are protected by placing and containing them within the carriers. In addition to the function of protecting the components from physical and environmental damage, they are used as an aid in the manufacturing or assembly processes after storage. For example, carriers containing the integrated circuits such as microprocessors are fed along the rails of the pick and place machines that automatically pick those microprocessors from the carriers and place it in a specific orientation at a specific location on the circuit board for reflow soldering. In general, carriers can be categorized into three types – tube, tray, and tape and reel.

Tubes

Tube carriers also called stick magazines, are an elongated hollow body made of plastic with antistatic coating, extruded in a rectangular shape. Each end of the tube is provided with a stopper to hold the components inside the tube and thus preventing them from falling out of the tube during transportation. They are used to feed the components to automatic pick and place machines for surface and through-hole board

mounting [5]. Figure 51 shows the picture of tube carriers containing quad flat node (QFN) package components inside it.

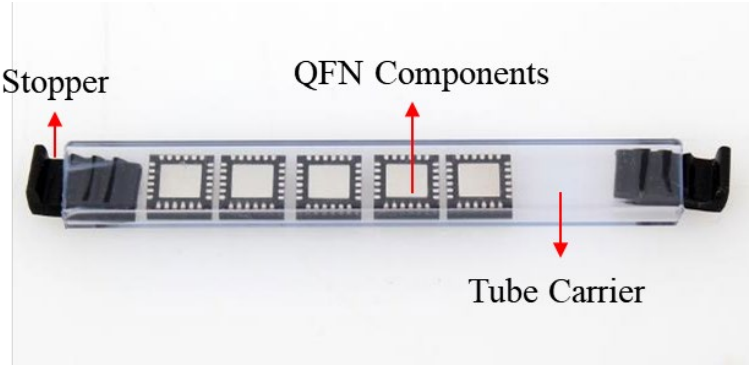

Figure 51 Tube carrier containing quad flat node (QFN) package components

Tray

Tray carriers are molded in rectangular shapes that nest the electronic components within a matrix of pockets that are uniformly spaced. Figure 52 shows the picture of a tray carrier. Trays are primarily designed for leaded components that require component lead isolation during transportation, handling, and manufacturing/assembly of those components. Unlike the tube carriers, the tray pockets prevent the component's leads from coming into contact with each other, thus protecting the components from physical damage during transportation and storage. The spacing provides exact locations for industry-standard automated-assembly equipment used for pick-and-place in board-assembly processes [41]. There are specific standards formulated by the electronic industries alliance (EIA) and joint electron device engineering council (JEDEC) that outlines requirements to store and handle the trays effectively. JEDEC publication 95 – Design guide 4.10 provides the standard design requirements for trays [42]. EIA 948 and EIA 960-B provides the requirements for automatic handling of trays

during the pick and place operations [43] [44]. They are usually of two types – bakeable and non-bakeable trays. With the bakeable trays, the components can be baked along with the trays inside the oven without having the components involved with any risk of damage due to additional handling. On the other hand, components have to be picked out of the non-bakeable trays for baking, which increases the chance of physical damages due to handling. The commonly used materials for manufacturing tray carriers in the current market are polyvinyl chloride, polystyrene, polyethylene terephthalate, polypropylene, and polycarbonate. The choice of material selection for the trays is based on the requirement of the maximum temperature rating. Trays are usually shipped in stacks of multiple single trays placed on top of each other for rigidity. These stacked trays that are loaded with components are protected with an empty cover tray on the top. Typically, the stack configurations are either five fully loaded trays with one empty cover tray or ten fully loaded trays with one cover tray [41]. Figure 53 shows the picture of stacked trays. The advantages of using the trays are attributed to its easy inspection of the loaded components and its reduced weight, thus reduced shipping cost.

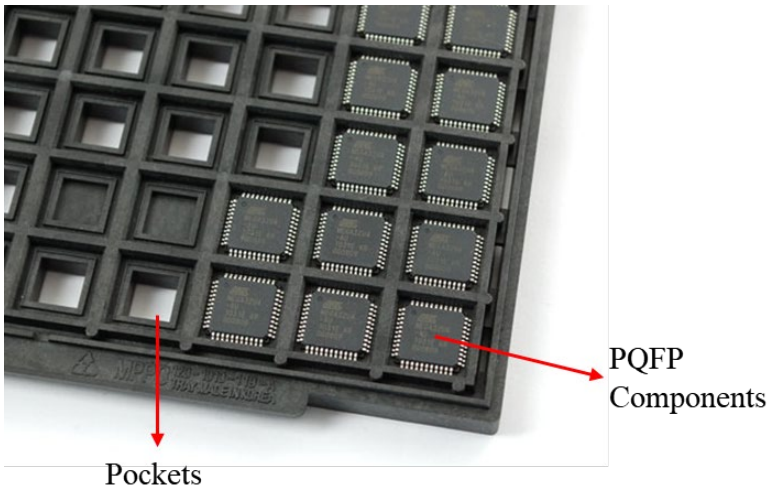

Figure 52 Tray carriers with pockets and loaded with Plastic Quad Flat Package (PQFP) components

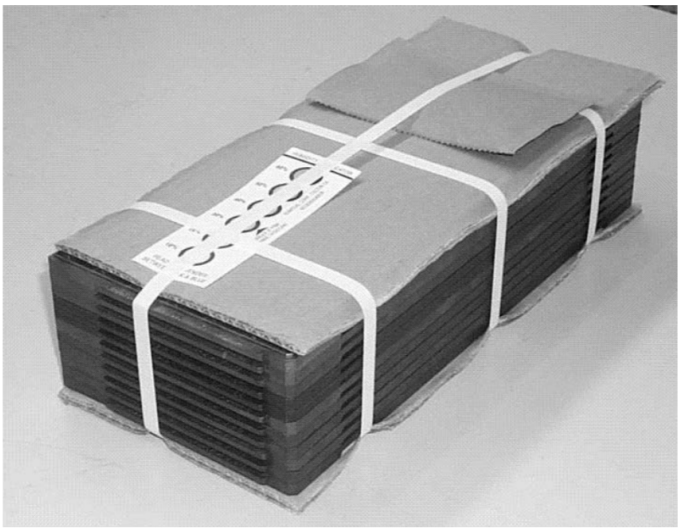

Figure 53 Trays stacked with the configuration of 10 loaded trays and one empty cover tray at the top

Tape and Reel

In tape and reel carriers, the electronic components are loaded onto a tape with sequential cavities along its length that are either in the form of punched holes or embossed pockets. This tape, known as carrier tape, is wound around a reel to feed the components for automatic pick and place operations for surface mounting on board

assemblies. The carrier tape is sealed by a cover tape on one side for embossed pockets and on both sides, for cavities to hold and retain the components, thus protecting the components from any physical damage and also free from dust and contaminants. The three elements of the tape and reel are carrier tape, cover tape, and reel. In general, the tape and reel carriers are categorized into two types based on the type of cavity found in carrier tape – punched hole type and embossed pocket type. In the former type, carrier tapes are punched with sequential holes to contain components, whereas, in the latter type, the carrier tapes are embossed in the form of pockets of a certain thickness to hold the components. Figure 54 shows the tape and reel, its elements, and its two types based on the cavity. Standards such as EIA 481–E formulated by automated component handling committee (ACH) of electronic components industry association (ECIA) in 2015 and IEC 60286-3 formulated by International Electrotechnical Commission (IEC) in 2019 provide specific requirements to store, handle, tape and de-tape the surface mount components effectively. They also provide dimensional requirements for the carrier tapes that, if not adhered to, may cause functional problems with the industry-standard automated feeding systems.

One important dimensional characteristic of the carrier tape is camber, which is defined as the curvature of the tape with respect to the x and y-axis on the plane in which the carrier tape is fed parallelly to the guideways. Camber shall not exceed 1 mm over 250 mm in either direction when the carrier tape is fed into guideways. Figure 55 shows this dimensional requirement for camber in carrier tapes [37] [45]. The standards also proposed general and storage requirements for the carrier tapes. Along with these

standards, EIA 468-C provides requirements for dimensions and tolerances for the automatic handling of components having two or more radial configured leads [46].

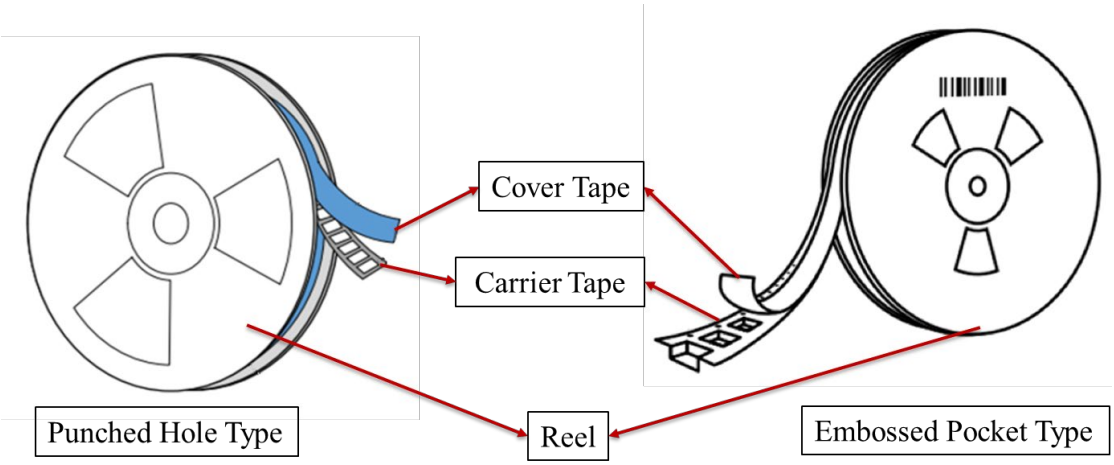

Figure 54 Two types of tape and reel along with its elements

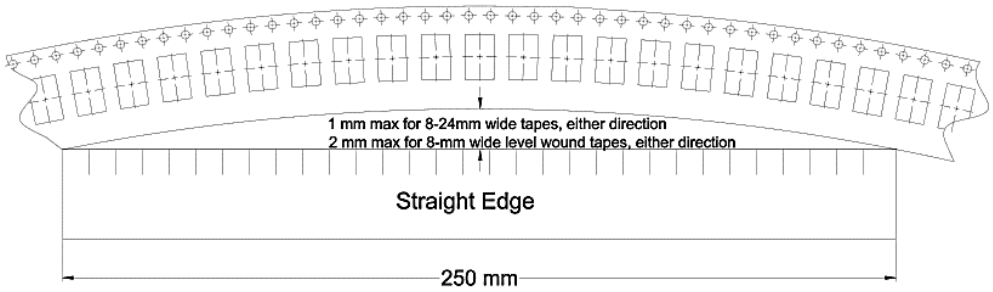

Figure 55 Dimensional requirement of camber in carrier tapes

Carrier Tape of Tape and Reel Carrier

The carrier tape is a continuous tape wound around the reel to accommodate electronic components for transport, storage, and automatic feeding to pick and place machines. These tapes incorporate sprocket holes that are punched on one or both the side ends of the tape depending on the tape width. These sprocket holes index with the sprockets of the pick and place machines to drive them along the guideways for

automatic feeding. Figure 56 shows the setup of the carrier tape containing components sliding along the guideways of the pick and place machine. Usually, the punched hole type carrier tapes contain small passive electronic components with thickness less than 0.9 mm approximately, for example, chip resistors and capacitors. The material that is commonly used for manufacturing the punched hole type is paper. The reason for using paper is because it does not require a high level of protection from physical damage during the transportation of passive components compared to the active leaded ICs. Components with thickness greater than 0.9 mm require more rigid protection from physical damage and ESD, and so they are loaded onto carriers with embossed pockets. This embossed pocket type carrier tapes are commonly made up of polymers such as polystyrene and polycarbonate. Some of the factors that influence the choice of selecting the materials for carrier tapes include susceptibility to warping and bending, risk of rough feeding into pick and place machine that may result in mis-pick errors, and, the requirement of tighter tolerances with dimensional integrity to restrict movement - rotation and tilting within the pocket that may otherwise result in physical damage of the leads and mis-picks [47].

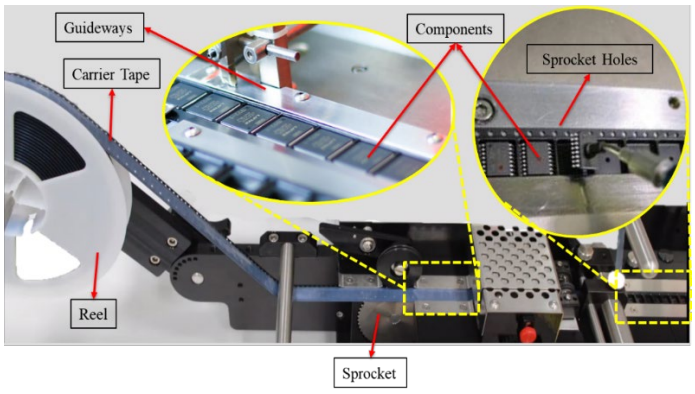

Figure 56 Carrier tape setup along the guideways of the pick and place machine for automatic component handling

Cover Tape of Tape and Reel Carrier

Cover tape is an antistatic, transparent polymeric thin film coated with the adhesive layer. The cover tapes are adhered to the top of carrier tapes after the components are loaded onto them, to protect and contain the loaded components during transportation and storage. During the automatic feeding operation of the carrier tapes along the guideways, the adhered cover tapes are peeled back using a peeling machine followed by pick and place operation of the contained components. Figure 57 shows the picture of cover tape adhered to the carrier tape along with the picture of cover tape peeled back from the carrier tape. Cover tapes are generally categorized into two types – heat-activated and pressure-sensitive. In heat-activated cover tapes, temperature, time and pressure are the parameters that are controlled in the sealing machine to adhere to the cover tape onto the edges of the carrier tape on both sides, sealing the cover tape to the carrier tape. Though these are the most widely used type of cover tape in the industry, it is marked with a downside of relatively inconsistent peel force compared to its counterparts. This uneven peel force causes the devices to pop out of their positions

within the pockets of the carrier tape, and this phenomenon is called as a trampoline that significantly slows down the production. On the contrary, the pressure-sensitive cover tape is adhered to the carrier tape by controlling the parameters such as pressure and time. These tapes provide smoother peel force and minimize the trampoline of components. However, these tapes leave behind a residue while peeling that builds up over time and causes jamming of the automatic feeder [47] [48].

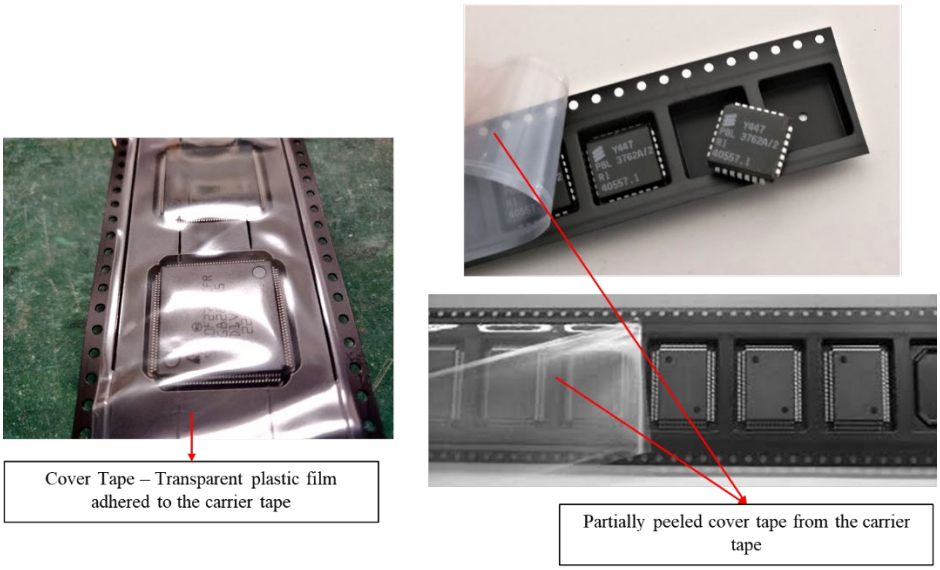

Figure 57 Picture showing the adhered and back peeled cover tape

Humidity Indicator Cards

Humidity indicator card (HIC) is an indicator of relative humidity (RH) levels inside the sealed moisture barrier bag that contains the components, carriers, and desiccants. The card is impregnated with certain chemicals that are sensitive to moisture, resulting in the change of color when the RH level exceeds the indicated level. This change in color allows for immediate inspection of RH level inside the bag;

however, the bag has to be cut open to inspect the RH level, which increases the risk of additional handling and processes such as vacuuming and re-sealing the bag. Typically, HIC is manufactured based on the compliance with IPC/JEDEC standard J-STD-033 and military standard MIL-I-8835A. According to IPC J-STD-033D, HIC should have three spots indicating 5% RH, 10% RH, and 60% RH in blue color initially. When the RH level exceeds these indicated values, the spot corresponding to that value changes its color from blue to pink, and in some cases, the changed color migrates out of the spot. The 5% RH and 10% RH indicator are assigned to moisture sensitivity level (MSL) 2A-5A components, and 60% RH indicator is assigned to MSL 2 parts. If the 10% RH spot is not blue for the MSL 2A-5A components that are sealed inside the bag, baking should be performed. If the 60% RH spot is not blue for the MSL 2 components, baking should be performed. Figure 58 shows the images of the HIC that comply with IPC/JEDEC J-STD-033D [39]. Table 28 shows the color indication of HIC that complies with IPC/JEDEC J-STD-033D at different RH environment.

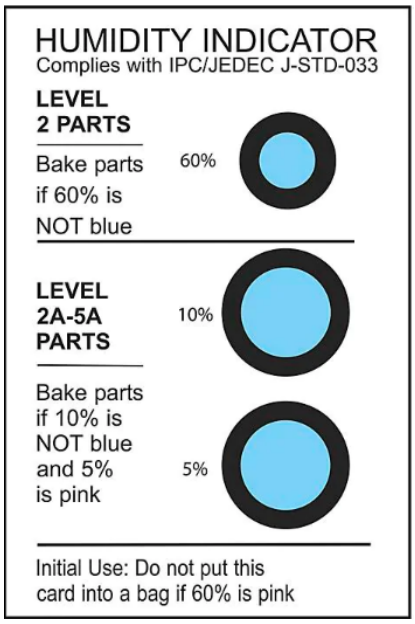

Figure 58 HIC that complies with J-STD-033D

Table 28 Color indication by HIC at different RH environment

	Indication at 2% RH Environment	Indication at 5% RH Environment	Indication at 10% RH Environment	Indication at 55% RH Environment	Indication at 60% RH Environment	Indication at 65% RH Environment
5% Spot	Blue	Lavender	Pink	Pink	Pink	Pink
10% Spot	Blue	Blue	Lavender	Pink	Pink	Pink
60% Spot	Blue	Blue	Blue	Blue	Lavender	Pink

Appendix B – Material Property Testing, Analysis and Validation

This section details the experiments that were conducted to test and validate some of the material properties of the received MBB samples.

Moisture Barrier Bag

Cross-Sectional Analysis – Thickness Measurement

The Dri-Shield 3700 series MBB was cut into a small strip from forming a V-shape to clearly identify the inner and the outer layers. The strip was then potted into a round shape with the V-shaped MBB strip showing its cross-section. The bottom side of the potted samples were then ground and polished to make a flat and clear cross-sectional view under the Zeiss Axiovert optical microscope. Figure 59 shows the V-shaped cross-sectional image obtained from the optical microscope that clearly identifies the three layers of the MBB. The thickness of each layer of the MBB was measured three times and their average was taken. The thickness of the MBB as a whole was measured using the same optical microscope and its average was calculated. Table 29 shows the values of the measured thickness with its last row indicating the thickness measured for the whole MBB. The last row of the Table 29 was measured independently and is not the addition of the thickness of the three layers. On an average the thickness of the MBB was found to 115.47 microns which is within the tolerance limits provided by the manufacturer (Refer Table 3). Also, the thickness of the outer layer of the MBB was found to be less in value compared to the inner layer of the MBB.

Table 29 Thickness of each layer of the MBB and the whole MBB in microns

	1st Measurement	2nd Measurement	3rd Measurement	Average
Outer Layer (µm)	34.98	35.09	36.72	35.60
Middle Layer (µm)	9.8	10.6	10.61	10.34
Inner Layer (µm)	67.05	67.32	69.77	68.05
MBB (Measured independently and not the addition of the three layers) (µm)	114.92	115.34	116.15	115.47

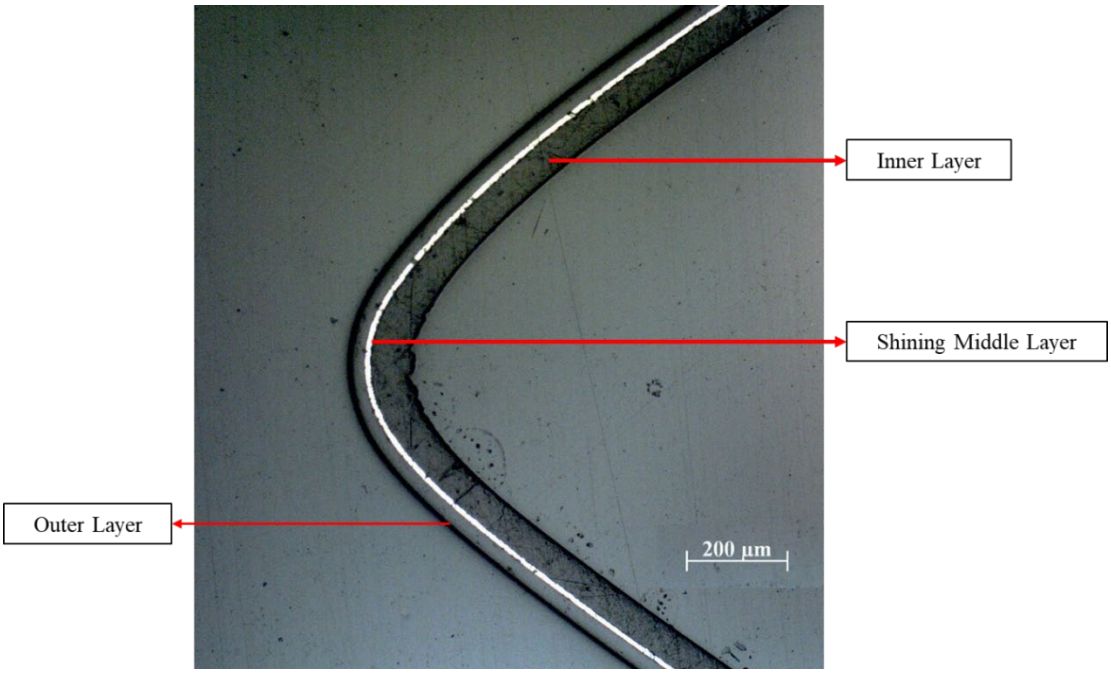

Figure 59 Optical microscopic image showing the cross-section of the MBB

Fourier Transform Infrared Spectroscopy (FTIR) Analysis

FTIR analysis was performed to identify and validate the inner and outer polymeric layers of the MBB. Agilent Cary 670 FTIR spectrometer in attenuated total reflection (ATR) mode was used for FTIR analysis of the Dri-Shied 3700 series MBBs. The MBB

samples was cut into rectangular shape of dimensions 2.5*1 cm^2. Infrared beam was allowed to through the diamond ATR crystal at different frequencies. The spectral output from FTIR was displayed in the form of graph with wavenumber along the x-axis and the absorbance along the y-axis. FTIR spectra was obtained for both the inner and the outer layers of the MBB to validate the polymeric materials as specified by the manufacturer.

(FTIR image obtained without any comparison with the FTIR library spectra has been included in the appendix section for now. The FTIR graph will be included after comparing the spectra with the library)

Energy-Dispersive X-ray Spectroscopy (EDS) Analysis

EDS analysis was performed to identify and validate the middle layer of the MBB. Similar to the sample preparation for the cross-sectional analysis, the MBB samples were cut into a V-shape and then ground and polished to view under the microscope of energy-dispersive x-ray spectrometer. The electron beam from the spectrometer was focused on the middle layer to obtain the elemental composition spectra from the EDS. Figure 60 shows the EDS spectra obtained for the middle layer of the MBB. The left side of the Figure 60 shows the point where the electron beam of the EDS was focused. The right side of the Figure 60 shows the EDS spectra with Aluminum as the major composition of the middle layer of the MBB, thus acting as a validation to the material specification provided by the Dri-Shield 3700 series manufacturer. Small traces of Carbon and Oxygen were also observed. The presence of Carbon in the middle layer can be attributed to the transfer of small amounts of Carbon from outer and inner

polymeric layers while grinding the sample. The possible explanation for the presence of small traces of Oxygen is that the Aluminum could have quickly reacted with the Oxygen present in the atmosphere to form Aluminum Oxide during the sample preparation.

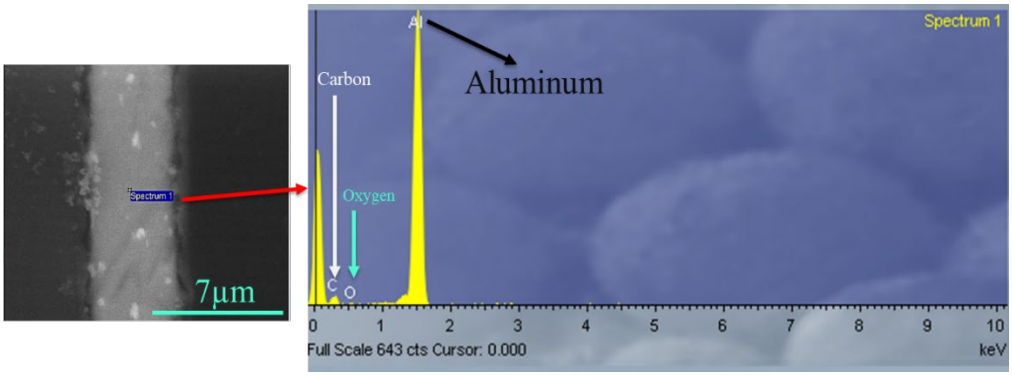

Figure 60 Figure showing the EDS spectra obtained for the middle layer of the MBB

Surface Resistance Analysis

The surface resistance of the MBB samples were measured using Signatone Pro-4 Four Point Resistivity System to validate the surface resistance property of the MBB. The Pro-4 system measures the surface resistivity which is different from surface resistance. The surface resistance (R_s) is defined as the ratio of a DC voltage (U) to the current (I_s) flowing between the two electrodes of specified configuration that are in contact with the same side of the material under test. On the other hand, surface resistivity (ρ_s) is defined as the ratio of DC voltage (U) per unit length (L) to the surface current (I_s) per unit width (D) [49]. The physical unit of surface resistivity (ρ_s) is Ohm (Ω). The physical unit of the surface resistance (R_s) is also Ohm (Ω). In order to differentiate between the two, surface resistivity is often expressed in Ohm/square

(Ω/sq) though it is not a valid physical unit from the dimensional analysis point of view. Equation (18) and equation (19) in combination with Figure 61 provides the interpretation of the difference between the surface resistance and resistivity respectively in the equation form. According to ANSI/ESD STM 11.11, surface resistance measured using the test method specified in this standard can be converted into surface resistivity by multiplying a conversion factor of 10, which is derived from the fixed geometry of the electrode assembly [50]. As shown in the Table 3, the reported surface resistance property was measured according to ANSI/ESD STM11.11. As a result, the surface resistance value of 1 x 10^4 to < 1 x 10^{11} Ohms can be converted into its equal surface resistivity of 1 x 10^5 to < 1 x 10^{12} Ohms/square by multiplying it with a conversion factor of 10. The converted surface resistivity property of the MBB still lies within the region of static dissipative region.

$$Surface\ Resistance\ , R_s(\Omega) = \frac{U}{I_s} \tag{18}$$

$$Surface\ Resistivity, \rho_s\ (\Omega/sq) = \frac{U/L}{I_S/D} \tag{19}$$

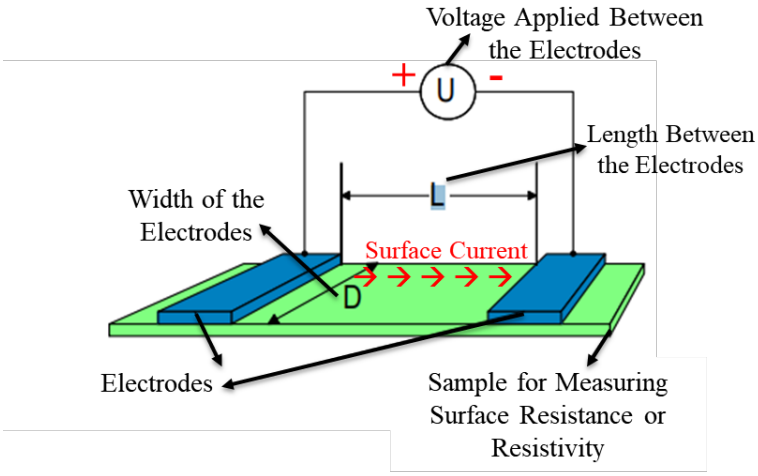

Figure 61 Image showing the basic setup for measuring the surface resistance or resistivity

Appendix C – Calibration Information of the Equipment

This section provides the calibration information of the equipment, devices and machines used in this thesis.

Weighing Scale

Amir digital kitchen weighing scale was used for measuring the weight of the desiccants in the experiments that were performed to determine the moisture adsorbing capability of the desiccants above 50^0C. The scale was calibrated before used for measuring the weights of the desiccant. For calibrating the scale, known weights of mass 20g, 50g, 100g and 200g were taken and placed on the weighing scale. It was observed that the weighing scale displayed the mass without any error. shows the picture showing the weighing scale displaying the exact mass of the known weights.

Figure 62 Picture showing the calibration of weighing scale used in the experiments

Temperature/Relative Humidity Chamber

ESPEC Temperature/relative humidity chambers were used for the aging experiments of MBBs and desiccants. The chambers were checked for calibration by

placing the Elitech wireless TH sensor inside them. Figure 63 shows the readings of the wireless TH sensor when the chamber was set at 60^0C/60% RH and 40^0C/60%RH.

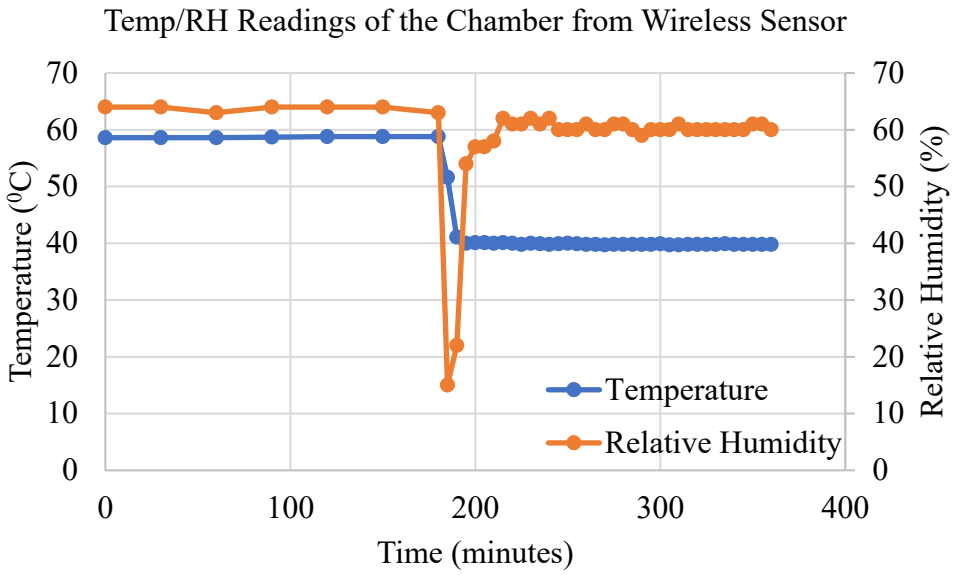

Figure 63 Graph showing the temperature and relative humidity of the chamber when set at 60^0C/60%RH and 40^0C/60%RH

Chapter 9: References

[1] JEDEC/EIA/IPC, "J-STD-048 - Notification Standard for Product Discontinuance," Joint Electron Device Engineering Council (JEDEC) Solid State Technology Association, Arlington, VA, 2014.

[2] B. Bartels, U. Ermel, P. Sandborn and M. G. Pecht, Strategies to the Prediction, Mitigation and Management of Product Obsolescence, John Wiley & Sons, 2012.

[3] E. Wong, S. Koh, K. Lee and R. Rajoo, "Comprehensive Treatment of Moisture Induced Failure-Recent Advances," *IEEE Transactions on Electronics Packaging Manufacturing,* vol. 25, no. 3, pp. 223-230, 2002.

[4] Joint Electron Device Engineering Council (JEDEC), "JEP 160 - Long-term Storage for Electronic Sold-State Wafers, Dice and Devices," JEDEC Solid State Technology Association, Arlington, Virginia, 2016.

[5] SAE, "GEIA-STD-0003A - Long Term Storage of Electronic Devices," SAE International, 2017.

[6] International Electrotechnical Commission (IEC), "IEC 62435: Electronic Components - Long-Term Storage of Electronic Semiconductor Devices," IEC Technical Committee, 2017.

[7] R. R. Madsen, "Application Report on Component Reliability After Long-Term Storage," Texas Instruments, 2008.

[8] Desco Industries, INC, "SCS - Static Control Bag Storage," January 2020. [Online]. Available: http://documents.staticcontrol.com/pdf/SCS_Bag_Storage.pdf. [Accessed 08 August 2020].

[9] K. Cleary, "What is the Expected Shelf LIfe of Your ESD Control Bags?," SCS, [Online]. Available: https://staticcontrol.descoindustries.com/ESD-Packaging-Shelf-Life.aspx. [Accessed 04 August 2020].

[10] W. Decker, D. Roy, C. Voght, C. Roy and P. Dabbert, "Metallized Polymer Films as Replacement for Aluminum Foil in Packaging Applications," *Proceedings of The Annual Technical Conference-Society of Vacuum Coaters,* vol. 47, p. 594, 2004.

[11] Desco Indusctires Inc, "Data Sheet of Moisture Barrier Bag Dri-Shield 3700," SCS, Sanford, North Carolina, 2019.

[12] ASTM, "ASTM F1249-20, Standard Test Method for Water Vapor Transmission Rate Through Plastic Film and Sheeting Using a Modulated Infrared Sensor," ASTM International, West Conshohocken, Pennsylvania, 2020.

[13] M. Tencer, "Moisture Ingress into Nonhermetic Enclosures and Packages. A Quasi-Steady State Model For Diffusion and Attenuation of Ambient Humidity Variations," in *1994 Proceedings - 44th Electronic Components and Technology Conference*, IEEE, 1994, pp. 196-209.

[14] J. Kuusipalo and K. Lahtinen, "Influence of Temperature and Mixing Ratio on Water Vapor Barrier Properties of Extrusion-Coated Paper," *International Journal of Polymer Analysis and Characterization,* vol. 10, no. 1-2, pp. 71-83, 2005.

[15] G. Scrivens, P. Gerst, B. C. MacDonald, D. Carabillo, A. P. Monahan, R. J. Timpano, J. Lippke, M. Ticehurst, G. Wood and K. O. Ryan, "The Humidity Exposure of Packaged Products," in *Accelerated Predictive Stability*, Elsevier, 2018, pp. 105-146.

[16] P. E. Keller and R. T. Kouzes, "Water Vapor Permeation in Plastics," Richland, WA, 2017.

[17] ANSI/ESD, "S541- ESD Association Standard for Protection of Electrostatic Discharge Susceptible Items - Packaging Materials," Electrostatic Discharge (ESD) Association, 2019.

[18] Advantek, "Polystyrene Black Tri-Laminate C-Series - Data Sheet," Advantek Inc., 2020.

[19] Advantek, "Type HUE Antistatic Heat Activated Cover Tape - Data Sheet," Advantek Inc., 2019.

[20] Advantek, "Type HUB Antistatic Heat Activated Cover Tape," Advantek Inc., 2017.

[21] C-PAK PTE LTD, "Technical Information of C-PAK TYPE BC-1051 (CL) EMBOSSED CARRIER TAPE," Singapore.

[22] Advantek. Inc, "Safety Data Sheet (SDS) of Tri-Laminate PS+C," 2018.

[23] C-PAK PTE LTD, "Safety Data Sheet of Cpak-PS-BC1051-CL," Singapore, 2017.

[24] B. A. Morris, The Science And Technology Of Flexible Packaging: Multilayer Films From Resin And Process To End Use, William Andrew, 2016.

[25] M. Sultan, T. Miyazaki and S. Koyama, "Optimization of Adsorption Isotherm Types for Desiccant Air-Conditioning Applications," *Renewable Energy,* vol. 121, pp. 441-450, 2018.

[26] U. S. Department of Defense, "MIL-D-3464E - Military Specification: Desiccants, Activated, Bagged, Packaging Use and Static Dehumidification," U. S. Government, 1987.

[27] Y. Chen, "Packaging Selection for Solid Oral Dosage Forms," in *Developing Solid Oral Dosage Forms*, Elsevier, 2017, pp. 637-651.

[28] "Tyvek® Bag Desiccants - Unit Size 1/2, 5 Gallon Pail S-5165," ULINE, [Online]. Available: https://www.uline.com/Product/Detail/S-5165/Desiccants/Tyvek-Bag-Desiccants-Unit-Size-1-2-5-Gallon-Pail. [Accessed 22 Nov 2021].

[29] C. D. Hatch, J. S. Wiese, C. C. Crane, K. J. Harris, H. G. Kloss and J. Baltrusaitis, "Water Adsorption on Clay Minerals as a Function of Relative Humidity: Application of BET and Freundlich Adsorption Models," *Langmuir,* vol. 28, no. 3, pp. 1790-1803, 2012.

[30] I. Reinas, J. Oliveira, J. Pereira, P. Mahajan and F. Pocas, "A Qunatitative Approach to Asses the Contribution of Seals to the Permeability of Water Vapor and Oxygen in Thermosealed Packages," *Food Packaging and Shelf Life,* vol. 7, pp. 34-40, 2016.

[31] ASTM, "ASTM F88 - Standard Test Method for Seal Strength of Flexible Barrier Materials," ASTM International, West Conshohocken, Pennsylvania, 2015.

[32] C. Yuan and A. Hassan, "Effect of Bar Sealing Parameters on OPP/MCPP Heat Seal Strength," *eXPRESS Polymer Letters,* vol. 1, no. 11, pp. 773-779, 2007.

[33] S. J. Dahman, "All Polymeric Compounds: Conductive And Dissipative Polymers in ESD Control Materials," *Electrical Overstress/Electrostatic Discharge Symposium, IEEE,* pp. 1-2, 2003.

[34] J. Pecht and M. Pecht, Long-Term Non-Operating Reliability of Electronic Products, CRC press, 2019.

[35] L. Struik, "Physical Aging in Plastics and Other Glassy Materials," *Polymer Engineering & Science,* vol. 17, no. 3, pp. 165-173, 1977.

[36] 3M, "Technical Data for 3M Clear Polycarbonate Carrier 2703," 3M Electronics Materials Solutions Division, St. Paul, Minnesota, 2017.

[37] Electronics Components Industry Association (ECIA), "EIA-481: 8 mm Through 200 mm Embossed Carrier Taping and 8 mm & 12 mm Punched Carrier Taping of Surface Mount Components for Automatic Handling," 2015.

[38] 3M Company, "3M™ Static Dissipative Heat Activated Cover Tape 2678 - Technical Data Sheet," 3M Electronics Materials Solution Division, St. Paul, Minnesota, 2017.

[39] IPC/JEDEC, "J-STD-033D: Handling, Packing, Shipping and Use of Moisture/Reflow Sensitive Surface Mount Devices," 2018.

[40] ULINE, "Uline Online Catalog," [Online]. Available: https://catalog.uline.com/Fall-Winter-US-2020/739/. [Accessed 2 Feb 2021].

[41] C. Troxtell, B. O'Donley, R. Purdom and E. Zuniga, "Semiconductor Packing Methodology," Texas Instrument, 2005.

[42] Joint Electron Device Engineering Council (JEDEC), "Design Requirements for Outlines of Solid State and Related Products - Design Guide 4.0 Generic - Shipping & Handling - Matrix Tray," JEDEC Solid State Technology Association, 2002.

[43] Electronics Components Industry Association (ECIA), "EIA-948 : Component Tray for Automati Handling," 2004.

[44] Electronics Components Industry Association (ECIA), "EIA-960-B: Assembly Component Tray - ACT," 2017.

[45] Internation Electrotechnical Commission (IEC), "IEC 60286-3: Packaging of Components for Automatic Handling - Part 3: Packaging of Surface Mount Components on Continuous Tapes," 2019.

[46] Electronic Components Indsutry Association (ECIA), "EIA 468-C: Lead Taping of Components in the Radial Coniguration for Automatic Handling," 2008.

[47] C. Maynes, "Choosing Carrier and Cover Tape for Tape-and-Reel," 3M Electronic Solutions Division, 2009.

[48] 3M, "Prevention of Pressure Sensitive Adhesive Cover Tape Jamming in Feeders with Nip Gear and/or Collecion Bin Systems," 3M Electronic Handling & Protection Division Surface Mount Supplies, Austin, 2001.

[49] W. A. Maryniak, T. Uehara and M. A. Noras, "Surface Resistivity and Surface Resistance Measurements Using a Concentric Ring Probe Technique," *Trek Application Note,* vol. 1005, pp. 1-4, 2003.

[50] ANSI/ESD, "STM11.11 ESD Association Standard Test Method for the Protection of Electrostatic Discharge Susceptible Items - Surface Resistance Measurement of Static Dissipative Planar Materials," Electrostatic Discharge (ESD) Association, 2015.

[51] P. Kumar and J. Han, "Packaging Materials for Non-Thermal Processing of Food and Beverages," *Emerging Food Packaging Technologies,* pp. 323-334, 2012.

[52] Association Connecting Electronics Industries (IPC), "Printed Board Handling and Storage Guidelines," 2016.

[53] U.S. Department of Defense, "MIL-HDBK-1131A: Handbook for Storage, Shelf Life, and Reforming Procedures for Aluminum Electrolytic Fixed Capacitors," 2004.